Study of Phase Tolerances for the European XFEL Undulator System

Yuhui Li, Bart Faatz and Joachim Pflueger

Deutsches Elektronen Synchrotron (DESY), Hamburg, Germany

December 2007, TESLA-FEL 2007-07

Study of Phase Tolerances for the European XFEL Undulator System

Yuhui Li, Bart Faatz and Joachim Pflueger

Deutsches Elektronen Synchrotron (DESY), Hamburg, Germany

Abstract

An integral part of the design study of undulators for FELs is the study of the impact of their errors on the FEL performance. Previous work mainly studied the influence of random errors for each pole. Some errors, however, for instance the girder deformation, are not random but periodic. In this report both random and periodic errors as well as a combination are studied. The results are limited to non-steering errors, i.e. a reduction in overlap between electrons and photon beam has been avoided throughout this study.
Key words: tolerance, undulator, XFEL

1 Introduction

In the European XFEL project, photons will be generated in the X-ray range of 12.4 keV to 0.2 keV [1]. Primarily because of the mirror limitations, high power X-ray radiation can hardly be accumulated in an optical resonator. Therefore, this facility generates high power radiation using Self-Amplified Spontaneous Emission (SASE) [2, 3]. Simulations show that the saturation length of SASE-XFEL is more than 100 meters [4]. Tolerances in $\Delta K/K$ are often related to the FEL bandwidth, which is in the order of the Pierce parameter ρ. In case of the XFEL, this is about 10^{-4}. In order to remain within this bandwidth, the variation in undulator gap should smaller than 1μm and the temperature variation should be limited to 0.08^{o}C.

To satisfy the tolerance requirement given by ρ is very difficult. Therefore more careful tolerance simulations must be performed in order to achieve the requirements with a relaxed tolerance budget. We distinguish between two kinds of undulator field errors. One kind is random error, for example because of the inhomogeneous field of magnet blocks. When its impact is calculated, random errors are induced to each undulator pole [6, 7, 8, 9]. Another kind of error changes along undulator as periodic function. This kind of error occurs for example because of girder deformation or temperature variations. Previous tolerance simulations concentrated mainly on the first kind of error. Therefore, this report mainly takes into account the latter one.

The European XFEL facility supplies 0.1 nm to 0.4 nm radiation by two devices which are called SASE1 and SASE2. The undulator gap for SASE1 is fixed and generates 0.1 nm radiation with 17.5 GeV electrons. The undulator gap for SASE2 can be changed, so 0.1 nm to 0.4 nm radiation can be generated at this same energy. On the other hand, SASE1 can also generate 0.4 nm radiation by changing the electron energy. We therefore simulate SASE1 with two settings: 0.1 nm radiation at 17.5 GeV for an undulator parameter $K_{\mathrm{rms}} = 3.3$ and 0.4 nm with 8.75 GeV with the same undulator

parameter. SASE2 is calculated for three settings: 0.1 nm radiation at 17.5 GeV with $K_{\rm rms} = 2.8$, 0.4 nm at 8.75 GeV electron and same $K_{\rm rms}$ value, 0.4 nm radiation for 17.5 GeV and $K_{\rm rms} = 6.1$. In the next sections, results are shown for SASE1. The results for SASE2 as well as details of simulations in general are shown at the end of this report.

2 Description of error types and their simulation models.

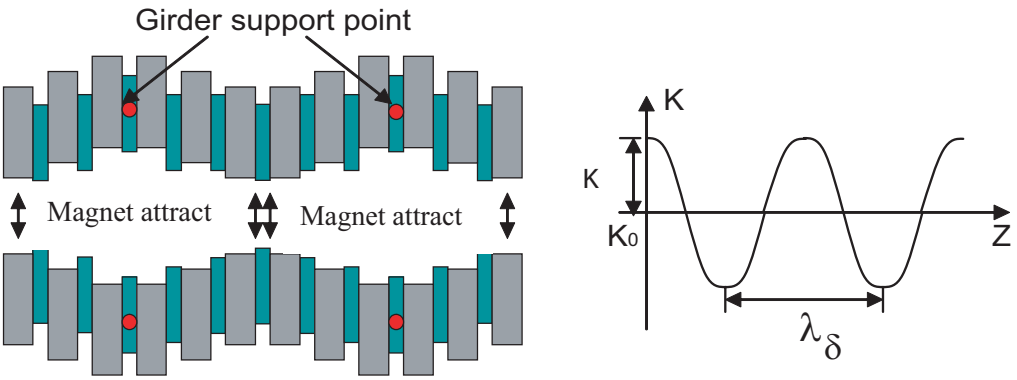

Figure 1: *Girder deformation due to magnetic forces. For one specific undulator gap, the field can be made homogeneous. For any other gap, a deformation can be expected which is close to a periodic sinusoidal shape.*

Figs. 1 and 2 show the girder deformation and gap tilt as sinus, triangle, sawtooth and (piecewise) constant error, respectively. The code Genesis 1.3 is used to simulate the error impact [10]. Because Genesis 1.3 uses the undulator parameter $K_{\rm rms}$ instead of gap to express the undulator field, we should discuss how the parameter $K_{\rm rms}$ changes because of these gap errors. As can be seen from Figs. 1 and 2, the error sources discussed here have a much longer period than the undulator period.

The peak magnetic field B_0 of a hybrid undulator depends on the undulator gap g, its period λ_u and constants a_1,a_2 and a_3 which depend on the undulator technology used [11]:

$$B_0 = a_1 \exp\left[a_2 \frac{g}{\lambda_u} + a_3 \left(\frac{g}{\lambda_u}\right)^2\right] . \tag{1}$$

Thus

$$dB_0 = B_0 \left(\frac{a_2}{\lambda_u} + \frac{2a_3}{\lambda_u^2} g\right) dg \approx B_0 \left(\frac{a_2}{\lambda_u} + \frac{2a_3}{\lambda_u^2} g_0\right) dg \,, \tag{2}$$

where g_0 is the nominal undulator gap. Therefore, in this approximation the undulator field error is proportional to the gap error.

Considering the vector potential $\mathbf{A_x}$ ($\nabla \times \mathbf{B} = \mathbf{A}$), the transverse velocity of an electron is:

$$\dot{x} = \frac{-e\mathbf{A_x}}{\gamma m} = -\frac{e}{\gamma m} \int \left[B_0 + \delta B(z)\right] \cos(k_u z) dz = \frac{\sqrt{2} c K(z)}{\gamma} \sin(k_u z) \,, \tag{3}$$

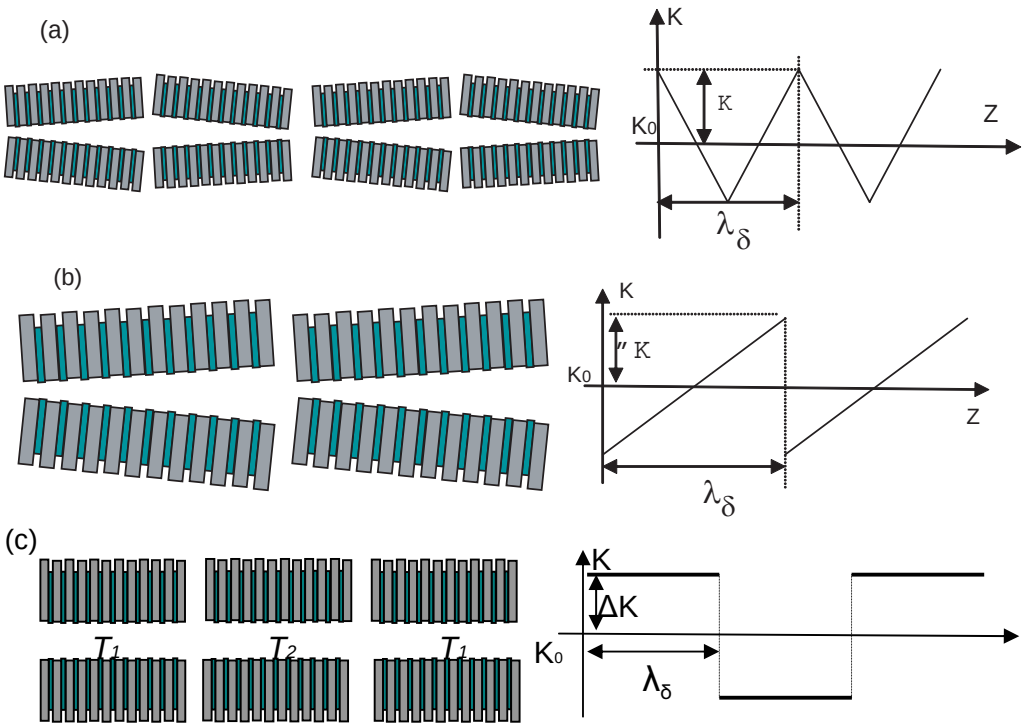

Figure 2: *Other gap variations simulated in this report have a triangle (a), sawtooth (b) or piecewise constant (c) distribution.*

with $k_u = 2\pi/\lambda_u$, $-e$ and m are the electron charge and mass, respectively, c is the speed of light and γ is the Lorentz factor.

Thus, the undulator parameter $K(z)$ is:

$$K(z)\sin(k_u z) = -\frac{e}{\sqrt{2}mc}\int [B_0 + \delta B(z)]\cos(k_u z)dz\,. \tag{4}$$

2.1 Sinus field error

The field error of a sinusoidal shape is described by $\delta B(z) = \delta B_0 \cos(k_\delta z)$, with $k_u >> k_\delta$. Therefore

$$\begin{aligned}\int \delta B(z)\cos(k_u z)dz &= \frac{1}{2}\delta B_0\left[\frac{\sin(k_u + k_\delta)z}{k_u + k_\delta} + \frac{\sin(k_u - k_\delta)z}{k_u - k_\delta}\right] \\ &= \delta B_0 \frac{k_u \sin(k_u z)\cos(k_\delta z) - k_\delta \cos(k_u z)\sin(k_\delta z)}{k_u^2 - k_\delta^2}\,.\end{aligned} \tag{5}$$

With the approximation $k_u >> k_\delta \Rightarrow k_u^2 - k_\delta^2 \approx k_u^2$, it is reasonable to neglect the term $k_\delta \cos(k_u z)\sin(k_\delta z)$ (see Fig. 3). So the integration of Eq. (5) is:

$$\int \delta B_0 \cos(k_\delta z)\cos(k_u z)dz \approx \frac{\sin(k_u z)}{k_u}\delta B_0 \cos(k_\delta z)\,. \tag{6}$$

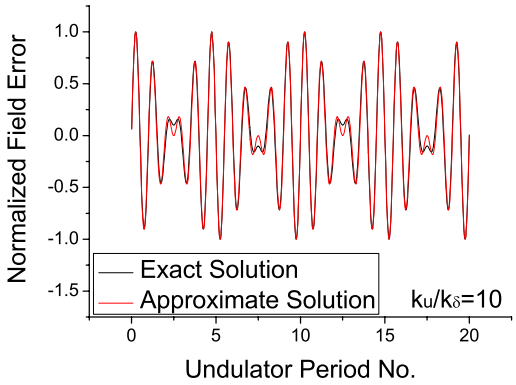

Figure 3: *Illustration of the effect of neglecting the term* $k_\delta \cos(k_u z)\sin(k_\delta z)$ *in Eq. (5). The largest impact is due to the smallest error period in our simulation,* $\lambda_\delta/\lambda_u = 10$*. One can see neglecting this term has little impact on Eq. (5).*

.

Therefore the undulator parameter $K(z)$ can be expressed as:

$$K(z) = -\frac{e\left[B_0 + \delta B_0 \cos(k_\delta z)\right]}{\sqrt{2}cmk_u} = K_0 + \Delta K \cos(k_\delta z)\,. \tag{7}$$

This equation shows that for sinus gap error, the undulator parameter K also has sinus error.

2.2 Linear field error (sawtooth and triangle).

Triangle and sawtooth field errors are linear errors $\delta B(z) = \delta B_0 k_\delta z$,

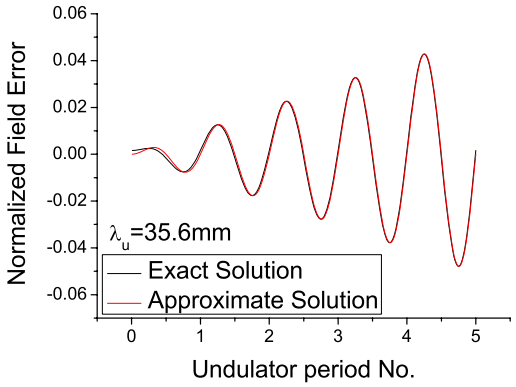

Figure 4: *Illustration of the effect of neglecting term* $\cos(k_u z)$ *in Eq. (8). One can see this approximation is reasonable.*

$$\int \delta B_0 k_\delta z \cos(k_u z)dz = k_\delta \delta B_0 \frac{k_u z \sin(k_u z) + \cos(k_u z)}{k_u^2} \approx \frac{\delta B_0 \cdot k_\delta z}{k_u}\sin(k_u z)\,, \tag{8}$$

where the approximation $k_u z \tan(k_u z) >> 1$ has been used. This is valid for all but the zero crossings of the sin-function. Fig. 4 shows the effect of neglecting the term $\cos(k_u z)$ in Eq. (8). So the undulator parameter $K(z)$ can be expressed by:

$$K(z) = K_0 + \Delta K \cdot k_\delta z \tag{9}$$

Eq. (9) means for the triangle or sawtooth gap error, the undulator parameter K also varies as triangle or sawtooth function.

3 Periodic error phase shake calculation.

Some papers have already investigated the impact of undulator field errors on the FEL performance [12, 13, 14, 15]. The error effect can be divided into beam wander and phase shake. Beam wander describes the reduced transverse overlap between electrons and radiation. Phase shake means the electron ponderomotive phase variation. Earlier studies show that large beam wander or phase shake can increase the saturation length and reduce the power. For different error distributions with similar rms beam wander and phase shake, the power at a fixed point should be similar.

In this report only non-steering errors are taken into account, so the phase shake is the only cause for power degradation.

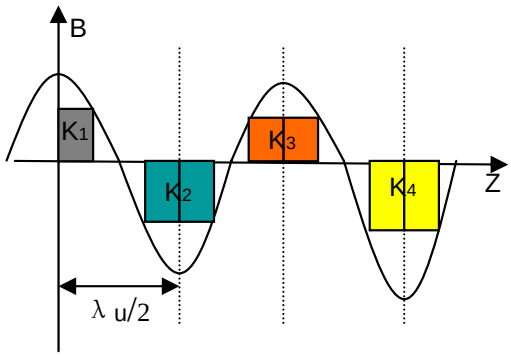

Figure 5: *Undulator parameter as used by Genesis 1.3. The K parameter is set for each half undulator period $K_1, K_2, \ldots, K_i$. The beam kick in one half undulator period corresponds to $K_i - K_{i-1}$.*

The undulator magnet field can be described as:

$$B(z) = B_i \cos(k_u z)\,, \tag{10}$$

where the subscript i denotes the magnet field for each half period. The change in transverse velocity for the i-th half undulator period is

$$\Delta\beta_{\perp i} = (-1)^{i+1} \frac{\sqrt{2}(K_i - K_{i+1})}{\gamma}\,, \tag{11}$$

where K_i on each half undulator period is defined as:

$$K_i = \frac{eB_i}{\sqrt{2}mck_u}\,. \tag{12}$$

Therefore the transverse velocity at the position of i-th half undulator period, which is an accumulation of all previous kicks, can be described as

$$\beta_{\perp i} = \frac{\sqrt{2}}{\gamma} \sum_{j=1}^{i} (-1)^{j+1} (K_j - K_{j+1}) \,. \tag{13}$$

On the other hand, the phase change is

$$\varphi' = \frac{k_u}{\beta_0} - k_s \frac{1 + p_x^2 + p_y^2 + K^2 + f_c K (u \exp(i\varphi) - c.c)}{2\beta_0 \gamma^2} \,, \tag{14}$$

where u denotes to the optical field. When we calculate the phase shake, this term normally can be neglected.

Because of the assumption that the beam remains on axis, the transverse velocity is very small. Therefore the term of p_x^2, p_y^2 can be neglected in Eq. (14). Comparing the term of K^2, the term of $f_c K(u \exp(i\varphi) - c.c)$ is also small and can be neglected too. The average electron velocity $\beta_0 \approx 1$. Thus the phase change can be expressed as:

$$\varphi' = k_u - k_s \frac{1 + K^2}{2\gamma^2} \,. \tag{15}$$

The undulator parameter K can be written as $K(z) = K_0 + \Delta K \cdot f(z)$, where K_0 is the nominal value, $\Delta K \cdot f(z)$ denotes the undulator error, ΔK expresses the error strength and $|f(z)| \leq 1$ expresses the error shape.

Therefore the phase at a position z is the integral of Eq. (15) :

$$\varphi(z) = \left(k_u - \frac{k_s (1 + K_0^2)}{2\gamma^2} \right) z - \Delta\varphi(z) \,. \tag{16}$$

The phase shake $\Delta\varphi$ generated by the undulator error is

$$\Delta\varphi(z) = \frac{k_u}{1 + K_0^2} \int_0^z \left((K_0 + \Delta K \cdot f(z'))^2 - K_0^2 \right) dz' \,. \tag{17}$$

Normally the field error is much smaller than the field itself, $\Delta K << K_0$, so the phase shake is:

$$\Delta\varphi(z) \approx \frac{k_u}{1 + K_0^2} \int_0^z 2K_0 \Delta K \cdot f(z') dz' \,. \tag{18}$$

If $f(z)$ is a periodic function, $f(z) = f(z + \lambda_\delta)$, we can use $x = z/\lambda_\delta,\ 0 < x \leq 1$ to normalize z. Thus

$$\Delta\varphi(x) = \frac{k_u}{1 + K_0^2} 2K_0 \cdot \Delta K \cdot \lambda_\delta \int_0^x f(x') dx' = \frac{k_u}{1 + K_0^2} 2K_0 \cdot \Delta K \cdot \lambda_\delta \cdot g(x) \,. \tag{19}$$

According to earlier work, the radiation power degradation is correlated to the rms value of phase shake $\Delta\varphi$.

$$\sigma_{\Delta\varphi} = \sqrt{\frac{1}{L} \int_0^L \left(\Delta\varphi(z') - \langle \Delta\varphi \rangle \right)^2 dz'} \,, \tag{20}$$

where L is the entire undulator length. For a periodic function, the $L = n\lambda_\delta$ can take the period length, $L = \lambda_\delta$, i.e. an integral over L or λ_δ gives the same result. On the other hand, the optimized wavelength of SASE-FEL always guarantee that $\langle \Delta\varphi \rangle = 0$ so the rms phase shake is:

$$\sigma_{\Delta\varphi} = \frac{k_u}{1+K_0^2} 2K_0 \cdot \Delta K \cdot \lambda_\delta \sqrt{\int_0^1 g^2(x)dx} = \alpha \frac{\Delta K}{K_0} \lambda_\delta \,. \tag{21}$$

Note that the rms phase shake is not only proportional to the error strength $\Delta K/K$ but also to the error period length λ_δ. To illustrate this analysis more carefully, Fig. 6 shows some simulation with sinus undulator field error. One can see that ΔK of the black sinus error is five times larger than the red error, while the error period λ_δ of the black error is ten time shorter than the red error. From Eq. (21) the red error has larger rms phase shake. Therefore the power growth with the black error undulator is better than the red one. The blue dot line is the power growth with ideal undulator field.

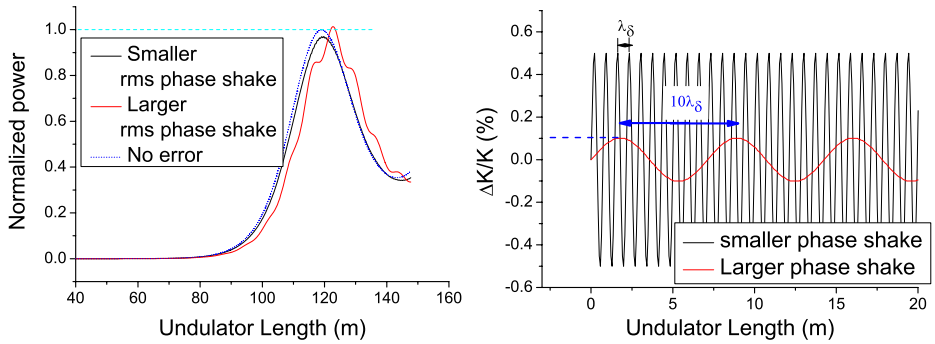

Figure 6: *Impact of two different sinus errors on power degradation. The ΔK of the black sinus error is five times larger than the red error, but the error period λ_δ of the black error is ten time shorter. From Eq. (21) the red error has a larger rms phase shake. Therefore the power growth with the black error undulator is better than the red one, as confirmed by the simulation.*

3.1 Phase shake expression for sinus error.

3.1.1 Periodic sinus error.

If the error field follows a sinus function, then:

$$K(z) = K_0 + \Delta K \sin(k_\delta z) \,. \tag{22}$$

So the phase change can be described by

$$\varphi' = \frac{k_u}{\beta_0} - k_s \frac{1 + (K_0 + \Delta K \sin(k_\delta z))^2}{2\beta_0 \gamma^2} \,. \tag{23}$$

The FEL resonant wavelength satisfies

$$\frac{k_u}{\beta_0} - k_s \frac{1+K_0^2}{2\beta_0\gamma^2} = 0 \,. \tag{24}$$

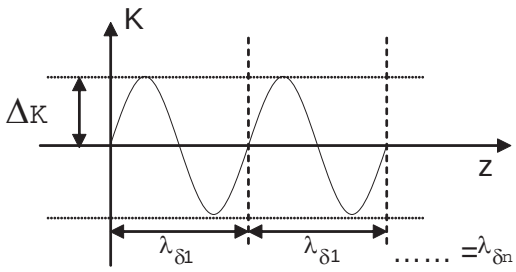

Figure 7: *Illustration for the constant sinus error. Error period and strength are defined as shown in this plot.*

Normally $\Delta K << K_0$, so the phase error is

$$\Delta\varphi(z) = -\frac{k_s K_0}{\beta_0 \gamma^2} \int_0^z \Delta K \sin(k_\delta z')dz' = -\frac{k_s K_0}{\beta_0 \gamma^2 k_\delta} \Delta K (1 - \cos(k_\delta z)) \,. \tag{25}$$

For the phase shake, the constant term can be neglected. therefore, the rms phase shake is:

$$\sigma_{\Delta\varphi} = \frac{k_s}{\beta_0 \gamma^2} \frac{K_0 \Delta K}{k_\delta} \sqrt{\frac{1}{n\lambda_\delta} \int_0^{n\lambda_\delta} \cos^2(k_\delta z)dz} = \frac{k_s}{\beta_0 \gamma^2} \frac{K_0 \Delta K}{\sqrt{2} k_\delta} = \frac{\sqrt{2} K_0^2}{\lambda_u (1 + K_0^2)} \frac{\Delta K}{K_0} \lambda_\delta \,. \tag{26}$$

Eq. (26) illustrates that the phase shake is proportional to the error strength and error period. Because the FEL power growth along the undulator is related to the phase as well, the power at a fixed longitudinal position within the undulator should show a similar correlation with the error strength and period.

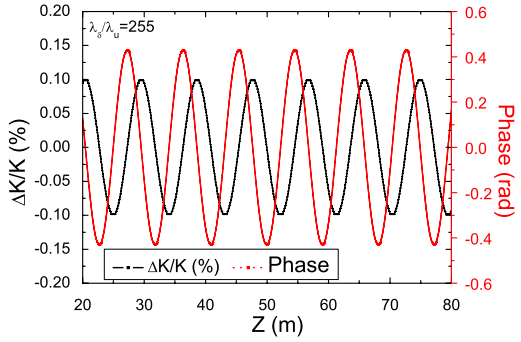

Figure 8: *Undulator parameter K and the corresponding phase as given by Eq. (25) for a periodic sinusoidal error.*

Fig. 8 gives K and the phase distribution along the undulator according to Eq. (25). The parameters for calculation are taken from SASE1 at 0.1nm.

3.1.2 Random sinus error.

So far the analysis only takes into account a periodic sinus function. In reality the undulators are separated into many segments. Also the sinus error does not neccesarily

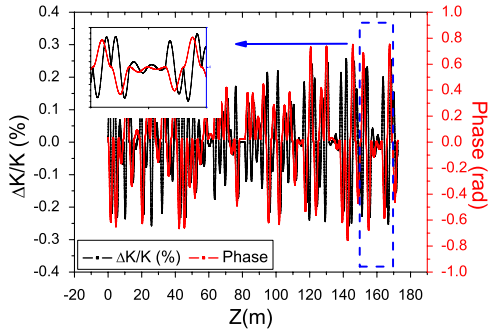

Figure 9: *Undulator parameter K and the corresponding phase as given by Eq. (29) for a sinusoidal error with random amplitude but constant period λ_δ.*

have a constant amplitude. Therefore, the effect of a sinus with random amplitude on the phase shake is studied. Fig. 9 illustrates the random undulator parameter and the phase along the undulator. One can see that the period is fixed but the sinus error has randomly different amplitude K_i for each period.

One question is how to compare the random to periodic error distributions. As mentioned above, the phase shake is the key reason for the power degradation, so naturally we compare the random to the periodic error having the same phase shake.

For a random field error, the undulator parameter can be represented as:

$$K_i(z') = K_0 + \Delta K_i \sin(k_\delta z')\,. \tag{27}$$

The subscript i means the ith error period. The corresponding phase error can be expressed as

$$\Delta\varphi_i(z) = -\frac{k_s K_0}{\beta_0\gamma^2 k_\delta}\Delta K_i(1-\cos(k_\delta z)), \qquad (i-1)\lambda_\delta < z < i\lambda_\delta\,. \tag{28}$$

From Eq. (28), it is easy to see that when $z = n\lambda_\delta$, the phase $\varphi = 0$. So the phase error in ith error period φ_i can be expressed as:

$$\begin{aligned}\Delta\varphi_i(z) = -\frac{k_s}{\beta_0\gamma^2}\int_0^{z-(i-1)\lambda_\delta} K_0\Delta K_i\sin(k_\delta z')[1-\cos(2k_u z')]dz' \\ \approx -\frac{k_s}{\beta_0\gamma^2}\frac{K_0\Delta K_i[1-\cos(k_\delta z)]}{k_\delta}\,.\end{aligned} \tag{29}$$

From Eq. (28), in each error period, the average phase error is

$$\Delta\bar{\varphi}_i = -\frac{k_s}{\beta_0\gamma^2}\frac{K_0\Delta K_i}{k_\delta}\,. \tag{30}$$

With ΔK_i homogeneously distributed in the range $[-\kappa, +\kappa]$, the average phase along the undulator should be zero.

So the phase shake is given by

$$\Delta\sigma_\varphi = \frac{k_s}{\beta_0\gamma^2}\frac{K_0}{k_\delta}\sqrt{\frac{1}{n\lambda_\delta}\int_0^{n\lambda_\delta}\Delta K_i^2[1-\cos(k_\delta z')^2 dz'}$$
$$= \frac{k_s}{\beta_0\gamma^2}\frac{K_0}{k_\delta}\sqrt{\frac{3}{2n}\sum_{i=1}^{n}\Delta K_i^2} \tag{31}$$

Because ΔK_i is homogeneously distributes in the range $[-\kappa, +\kappa]$,

$$\frac{1}{n}\sum_{i=1}^{n}\Delta K_i^2 = \frac{1}{2\kappa}\int_{-\kappa}^{\kappa}x^2 dx = \frac{\kappa^2}{3} \tag{32}$$

Therefore, the rms phase shake expressed by Eq. (31) is

$$\sigma_{\Delta\varphi} = \frac{k_s}{\beta_0\gamma^2}\frac{K_0}{k_\delta}\sqrt{\frac{3}{2n}\sum_{i=1}^{n}\Delta K_i^2} = \frac{k_s}{\beta_0\gamma^2}\frac{K_0\kappa}{\sqrt{2}k_\delta} = \frac{2k_u}{1+K_0^2}\frac{K_0\kappa}{\sqrt{2}k_\delta}\,. \tag{33}$$

Comparing Eq. (33) to Eq. (26), to guarantee that the phase shake of random and periodic cases are the same, $\kappa = \Delta K$.

On the other hand, we also want to set κ to a value that the RMS error of periodic and random cases can be the same. This corresponds to:

$$\sqrt{\frac{1}{n\lambda_\delta}\int_0^{n\lambda_\delta}\Delta K_i^2\cos^2(k_\delta z')dz'} = \sqrt{\frac{1}{n\lambda_\delta}\int_0^{n\lambda_\delta}\Delta K^2\cos^2(k_\delta z')dz'}$$
$$\Rightarrow \frac{1}{n}\sum_{i=1}^{n}\Delta K_i^2 = \Delta K^2 \Rightarrow \frac{1}{2\kappa}\int_{-\kappa}^{\kappa}x^2dx = \frac{\kappa^2}{3} = \Delta K^2 \Rightarrow \kappa = \sqrt{3}\Delta K \tag{34}$$

From $\kappa = \Delta K$ and Eq. (34), one can see that if the RMS error value is same, then the phase shake of the random error is larger, and the power correspondingly smaller.

3.2 phase shake expression for triangle error.

3.2.1 Periodic triangle error.

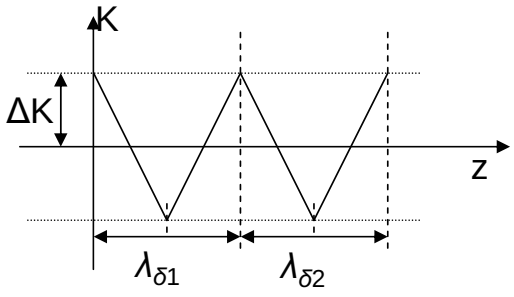

Figure 10: *Illustration for the periodic triangle error. Error period and error strength are defined as it is shown in this plot.*

From Fig. 2, in case of a triangle error shape, for each undulator segment the parameter K changes linearly. Similar to the sinus error shape, first we analyse the phase shake of this kind of error. In each error period, the K value can be described as:

$$K(z) = \begin{cases} \frac{-4\Delta K}{\lambda_\delta}(z - n\lambda_\delta) + \Delta K + K_0, & n\lambda_\delta \le z < (n+1/2)\lambda_\delta \\ \frac{4\Delta K}{\lambda_\delta}(z - n\lambda_\delta) - 3\Delta K + K_0, & (n+1/2)\lambda_\delta \le z < (n+1)\lambda_\delta \end{cases} \tag{35}$$

So the phase error variation is:

$$\Delta\varphi' = \begin{cases} -\frac{k_s}{\beta_0\gamma^2}K_0\Delta K\left[1 - \frac{4}{\lambda_\delta}(z - n\lambda_\delta)\right], & n\lambda_\delta \le z < (n+1/2)\lambda_\delta \\ -\frac{k_s}{\beta_0\gamma^2}K_0\Delta K\left[-3 + \frac{4}{\lambda_\delta}(z - n\lambda_\delta)\right], & (n+1/2)\lambda_\delta \le z < (n+1)\lambda_\delta \end{cases} \tag{36}$$

It can be easily proven that the phase change after each error period is zero. Therefore, the phase error is

$$\Delta\varphi = \begin{cases} -\frac{k_s}{\beta_0\gamma^2}K_0\Delta K\left[z - \frac{2}{\lambda_\delta}z^2\right], & 0 \le z < 1/2\lambda_\delta \\ -\frac{k_s}{\beta_0\gamma^2}K_0\Delta K\left[-3z + \frac{2}{\lambda_\delta}z^2 + \lambda_\delta\right], & 1/2\lambda_\delta \le z < \lambda_\delta \end{cases} \tag{37}$$

Fig. 11 shows K and the corresponding phase.

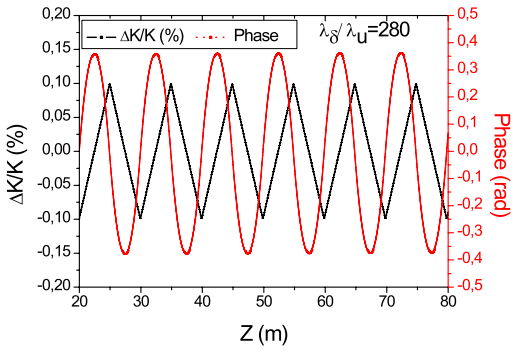

Figure 11: *Undulator parameter K and the phase for a periodic triangle error field.*

The average phase error is zero.

$$\Delta\bar{\varphi} = \frac{1}{\lambda_\delta}\int_0^{\lambda_\delta}\Delta\varphi(z')dz'$$

$$= -\frac{k_s}{\beta_0\gamma^2}K_0\Delta K\left(\int_0^{\lambda_\delta/2} z' - \frac{2}{\lambda_\delta}z'^2dz' + \int_{\lambda_\delta/2}^{\lambda_\delta} -3z' + \frac{2}{\lambda_\delta}z'^2 + \lambda_\delta dz'\right) = 0 \tag{38}$$

Thus the phase shake is

$$\sigma_{\Delta\varphi} = \frac{k_s}{\beta_0\gamma^2}\sqrt{\frac{1}{\lambda_\delta}\int_0^{\lambda_\delta}\varphi^2(z')dz'}$$

$$= \frac{k_s}{\beta_0\gamma^2}K_0\Delta K\sqrt{\frac{1}{\lambda_\delta}\int_0^{\lambda_\delta/2}\left(z' - \frac{2}{\lambda_\delta}z'^2\right)^2dz' + \frac{1}{\lambda_\delta}\int_{\lambda_\delta/2}^{\lambda_\delta}\left(-3z' + \frac{2}{\lambda_\delta}z'^2 + \lambda_\delta\right)^2dz'}$$

$$= \frac{k_s}{\beta_0\gamma^2}\sqrt{\frac{1}{120}}K_0\Delta K\lambda_\delta = \frac{4\pi K_0^2}{\lambda_u(1+K_0^2)}\frac{1}{\sqrt{120}}\frac{\Delta K}{K_0}\lambda_\delta \quad (39)$$

From Eq. (39), it can be seen that as with the sinus error shape, for the triangle error the phase shake is proportional to the error strength and the period.

3.2.2 Random triangle error

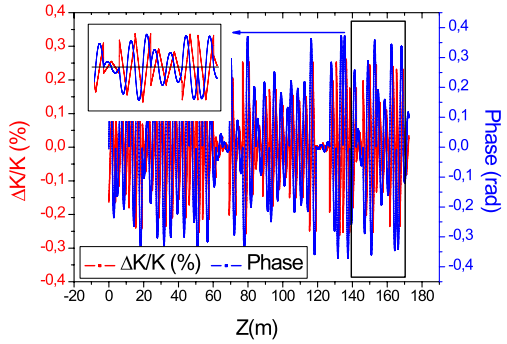

Figure 12: *Undulator parameter K and the phase for a random triangle error field.*

Then we take into account the phase shake induced by the random error. Inside *ith* error period, the phase error change is

$$\Delta\varphi' = \begin{bmatrix} -\frac{k_s}{\beta_0\gamma^2}K_0\Delta K_i\left[1-\frac{4}{\lambda_\delta}(z-i\lambda_\delta)\right], & i\lambda_\delta \le z < (i+1/2)\lambda_\delta \\ -\frac{k_s}{\beta_0\gamma^2}K_0\Delta K_i\left[-3+\frac{4}{\lambda_\delta}(z-i\lambda_\delta)\right], & (i+1/2)\lambda_\delta \le z < (i+1)\lambda_\delta \end{bmatrix} \quad (40)$$

The integration of Eq. (40) over one error period is zero, so the phase doesn't change after one complete error period. Therefore it can be described as

$$\Delta\varphi_i(z) = \begin{bmatrix} -\frac{k_s}{\beta_0\gamma^2}K_0\Delta K_i\left[z-\frac{2}{\lambda_\delta}z^2\right], & 0 \le z < 1/2\lambda_\delta \\ -\frac{k_s}{\beta_0\gamma^2}K_0\Delta K_i\left[-3z+\frac{2}{\lambda_\delta}z^2+\lambda_\delta\right], & 1/2\lambda_\delta \le z < \lambda_\delta \end{bmatrix} \quad (41)$$

It can be easily proven that the average phase error is zero, resulting in

$$\sigma_{\Delta\varphi} = \frac{k_s}{\beta_0\gamma^2}\frac{1}{\sqrt{120}}\sqrt{\frac{1}{n\lambda_\delta}\sum_{i=1}^{n}\int_0^{\lambda_\delta}\varphi_i^2(z)dz} = \frac{k_s}{\beta_0\gamma^2}K_0\lambda_\delta\frac{1}{\sqrt{120}}\sqrt{\frac{1}{n}\sum_{i=1}^{n}K_i^2} \quad (42)$$

It is assumed that ΔK_i is homogeneously distributed in the range $[-\kappa, +\kappa]$,

$$\frac{1}{n}\sum_{i=1}^{n}\Delta K_i^2 = \frac{1}{2\kappa}\int_{-\kappa}^{\kappa}x^2dx = \frac{\kappa^2}{3}.$$

Therefore, the RMS phase shake is

$$\sigma_{\Delta\varphi} = \frac{k_s}{\beta_0\gamma^2}\frac{1}{\sqrt{120}}\frac{\kappa}{\sqrt{3}}K_0\lambda_\delta = \frac{2k_u}{1+K_0^2}\frac{1}{\sqrt{120}}\frac{\kappa}{\sqrt{3}}K_0\lambda_\delta\,. \quad (43)$$

Comparing Eq. (43) to Eq. (39), the phase shake of constant and random error are the same. This is different for the sinus case as shown before. Therefore, when the RMS error is the same, so is the phase shake.

3.3 phase shake expression for sawtooth error

3.3.1 Periodic sawtooth error

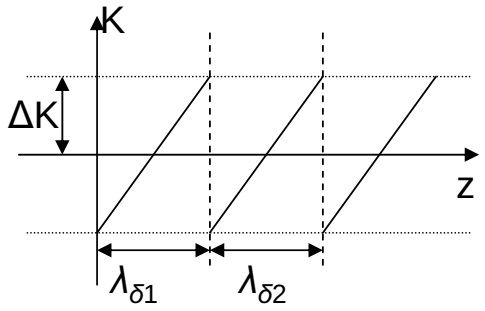

Figure 13: *Illustration for the periodic sawtooth error. Error period and strength are defined as shown in this plot.*

The error field shown in Fig. 13 can be described as

$$K(z) = K_0 + \frac{2\Delta K}{\lambda_\delta}(z - n\lambda_\delta) - \Delta K, \quad n\lambda_\delta < z < (n+1)\lambda_\delta\,. \tag{44}$$

The corresponding change in phase error is

$$\Delta\varphi'(z) = -\frac{k_s}{\beta_0\gamma^2}K_0\Delta K\left(\frac{2}{\lambda_\delta}(z - n\lambda_\delta) - 1\right), \quad n\lambda_\delta < z < (n+1)\lambda_\delta\,. \tag{45}$$

So after one error period the phase error changes zero

$$\int_0^{\lambda_\delta}\varphi'(z)dz = -\frac{k_s}{\beta_0\gamma^2}K_0\Delta K\int_0^{\lambda_\delta}\left(\frac{2}{\lambda_\delta}z - 1\right)dz = 0\,. \tag{46}$$

Thus, the phase error is

$$\Delta\varphi(z) = -\frac{k_s}{\beta_0\gamma^2}K_0\Delta K\left(\frac{(z - n\lambda_\delta)^2}{\lambda_\delta} - (z - n\lambda_\delta)\right), \quad n\lambda_\delta < z < (n+1)\lambda_\delta\,. \tag{47}$$

The average phase error is:

$$\Delta\bar{\varphi} = \frac{1}{\lambda_\delta}\int_0^{\lambda_\delta}\varphi(z)dz = \frac{k_s}{\beta_0\gamma^2}\frac{K_0\Delta K\lambda_\delta}{6} \tag{48}$$

Finally, the RMS phase shake is

$$\begin{aligned}\sigma_{\Delta\varphi} = \frac{k_s}{\beta_0\gamma^2}K_0\Delta K\sqrt{\frac{1}{\lambda_\delta}\int_0^{\lambda_\delta}\left(\frac{z^2}{\lambda_\delta} - z + \frac{\lambda_\delta}{6}\right)^2 dz} &= \frac{k_s}{\beta_0\gamma^2}\sqrt{\frac{1}{180}}K_0\Delta K\lambda_\delta \\ &= \frac{4\pi K_0^2}{\lambda_u(1+K_0^2)}\frac{1}{\sqrt{180}}\frac{\Delta K}{K_0}\lambda_\delta\,.\end{aligned} \tag{49}$$

As before, the phase shake is proportional to the error strength and error period. Fig. 14 shows K and the phase along the undulator.

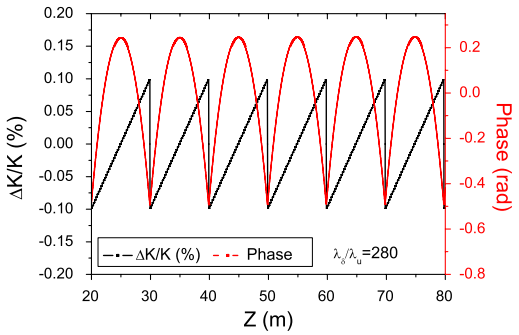

Figure 14: *Undulator parameter K and the phase for a periodic sawtooth error field.*

3.3.2 Random sawtooth error

Then we analyse the random case. The phase error in *ith* error period is:

$$\Delta\varphi_i(z) = -\frac{k_s}{\beta_0\gamma^2}K_0\Delta K_i\left(\frac{(z-i\lambda_\delta)^2}{\lambda_\delta} - (z-i\lambda_\delta)\right), \quad i\lambda_\delta \le z < (i+1)\lambda_\delta\,. \tag{50}$$

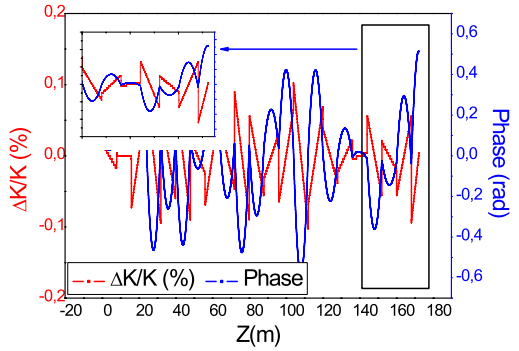

Figure 15: *Undulator parameter K and the phase for a random sawtooth error field.*

Fig. 15 plots the random error and the phase along the undulator for SASE1 parameters. We assume that ΔK_i homogeneously distributes in the range $[-\kappa, \kappa]$, so the average of the phase error is zero. The phase shake is

$$\sigma_{\Delta\varphi} = \frac{k_s}{\beta_0\gamma^2}K_0\sqrt{\frac{1}{n\lambda_\delta}\sum_{i=1}^{n}\Delta K_i^2\int_0^{\lambda_\delta}\left(\frac{z^2}{\lambda_\delta}-z\right)^2 dz} = \frac{k_s}{\beta_0\gamma^2}\frac{K_0\lambda_\delta}{\sqrt{30}}\sqrt{\frac{1}{n}\sum_{i=1}^{n}\Delta K_i^2}\,. \tag{51}$$

With ΔK_i homogeneously distributed in the range $[-\kappa, \kappa]$, the phase shake is

$$\sigma_{\Delta\varphi} = \frac{k_s}{\beta_0\gamma^2}\frac{\kappa K_0\lambda_\delta}{\sqrt{3}}\frac{1}{\sqrt{30}} = \frac{2k_u}{1+K_0^2}\frac{\kappa K_0\lambda_\delta}{\sqrt{3}}\frac{1}{\sqrt{30}} \tag{52}$$

Comparing Eq. (49) to Eq. (52), in order for the phase shake to be the same $\kappa = \Delta K/\sqrt{2}$.

3.4 phase shake expression for a piecewise constant error

3.4.1 Periodic constant error

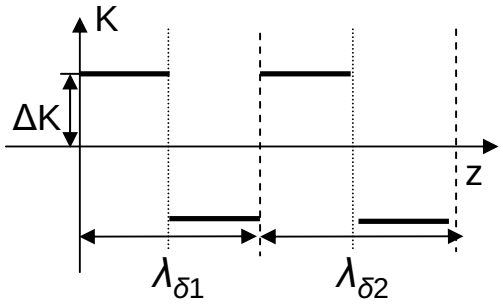

Figure 16: *Illustration for the periodic, piecewise constant error.*

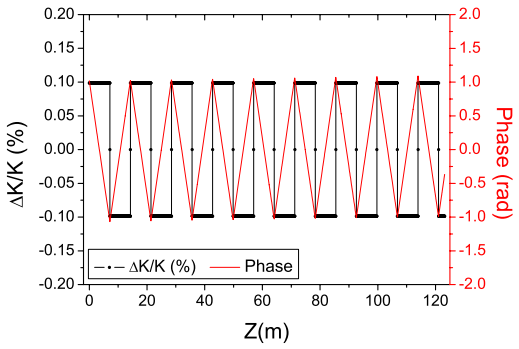

Figure 17: *The value distribution of undulator parameter K and phase $\varphi(z)$ along the undulator. The error amplitude is constant for different error period.*

For the constant error illustrated in Fig. 16, the change in electron phase error is:

$$\Delta\varphi'(z) = \pm\frac{k_s K_0}{\beta_0\gamma^2}\Delta K \tag{53}$$

For the periodic constant error shown in Fig. 17, the phase error is

$$\Delta\varphi(z)\begin{cases} -\frac{k_s}{\beta_0\gamma^2}\Delta K(z - n\lambda_\delta/2), & n\lambda_\delta/2 \le z < (n+1)\lambda_\delta/2 \\ -\frac{k_s}{\beta_0\gamma^2}\Delta K[(n+2)\lambda_\delta/2 - z], & (n+1)\lambda_\delta/2 \le (n+2)\lambda_\delta/2 \end{cases} \quad n = 0, 2, 4, ... \tag{54}$$

The average phase error is

$$\Delta\bar{\varphi} = -\frac{k_s}{\beta_0\gamma^2}\frac{1}{2}\Delta K\frac{\lambda_\delta}{2}\,. \tag{55}$$

Therefore, the phase shake is

$$\sigma_{\Delta\varphi} = \frac{k_s}{\beta_0\gamma^2}\sqrt{\frac{1}{\lambda_\delta/2}\int_0^{\lambda_\delta/2}(\Delta K z - \frac{1}{2}\Delta K\lambda_\delta/2)^2 dz} = \frac{k_s}{\beta_0\gamma^2}\frac{1}{\sqrt{12}}\Delta K\frac{\lambda_\delta}{2}$$

$$= \frac{4\pi K_0^2}{\lambda_u(1+K_0^2)} \frac{1}{2\sqrt{12}} \frac{\Delta K}{K_0} \lambda_\delta \,. \tag{56}$$

3.4.2 Random constant error

Unlike for the other error types mentioned before, the electron phase in each error period depends on the phase in the former error periods. So for the randomly distributed constant error, even when the mean and RMS values of K are same, the phase shake still may be significantly different.

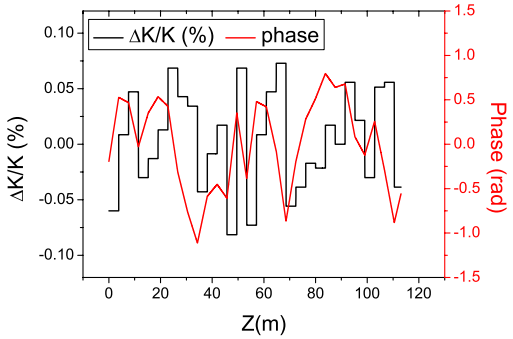

Figure 18: *The distribution of undulator parameter K and phase $\varphi(z)$ along the undulator. The error amplitude is random for different error periods.*

3.5 Compare sawtooth and triangle error

The error of triangle and sawtooth both have a linear gap dependence. However, even for the same error strength and period, their phase shake is not equal. For Eqs. (39) and (49), the ration between their phase shake is $\sqrt{\frac{180}{120}} \times 2 = 2.45$, which matches the calculation and later simulations well.

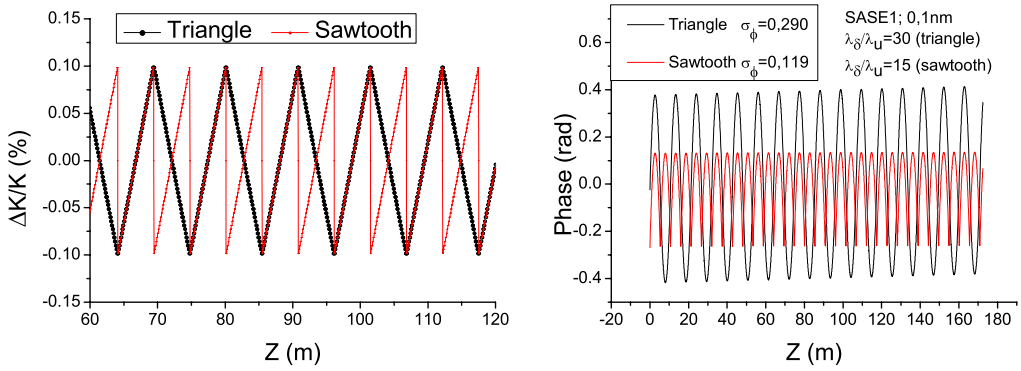

Figure 19: *Comparison of phase and phase shake for triangle and sawtooth errors. The error strength and period are the same. It is can be seen that the triangle has larger phase shake.*

4 Numerical evaluation of the tolerance simulations.

Before performing the simulations, a number of issues have to be addressed. Since the main interest of this report is the influence of phase shake on the FEL performance, the electron beam has to remain on axis in order to avoid gain degradation due to reduced overlap between electron beam and photons. This this briefly addressed in Sec. 4.1.

Another important point is the validity of the results. Because it is practically impossible to study the effect of errors with time dependent simulations, all results in this report have been obtained using steady state simulations. This means that one has to give an initial power (the shot noise power) and wavelength. The effect of choice of wavelength is discussed in in Sec. 4.2.

Finally, the results have to be presented in a transparent way. Several methods of representation have been used so far. The choice for this report and the reason for the choice is addressed in Sec. 4.3.

4.1 Treatment to keep the beam on axis.

For the sawtooth and constant error as well as the random triangle error, the field is discontinuous between two error periods. This kicks the beam and after accumulation of these kicks, deviation of the beam center from the main axis will grow.

To compensate this kick, a point is added between two error periods on which the undulator parameter K is the average value of the two. By this treatment the beam can be kept on axis. Fig. 20 shows the result using a sawtooth error field as example. Since usually the beam orbit can always be corrected at the beginning and end of each undulator segment, this addition does not limit the validity of the results presented here.

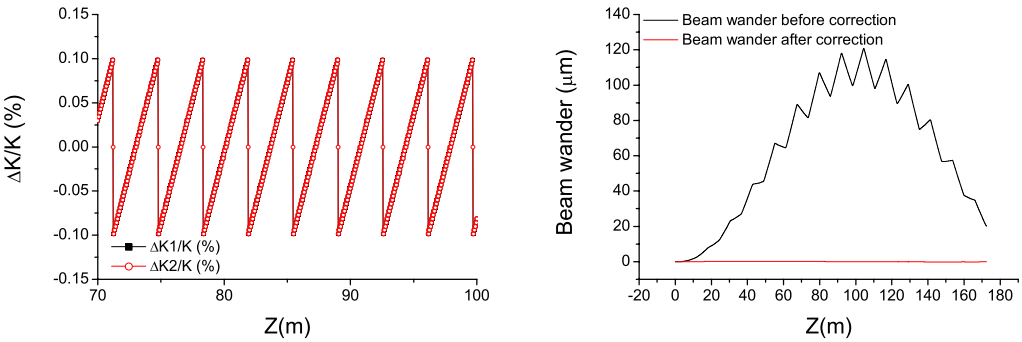

Figure 20: *Comparison of the beam wander before and after correction of K after each error period for a periodic sawtooth error distribution. The left plot compares the error field before and after treatment. One can see the field is the same except for one point at the joint position of two error periods. The right plot shows the orbit before and after correction.*

4.2 Discussion of the error impact on the optimized wavelength.

Because all of the simulations in this report are steady-state, first we argue the field error's impact to the optimized wavelength. The wavelength shift by field error is

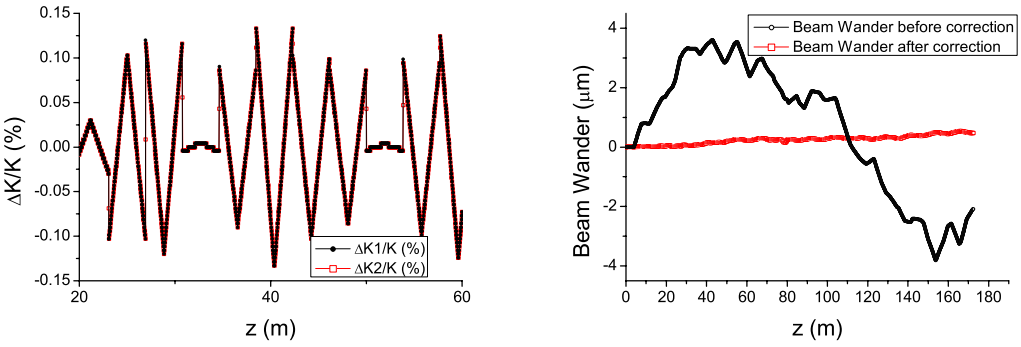

Figure 21: *Same correction as in Fig. 20, but this time for a random triangle error distribution. The left plot again compares the error field before and after treatment. One can see the field is the same except for one point at the joint position of two error periods. The right plot shows the orbit before and after correction.*

$$\Delta\lambda_s = \frac{\lambda_u}{2\gamma^2}\left[\frac{(K_0+\Delta K(z))^2 - K_0^2}{2}\right] \approx \frac{\lambda_u}{2\gamma^2}\left[\frac{2K_0\langle\Delta K\rangle + \langle\Delta K^2\rangle}{2}\right] = \frac{\lambda_u}{8\gamma^2}\Delta K^2\,, \quad (57)$$

where the average of the error $\langle\Delta K\rangle = 0$ is satisfied for all error types irrespective of whether periodic or random error are simulated and $\langle\Delta K^2\rangle = \Delta K^2/2$ for sinus and $\langle\Delta K^2\rangle = \Delta K^2/3$ for triangle and sawtooth.

We choose the larger $\langle\Delta K^2\rangle = \Delta K^2/2$ to evaluate the wavelength deviation. So

$$\frac{\Delta\lambda_s}{\lambda_{s0}} = \frac{\Delta K^2}{4(1+K_0^2/2)} < \frac{\Delta K^2}{2K_0^2}\,. \quad (58)$$

For SASE1 $K = 3.3$. When $\Delta K/K_0 = 0.5\%$, which is normally a large field error, according to Eq. (58) the wavelength shift is much smaller than the Pierce parameter. Therefore, the impact to the optimized wavelength can be neglected. We do some simulation to test the analysis above. In our case the optimized wavelength without any error is $\lambda_{s0} = 9.7852\times10^{-11}m$, so the cases of wavelength shift $\Delta\lambda_s/\lambda_{s0} = \pm10^{-5}$ and 0 are calculated. The error strength is $\Delta K/K_0 = 0.5\%$ and the error period is $\lambda_\delta = 90\lambda_u$. Fig. 22 shows the result. As can be seen, the influence by the wavelength shift can be neglected. Consequently in the simulations that follow, the optimized wavelength has not been varied.

4.3 Choice of criterium for evaluation of error impact.

It is important to find a suitable criterium to determine the influence of the error. Natural candidates are the saturation length and saturation power. But in many cases, if undulator error is induced, in the saturation region the power oscillates. Therefore the saturation point is difficult to determine. However, we still try to find the saturation point and then obtain Fig. 23. From this one can see that for a certain error strength, the saturation length and saturation power oscillate with the error period. Therefore, saturation power or saturation length can hardly be used as the number of merit.

Then we choose the radiation power at a fixed point as the criterium. To take into account the magnetic field error for the whole undulator length, the fixed point should

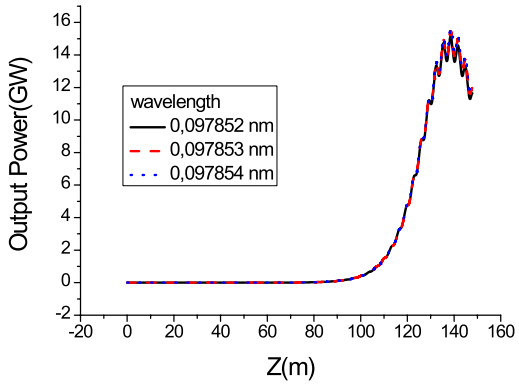

Figure 22: *Power growth for different wavelengths. This plot illustrates that small undulator field error has no apparent impact to the optimized wavelength.*

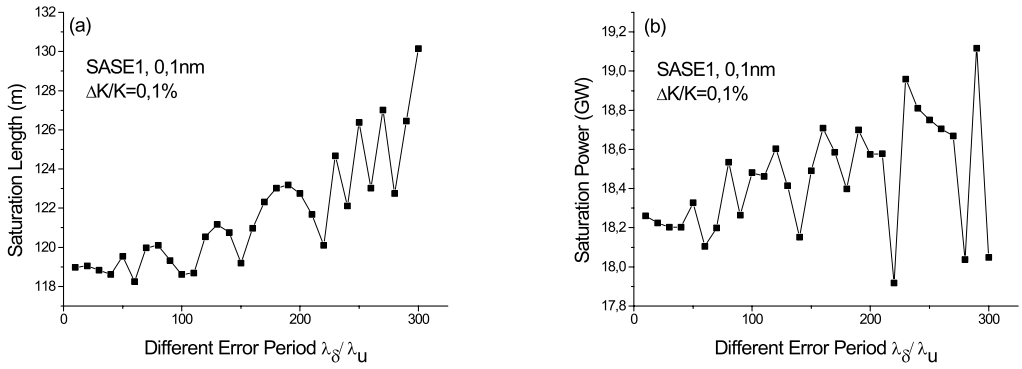

Figure 23: *The saturation length (a) and power (b) with different error period (sinus error has been used). This plot shows that the changing tendency of saturation length and saturation power with different error period is not clear. Therefore, they are not suitable criteria to evaluate the error impact.*

be close to saturation. But saturation is not a good choice because it is already beyond the exponential gain regime. Therefore we take the 95% of the saturation length instead.

Fig. 24 illustrates the power versus error period. Apparently the oscillation is greatly reduced compared to the choice of saturation length or saturation power. If the error period λ_δ is large, some oscillations still exist. We investigate the (inverse) gain length, which is shown in Fig. 25. One can see it oscillates as well. We know that the oscillation period equals the error period λ_δ, thus if it is large, an apparent impact to the radiation can be shown. A detailed analysis will be given in appendix B.

5 Influence of Field errors on the SASE1 performance

In this section we introduce the method of our error tolerance calculation and the results for SASE1.

SASE1 uses 17.5 GeV electrons to generate 0.1 nm. The undulator's gap of SASE1 is fixed, but the wavelength can still be changed by adjusting the electron energy. Therefore

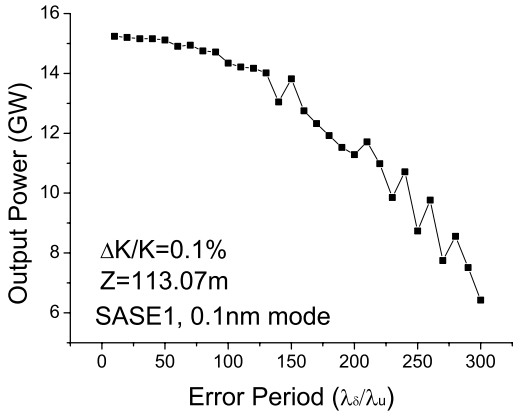

Figure 24: *The power at a fixed point. This plot shows that the changing of power at a fixed point with different error period is much more clear than the saturation power and saturation length.*

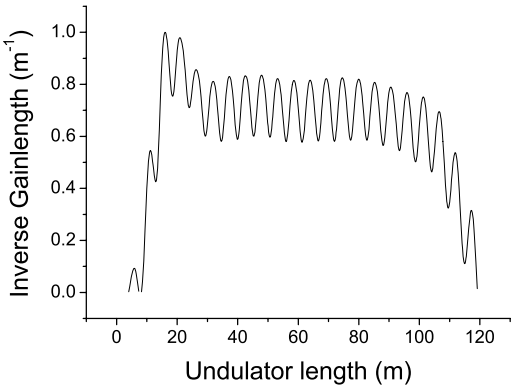

Figure 25: *Power increment with undulator deformation. The power increment along the undulator oscillates due to the field error. This is not suitable to evaluate the error impact.*

0.4 nm radiation with 8.75 GeV electrons has also been simulated.

From the design, the SASE1 undulator segment length is about 5 meters. For these simulations however, we do not include the intersections but simulate one long undulator instead. The main parameters for SASE1 are listed in Table 1:

5.1 Simulation Method

As mentioned in Sec. 2, the impact of four error types (sinus, sawtooth, triangle, constant) is simulated. The radiation power at a fixed point (95% of the saturation length for an ideal undulator) is chosen to evaluate the effect. For each error type, the simulation is divided into two steps: first the periodic error is simulated and then the random error. The periodic and random errors for different types are shown in Fig. 26. From the analysis in Sec. 3 we expect that the the rms phase shake can be changed either by adjusting the error strength $\Delta K/K$ or the error period λ_δ. Because the rms phase

Table 1: *SASE1 Parameters*

Wavelength	Electron energy	Energy spread	Undulator period	K parameter
0.1 nm	17.5 GeV	1.5 MeV	35.6 mm	3.3
0.4 nm	8.75 GeV	1.5 MeV	35.6 mm	3.3

shake correlates to the power degradation, each combination of $\Delta K/K$ and λ_δ corresponds to a certain power degradation. The aim is to find the relation between the power degradation and these two parameters. To achieve this, we choose 9 different error strengths: $\Delta K/K = 0.1\%, 0.15\%, \ldots, 0.5\%$ and for each $\Delta K/K$, 30 different error periods $\lambda_\delta/\lambda_u = 10, 20, \ldots, 300$ are chosen. Thus the power growth with in total 270 combinations of $\Delta K/K$ and λ_δ is calculated.

As shown in Fig. 24, some oscillation still exists. Therefore, to achieve a smooth dependence, we choose the Bolzmann function to fit the 30 points for each $\Delta K/K$, which can be represented as $Y(x) = A_2 + (A_1 - A_2)/(1 + exp(x - x_0)/dx)$, where A_1, A_2, x_0, dx are coefficient to be determined. With this fitted curve, we can evaluate the power with arbitrary λ_δ for a given error strength. Intermediate values for $\Delta K/K$ and λ_δ can be obtained by interpolation.

Using the fitted curve we can evaluate the combinations of the chosen $\Delta K/K$ and λ_δ which reduce the power by 10%, 20%, 30% and 40%. In order to obtain information for all of the possible combinations of $\Delta K/K$ and λ_δ we should fit each of these curves of constant power again. As mentioned in Sec. 3, the rms phase shake, which gives a certain power reduction, is proportional to the product of $\Delta K/K$ and λ_δ. Therefore, we can fit the curve with $y = ax^b$ with a and b the coefficients which should be determined. The expected value of $b = -1$, indicating that the power reduction is proportional to both $\Delta K/K$ and λ_δ.

For the random errors, we choose three points (combination of $\Delta K/K$ and λ_δ) from each curve where $10\%, 20\%, 30\%$ power degradation can be expected. Thus totally 9 points are chosen. For each point, we fix the λ_δ and set a suitable κ for $\Delta K/K$ that if $\Delta K_i/K$ randomly varies in the range of $[-\kappa, \kappa]$, the rms phase shake is similar to the one of periodic error. In Sec. 3 it is already discussed how to determine the κ for different error types. For each point 100 random simulations are done, resulting in a total of 900 random error simulations.

5.2 Simulation for SASE1 at 0.1 nm

5.2.1 Sinus error

1. Periodic sinus error

As mentioned above, the first step is to calculate the power variation for different error periods at a given error amplitude. Fig. 28 illustrates the result. The error strength in this example is $\Delta K/K = 0.1\%$. From the left plot one can see that the correlation between the error period and power is good but not perfect. In general the power decreases when the error period increases. The plot on the right shows the corresponding phase shake and beam wander. The beam wander is kept small and the rms phase shake increases linearly with error period. This confirms the conclusion from section 3 that the rms phase shake is proportional to the error period. In appendix B one reason why the power oscillates with increasing λ_δ will be discussed.

From the fit shown in Fig. 28 and similar curves for other error strength, one obtains Fig. 29. It shows four curves with each point ($\Delta K/K$ and λ_δ) on the same curve having

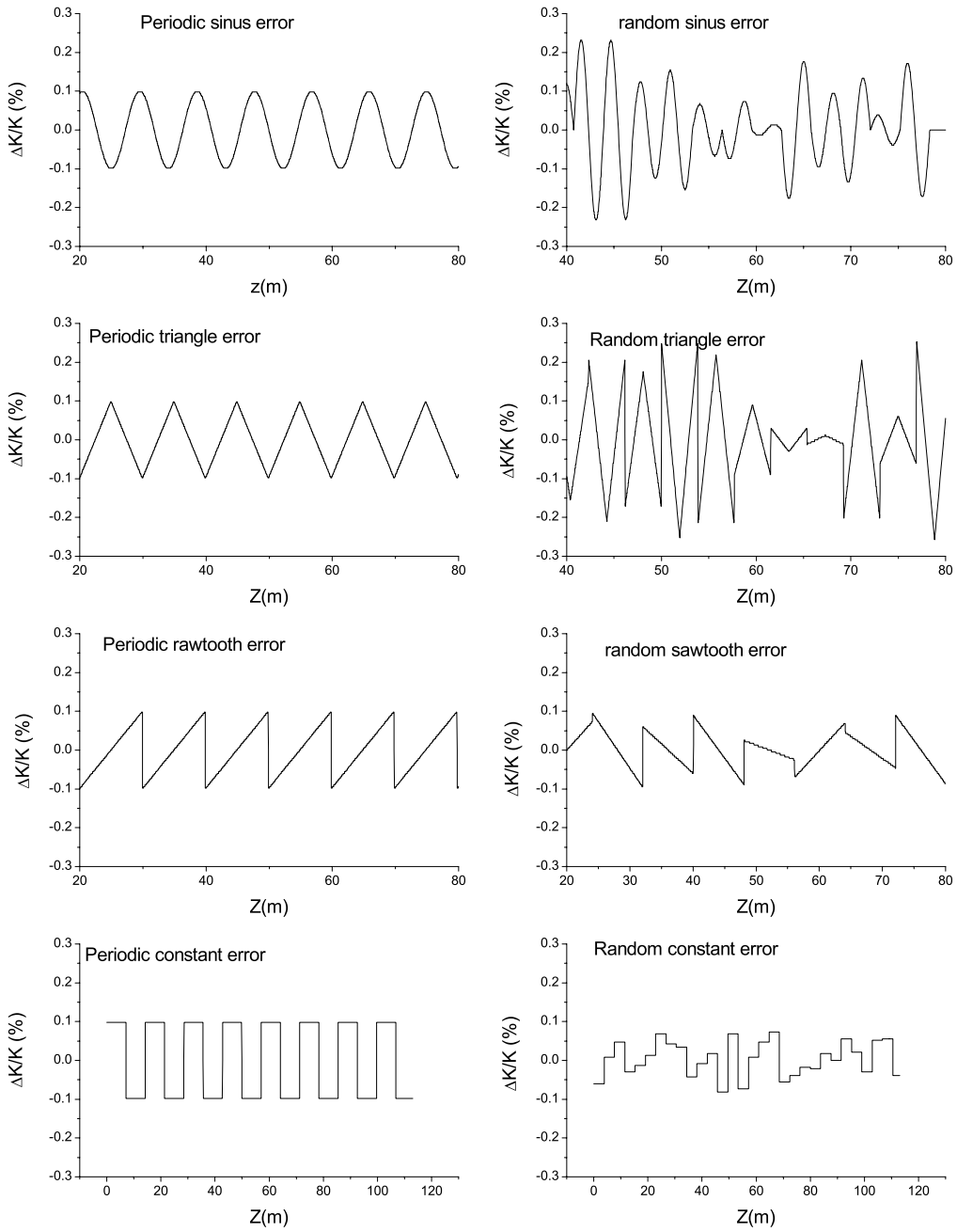

Figure 26: *The periodic and random error for the four error types. In the periodic error the error strength is the same for different error period, while in the random error, the error strength is randomly changing for each error period.*

the same power, normalized to the power P_0 at the same position of 113.07 m for an ideal undulator. From Fig. 29 one can see that a larger error period with smaller error strength results in the same power.

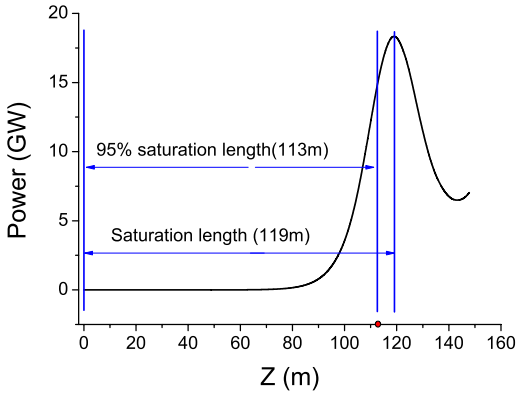

Figure 27: *The power growth for an ideal undulator for SASE1, 0.1 nm. The saturation length* $L_{sat.} = 119$ *m, so the* 95% *of* $L_{sat.}$ *is 113 m and this length is selected to evaluate the power.*

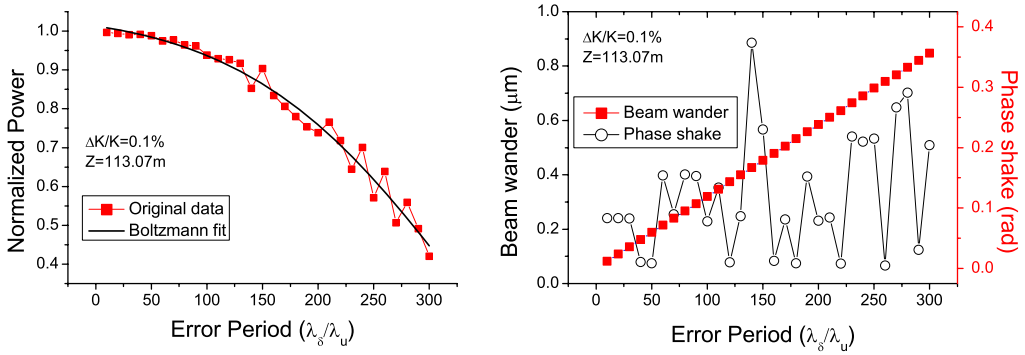

Figure 28: *Left: Normalized power versus error period at a fixed position for an error strength* $\Delta K/K = 0.1\%$*. The results are for a sinus error at 0.1 nm for SASE1. One can see that the power decreases when the error period increases. Right: Phase shake and beam wander versus error period. The beam wander is kept small and the phase shake increases linearly with error period.*

Fig. 30 shows the fitting result with the function $y = ax^b$. One can see that the value of b is close to -1, confirming the linear dependence on error period and strength. With an undulator segment length of 5 m and a four points support structure, e.g. a deformation length of about 1.2 m, Fig. 30 shows that if 10% power degradation is acceptable, the error strength can be as large as $\Delta K/K = 0.366\%$.

To illustrate the correlation between the rms phase shake and the power, Fig. 31 shows the normalized power versus the rms phase shake for all 270 different periodic simulations combining different $\Delta K/K$ and λ_δ. The good correlation between phase shake and the power shown in Fig. 31 is important because the phase shake of an undulator system is easily calculated from magnetic measurements.

2. Random sinus error

Although the undulator girder deformation is homogeneous and therefore the sinus error

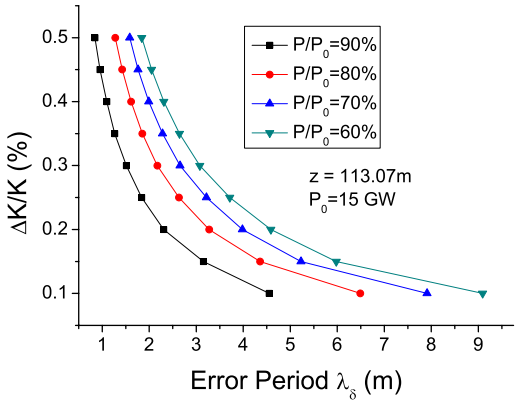

Figure 29: *Curves of constant power for different error period and strength for SASE1 at 0.1 nm. A sinus error shape has been simulated.*

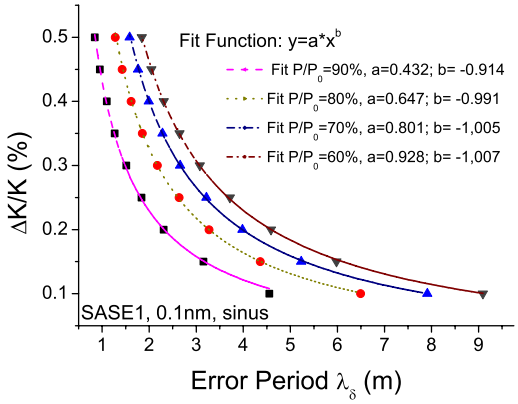

Figure 30: *Fitting result for Fig. 29.*

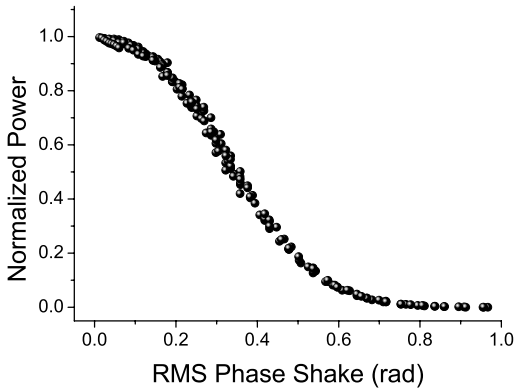

Figure 31: *Correlation between the phase shake and the power for the sinus error of constant amplitude. Parameters for SASE1 at 0.1 nm have been used.*

to large extent periodic, the random sinus error has been simulated for later comparison with sawtooth and triangle error distributions. As mentioned in section 5.1, 9 different error periods λ_δ are chosen and for each λ_δ 100 different random error distributions of ΔK are simulated, such that there are 900 random simulations in total. The error period and strength are chosen based on the curves in Fig. 29 to make the power in the range of $P/P_0 = 70\%$ to 90%. Finally, we calculate the rms phase shake and the rms beam wander for each random simulation. Fig. 32 shows the result. One can see that for the random sinus error, the correlation between power and rms phase shake is similar to that for the periodic error in Fig. 31, although the spread is larger. In appendix B the results are analyzed in more detail. Note that some of the points at small phase shake show a larger power reduction due to a larger beam wander (black points in Fig. 32).

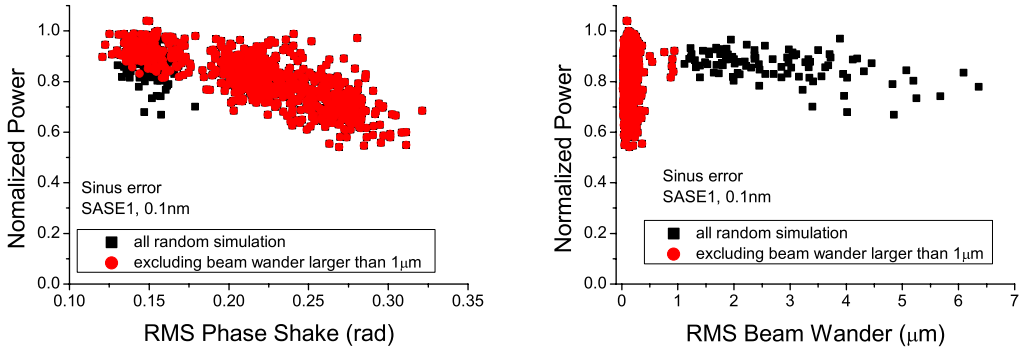

Figure 32: *Left: the relation between the RMS phase shake and the power using random sinus error distributions. The black points are all of the 900 simulations, the red points show the simulations in which beam wander is less than 1 μm. Right: the relation between the beam wander and the power. Because the beam wander is very small ($\leq 6\mu m$) compared to the beam transverse size (≈ 30 μm), there is no apparent correlation. The power degradation is mainly determined by rms phase shake.*

5.2.2 Triangle error shape

1. Periodic triangle error

Similar to the sinus error shown in Fig. 28, Fig. 33 shows the result of $\Delta K/K = 0.1\%$ for a periodic triangle error. It can be see that the points of constant power in Fig. 34 show a similar behaviour as for the sinus error. Fitting with the function $y = ax^b$ shown on the right therefore shows again b close to -1. Because two undulator segments construct one triangle period and one undulator length is 5 m long for SASE1, the triangle period is 10 m. Thus from Fig. 34 an error of $\Delta K/K = 0.058\%$ reduces the power by 10%.

Similar to the case of sinus error, Fig. 35 also shows a good correlation between rms phase shake and power degradation for a periodic error distribution.

2 Random triangle error

As analyzed in section 3, if $\kappa = \sqrt{3}\Delta K$, the phase shake of periodic and random triangle errors are the same. Here κ is the limitation for the variation range of random ΔK_i of each period ($-\kappa \leq \Delta K_i \leq \kappa$), ΔK is the error strength for periodic triangle error.

Fig. 36 shows the result of calculation for random triangle error. Comparing to Fig. 35, the power spread is large. Excluding those points that have a large rms beam

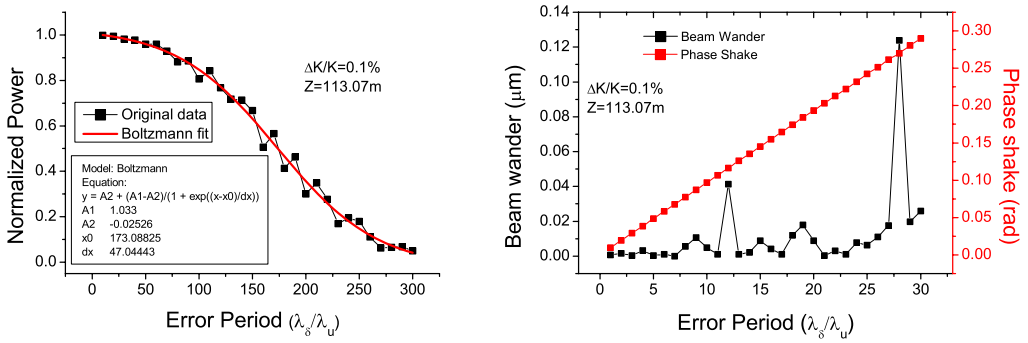

Figure 33: *Left: Normalized power versus error period at a fixed position for an error strength* $\Delta K/K = 0.1\%$*. The results are for a periodic triangle error of SASE1 at 0.1 nm. One can see that the power decreases when the error period increases. Right: Phase shake and beam wander versus error period. The beam wander is kept small and the phase shake increases linearly with error period.*

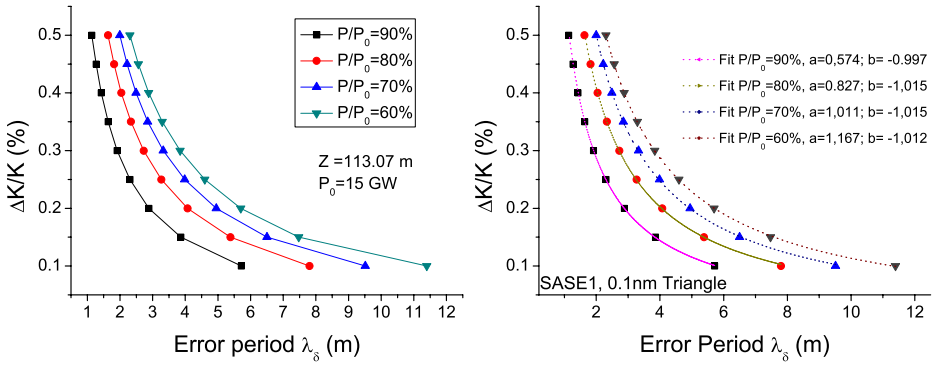

Figure 34: *Left: Output power versus error period and strength for SASE1 at 0.1 nm. A triangle error shape is used. Each curve shows a different power level. Right: fitting result for the same simulation shown on the left.*

wander($> 10\mu m$), the remaining points, shown in red, show a much better correlation. Because in this report we only take into account the non-steering errors, the effect of both errors simultaneously has not been studied further.

5.2.3 Sawtooth error shape

Similar to the simulation methods of sinus and triangle error, the simulation for sawtooth error also takes into account periodic sawtooth error and random sawtooth error.

1. Periodic sawtooth error

Fig. 37 shows the power degradation with error period varying from $\lambda_\delta/\lambda_u = 10$ to $\lambda_\delta/\lambda_u = 400$ and with an error strength $\Delta K/K = 0.1\%$. The result is similar to the ones shown before for sinus and triangle error. From the right plot of Fig. 37 one can again see the linear dependence of phase shake on error period.

By fitting the power degradation with error period λ_δ for different error strengths

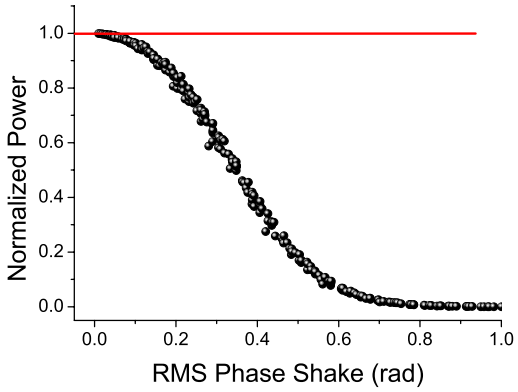

Figure 35: *Correlation between the rms phase shake and the power for the periodic triangle error for SASE1 at 0.1 nm.*

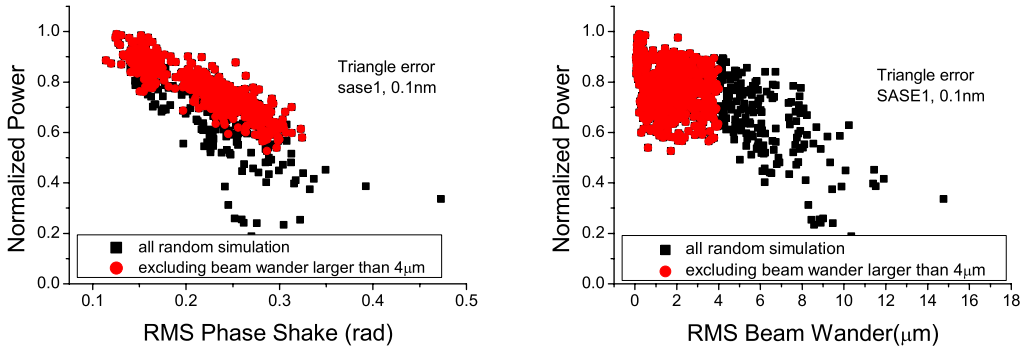

Figure 36: *Left: the correlation between the phase shake and the power for triangle errors with random amplitude. The black point are all of the 900 simulations, the red points are those with a beam wander less than* $4\mu m$*. The correlation between the power and the phase shake is better than the random error simulation for sinus error. Right: the correlation between the beam wander and the power. For those points where beam wander is large* ($\approx 10\mu m$) *compared to the beam size* ($\approx 30\mu m$)*, the power reduction is determined by a combination of phase shake and overlap. Excluding the points with large beam wander shows a good correlation between phase shake and power.*

$\Delta K/K$, λ_δ and $\Delta K/K$ can be found for every power degradation. The result is shown in Fig. 38. Similar to the method for sinus and triangle error, we fit the separated points on the left of Fig. 38 again to obtain the curves on the right. By this fitting plot, we can find the error tolerance for different power degradation and the certain undulator structure.

Another interesting point is to find the correlation between the rms phase shake and the power degradation for sawtooth error. Fig. 39 gives the result. One can see that the correlation is still good.

2. Random sawtooth error

As shown in Sec. 3.3.2, the rms phase shake of periodic and random sawtooth error is the same if the random variation range κ of random error strength ΔK_i satisfies $\kappa = \Delta K/\sqrt{2}$,

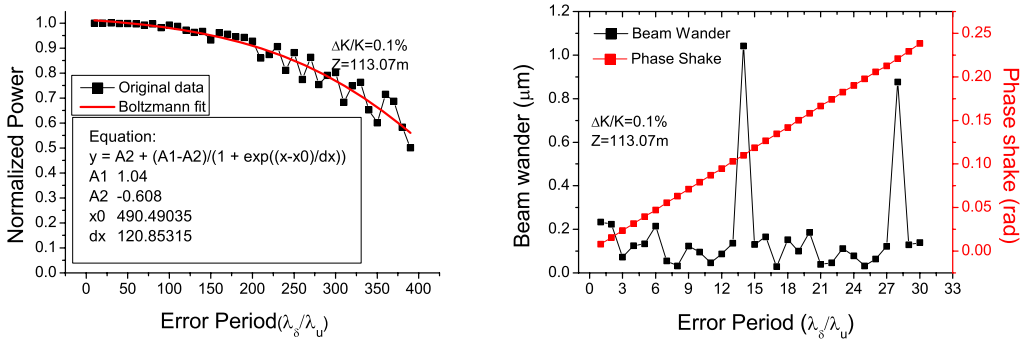

Figure 37: *Left: Normalized power versus error period at a fixed position for an error strength* $\Delta K/K = 0.1\%$*. The results are for a periodic sawtooth error at 0.1 nm for SASE1. One can see that the power decreases when the error period increases. Right: Phase shake and beam wander versus error period. The result is similar to the corresponding plots of the sinus and triangle error.*

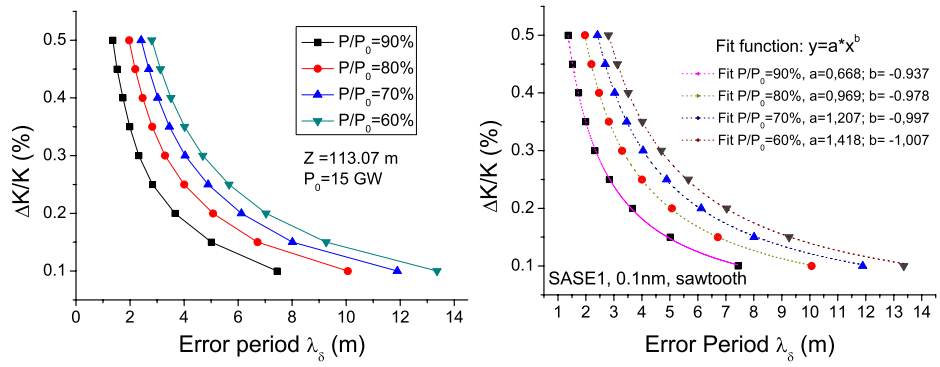

Figure 38: *Left: power degradation with different* λ_δ *and* $\Delta K/K$ *for SASE1 at 0.1 nm for a sawtooth error. Right: fitting curve for power degradation points shown in teh left plot.*

where ΔK is the periodic error strength.

Fig. 40 shows the random simulation result for sawtooth error. The radiation power still decreases as the rms phase shake increases but the spread for a certain rms phase shake is larger than that of periodic error.

5.2.4 Piecewise constant error

1. periodic 'constant' error

Fig. 41 shows the power degradation versus error period λ_δ. One can see similar results as for the calculations for other error types. By the fitting curves shown in Fig. 41, we can get Fig. 42, which gives the combinations of $\Delta K/K$ and λ_δ for which a certain power degradation can be expected.

To find the error tolerance for the certain structure, the separated points in on the left of Fig. 42 are fitted again to get the curves on the right. Fig. 43 shows the correlation between the power degradation and the rms phase shake. We can again find a good

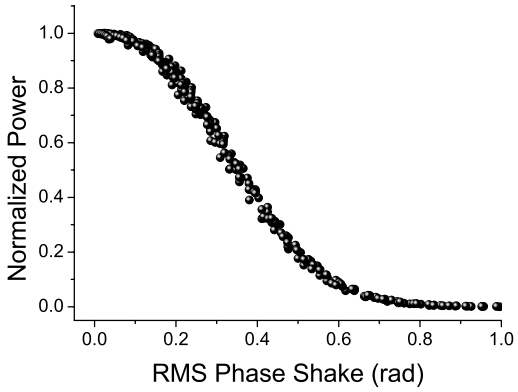

Figure 39: *Correlation between the phase shake and the power for the periodic sawtooth error for SASE1 at 0.1 nm mode. One can see that this correlation is good.*

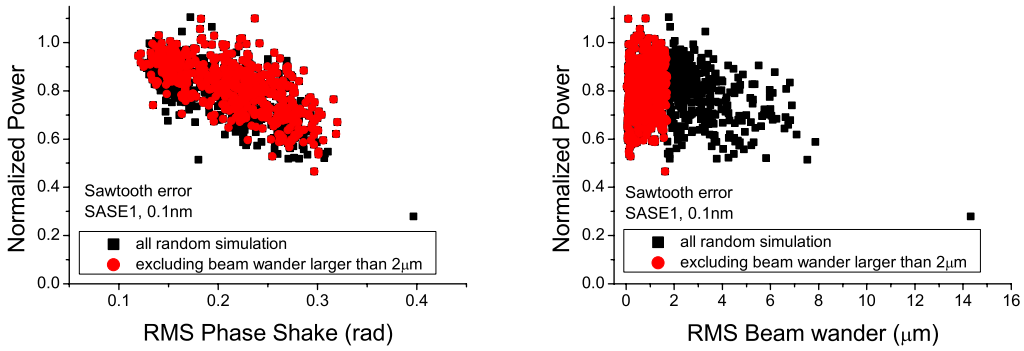

Figure 40: *Left: the correlation between the phase shake and the power with random simulation. The black points show all of the 900 simulation, the red points the simulations in which beam wander is less than 2μm. Right: the correlation between the beam wander and the power.*

correlation.

2. random error

Similar to the simulation for the other error types, we simulate the power degradation with random error. The result shown in Fig. 44 is different from the corresponding plots for the other error types. The largest power degradation and the largest rms phase shake are much larger than the ones of the other error types. This is because the rms phase shake for the whole undulator system is determined not only by the error strength but also by the distribution of the error.

5.2.5 Comparison of phase shake for different distributions

We have already shown the good correlation between the rms phase shake and the power degradation for each error type. It is also important to compare the correlations of different error types. Fig.45 shows the result. As can be seen from this plot, the same rms phase shake generated by different error tpyes gives the same power degradation. There-

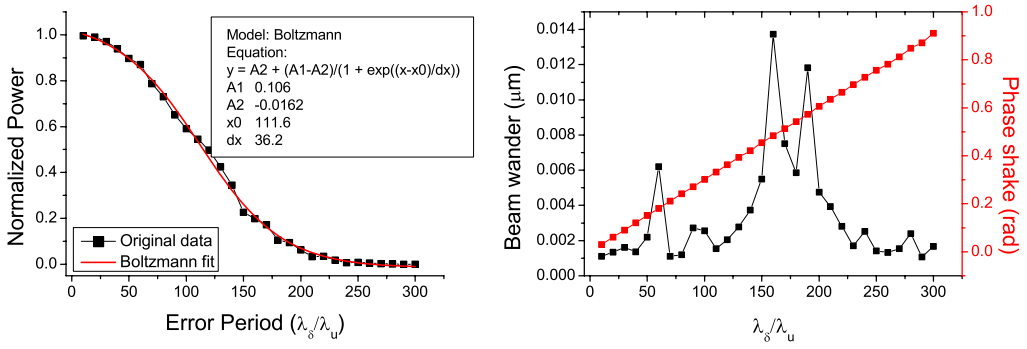

Figure 41: *Left: Normalized power versus error period at a fixed position for an error strength* $\Delta K/K = 0.1\%$*. The results are for a periodic 'constant' error at 0.1 nm for SASE1. One can see that the power decreases when the error period increases. Right: Phase shake and beam wander versus error period. The result is similar to the corresponding plots of the sinus, triangle and sawtooth error.*

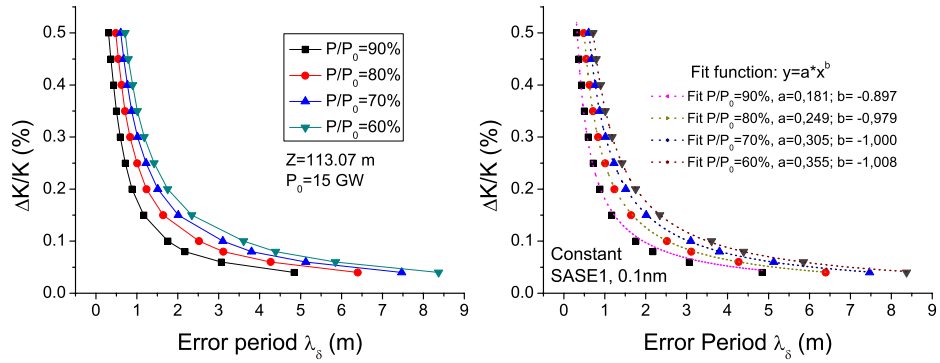

Figure 42: *Left: power degradation with different* λ_δ *and* $\Delta K/K$ *for SASE1 at 0.1 nm for a 'constant' error. Right: fitting curve for points shown on the left.*

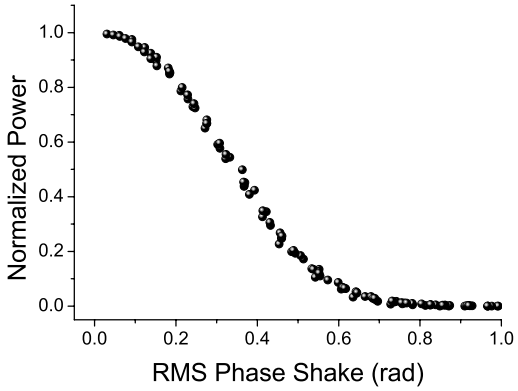

Figure 43: *Correlation between the phase shake and the power for the constant error for SASE1 at 0.1 nm.*

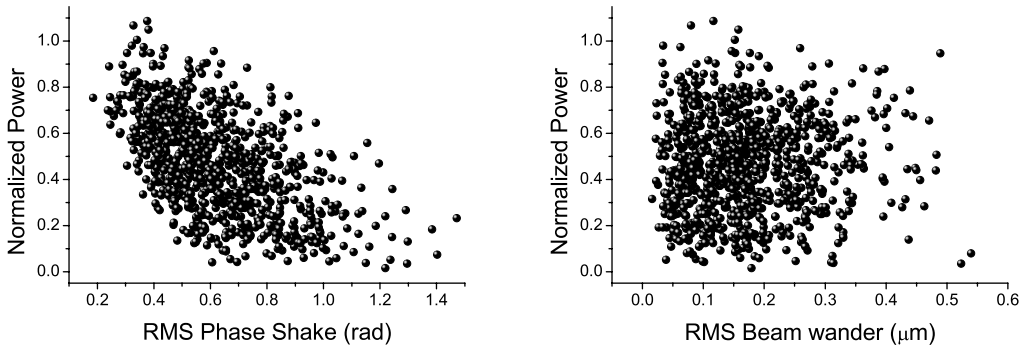

Figure 44: *Left: the correlation between the phase shake and the power with random simulation. One can see that the phase shake has a large spread; Right: the correlation between the power and the beam wander. Compared to all previous simulation results, the beam wander is very small.*

fore, we can consider the rms phase shake as a key parameter for the power degradation. Because the rms phase shake can be calculated from magnetic measurements only, the expected FEL performance can be estimated directly.

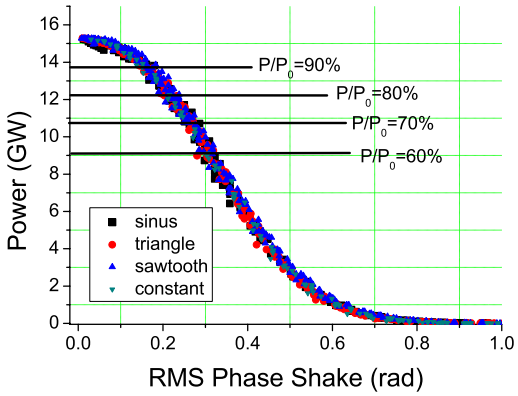

Figure 45: *The power degradation with rms phase shake. One can see that the power corresponds to the phase shake well, independent of the error shape. The error strength is periodic here.*

5.3 Simulation for SASE1 at 0.4 nm

The undulator of SASE1 has a fixed gap, which means in principle the undulator parameter can not be changed. With a 17.5 GeV electron beam, 0.1 nm radiation can be generated. But it is also possible that SASE1 can change its operation mode to a radiation wavelength of 0.4 nm by adjusting the electron energy from 17.5 GeV to 8.75 GeV. It is important to find the error tolerance for this different beam energy. In this section we thereore calculate the error tolerance for SASE1 with 0.4 nm. The analysis method is the same as for SASE1 at 0.1 nm. Fig. 46 shows the power growth for an ideal undulator, with a saturation power and length of 22.21 GW and 64.51 m, respectively. So 95% of

the saturation length is 61.3 m which is the point used to determine the power.

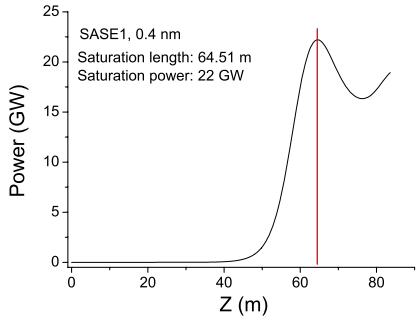

Figure 46: *The power growth with an ideal undulator for SASE1 at 0.4 nm.*

In this section, we also analyze the tolerance for sinus, triangle, sawtooth and constant error types. As the analysis method is introduced for SASE1 at 0.1 nm, in this section we only list the key plots to show the results (see Fig. 47 50).

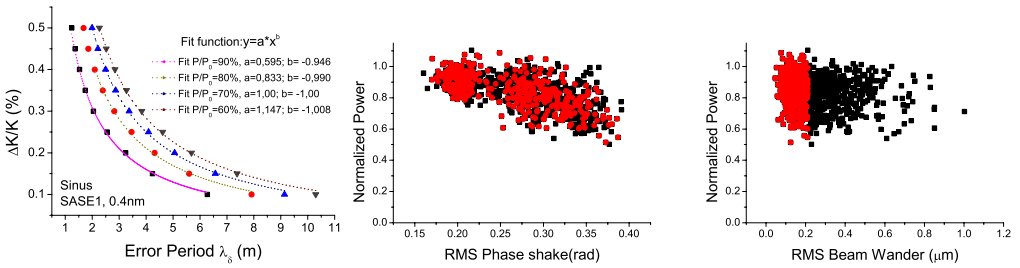

Figure 47: *Left: the periodic sinus error impact for SASE1 at 0.4 nm. Middle: random sinus error simulation for SASE1,* 0.4 *nm. The correlation between the phase shake and the power with random simulation. The black points show all of the 900 simulation, the red points the simulations in which beam wander is less than 0.2μm. Right: the correlation between the beam wander and the power.*

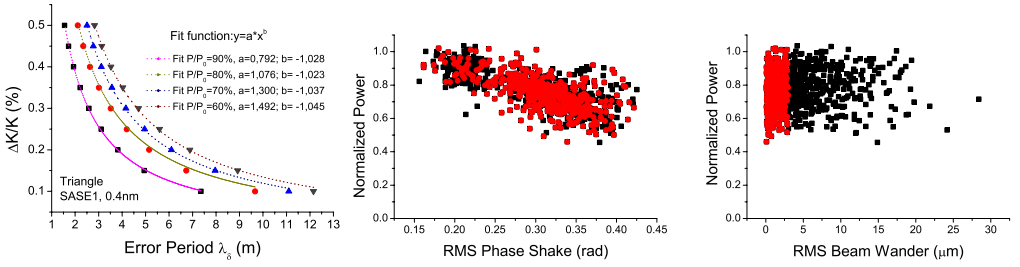

Figure 48: *Left: the periodic triangle error impact for SASE1 at 0.4 nm. Middle: random triangle error simulation for SASE1,* 0.4 *nm. The correlation between the phase shake and the power with random simulation. The black points show all of the 900 simulation, the red points the simulations in which beam wander is less than 2.5μm. Right: the correlation between the beam wander and the power for the same random simulations.*

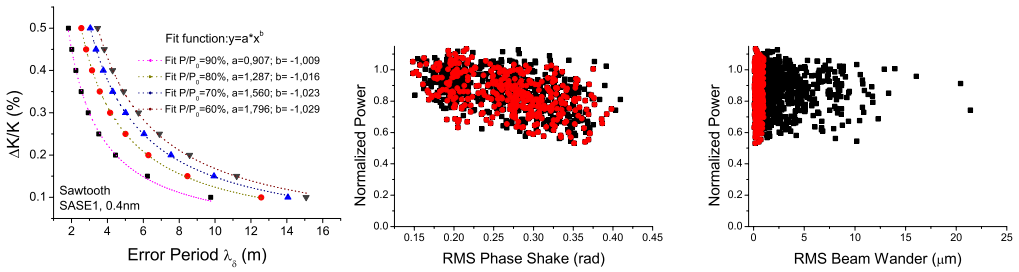

Figure 49: *Left: the periodic sawtooth error impact for SASE1 at 0.4 nm. Middle: random sawtooth error simulation for SASE1, 0.4 nm. The correlation between the phase shake and the power with random simulation. The black points show all of the 900 simulation, the red points the simulations in which beam wander is less than 1 μm. Right: the correlation between the beam wander and the power for the same random simulations.*

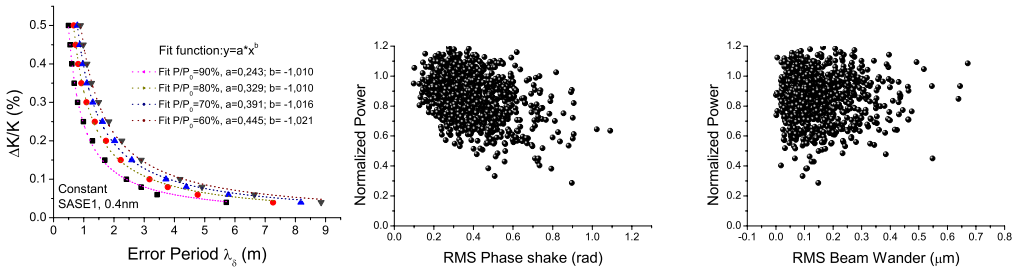

Figure 50: *Left: the periodic constant error impact for SASE1 at 0.4 nm. Middle: random 'constant' error simulation for SASE1, 0.4 nm. The correlation between the phase shake and the power with random simulation. Right: the correlation between the beam wander and the power. One can see the beam wander is very small.*

5.4 Comparison of results at 0.1 nm and 0.4 nm for SASE1

The error tolerance is different for the 0.1 nm and 0.4 nm. From Fig. 51 one can see that the error tolerance for 0.1 nm is tighter than for 0.4 nm mode. It can be shown that the rms phase shake is only determined by the undulator system. This means for the same power degradation, 0.4 nm permits larger rms phase shake than the 0.1 nm mode. We can try to explain this phenomenon by the Pierce parameter. The pierce parameter ρ is:

$$\rho = \frac{1}{\gamma}\left[\left(\frac{Kf_c\lambda_u}{8\pi\sigma_b}\right)^2 \frac{I_p}{I_A}\right]^{1/3} \tag{59}$$

In these two modes only electron energy γ and σ_b are different. For 0.1 nm $\gamma = 3.4\times10^4$, $\sigma_b = 35.7\,\mu$m; for 0.4 nm, $\gamma = 1.7\times10^4$, $\sigma_b = 48.3\,\mu$m. So the Pierce parameters are 4×10^{-4} and 6.5×10^{-4} respectively for 0.1 nm and 0.4 nm. Thus ρ of 0.1 nm mode is smaller than 0.4 nm mode. Because the Pierce parameter correlates to the SASE-FEL bandwidth, the larger bandwidth permits bigger rms phase shake.

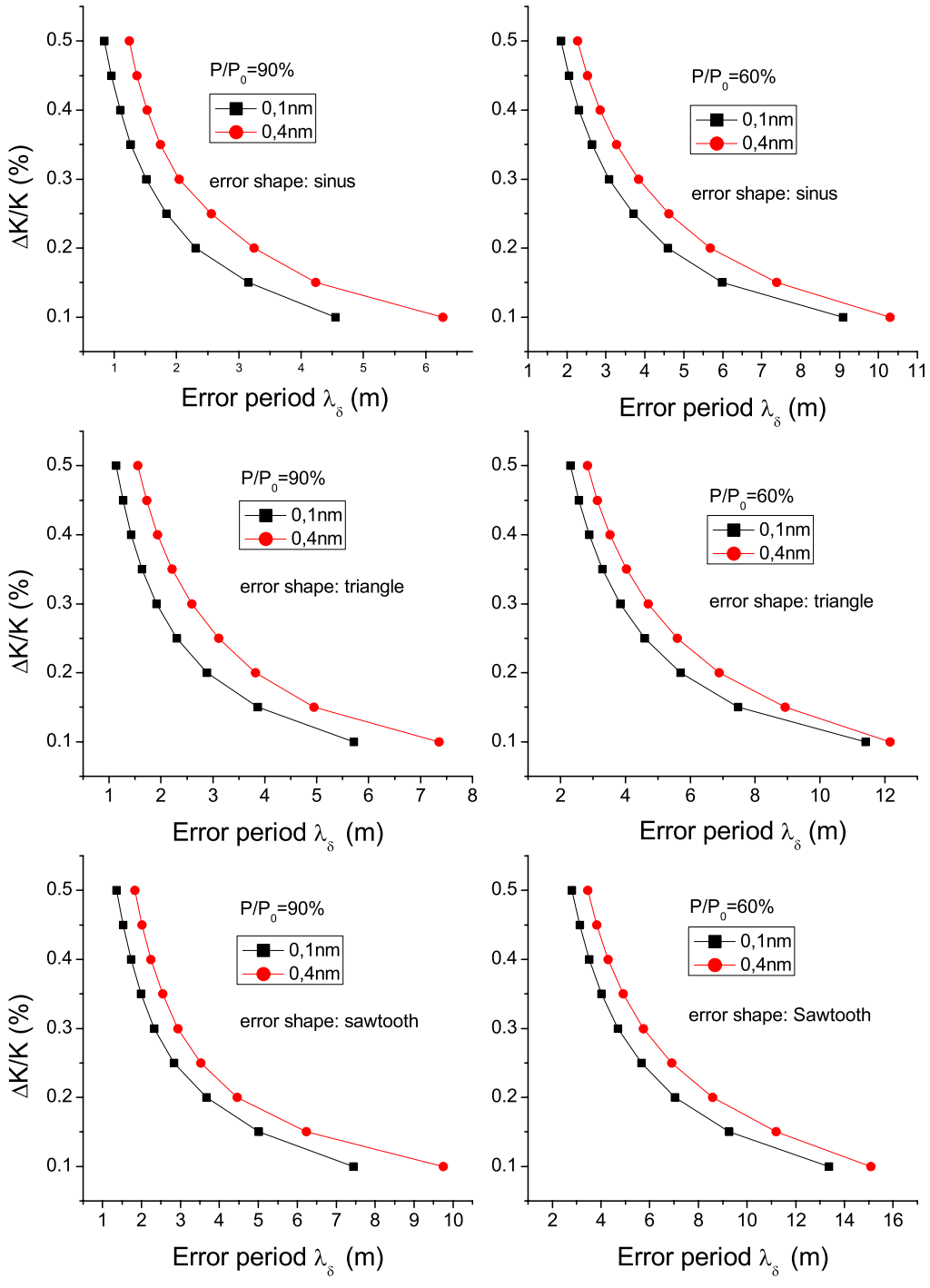

Figure 51: *Tolerance comparison of 0.1 nm and 0.4 nm for SASE1.*

6 Simulation for combined error and temperature compensation by adjusting the undulator gap

6.1 Combination different errors

In the sections before the influence of four different error types are illustrated separately. In practice these errors are combined. Therefore, it is also necessary to investigate the effect of a combination of errors.

In principal the girder deformation is to large extend homogeneous. Therefore, the sinus error has been assumed periodic in this section. The triangle, sawtooth and piecewise constant error are all caused by inaccuracy of motor movement and are therefore random. We assume that the girder deformation is 20 μm and the motor movement accuracy is 2 μm. Fig. 52 shows the error combination. The black curve in the right plot is the final combined K value.

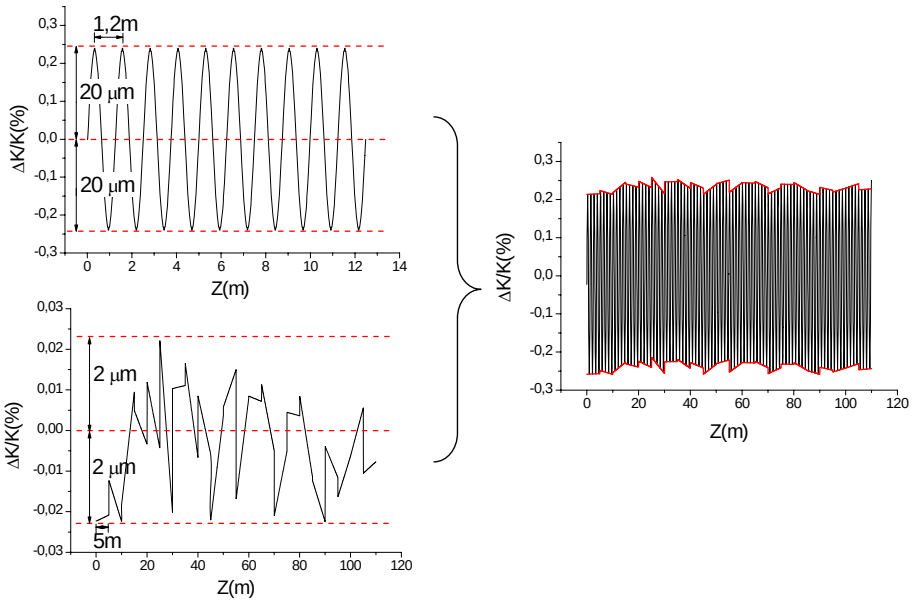

Figure 52: *The illustration of combined field error. The girder deformation with an amplitude of 20 μm and a period of 1.2 m is periodic, whereas a combination of triangle, constant and sawtooth error with an amplitude of 2 μm is random.*

More than 100 combined random errors are generated and the power degradation versus the rms phase shake is shown in the Fig. 53. One can see that the largest power degradation is around 30%.

For the point with the largest power degradation we do the time dependent simulation. The result is shown in Fig. 54. One can see that the Gaussian-fitted peak power with error undulator field shows around 40% reduction in power compared to the simulation without error. A similar time-dependent simulation with a flat top current distribution shows a 35% reduction in power, indicating that the increased reduction in power is caused by the current distribution used.

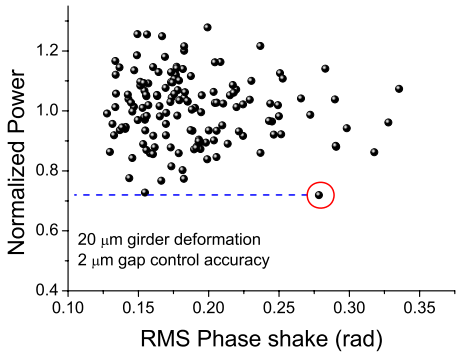

Figure 53: *The power degradation due to combined periodic sinus and random sawtooth/constant error*

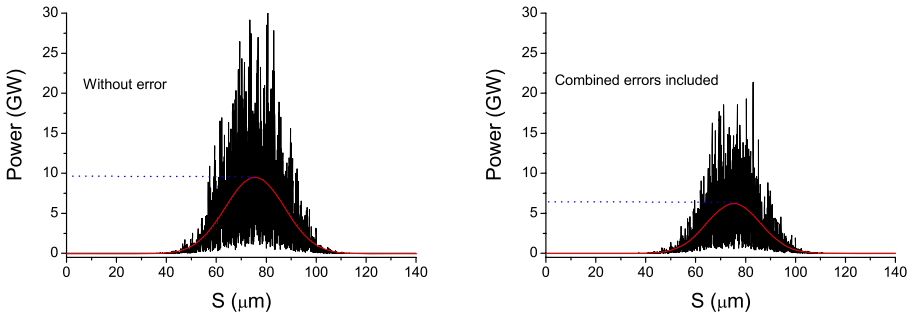

Figure 54: *The comparison of time dependent simulation results between the power without error and with combined errors.*

6.2 Linear temperature variation and compensation by adjusting the undulator gap

Over the length of the undulator, which typically exceeds 100 m, a small temperature gradient accumulates to several degrees. One degree temperature change corresponds to 0.1% change of K which would already reduce the radiation power measurably. In order to evaluate the impact of temperature variation, we assume that the temperature changes linearly. Fig. 55 illustrates the impact of this kind of temperature gradient. One can see that only 1 degree temperature gradient over 140 meters reduces the power by more than 50%.

Because the temperature variation considered here is linear over the whole undulater, this error variation is a sawtooth error with a 140 m period. Because of the long λ_δ, even the a small error strength $\Delta K/K$ is still too large. One way to compensate the temperature's impact is by adjusting the undulator gap. The gap can be adjusted when detecting temperature variation larger than 0.1 degree which is the assumed accuracy of temperature measurement. Fig. 56 shows the result. One can see that after adjusting the undulator gap to compensate the impact of temperature variation, the linear variation field changes to a periodic sawtooth field. By this kind of compensation, even a 5 degree teperature variation can be compensated.

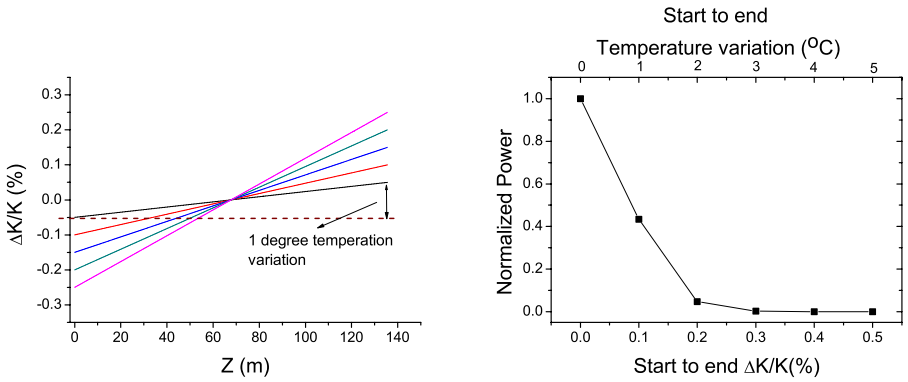

Figure 55: *Power reduction due to a linear increase of K over the undulator length. Left: The range over which K increases. Right: The power versus relative change in K over the undulator length. The top scale gives a corresponding temperature scale for comparison.*

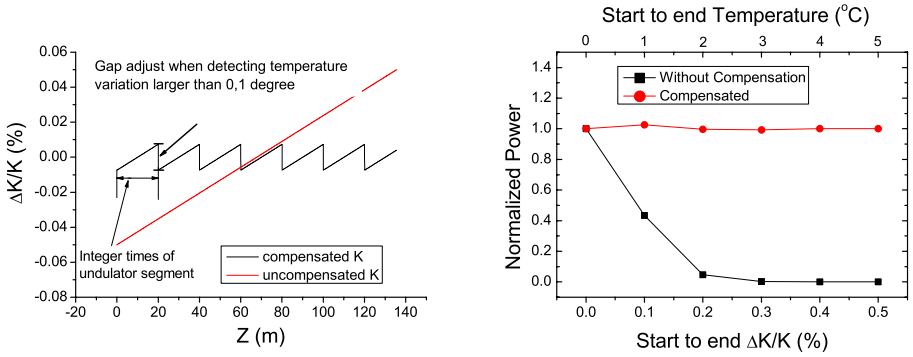

Figure 56: *Same as in Fig. 55, but the K variation is compensated by adjusting the undulator gap after each undulator where a temperature measurement shows a deviation larger than 0.1 degree. This results in a sawtooth like K value (left) and a corresponding recovering of the power (red curve on the right).*

7 Influence of phase shifter errors for SASE1

Inside an undulator segment, the undulator magnetic field will guarantee the synchronous relationship between electrons and field that after each undulator period the phase change between them is $\phi = 2\pi$. To keep the synchronous relationship between the electrons and radiation in the intersection between two undulator segments, a phase shifter is installed. Fig. 57 shows the Permanent Magnet (PM) phase shifter designed for the European XFEL project. By adjusting the shifter gap, the field $B_d(z)$ can be adjusted to a suitable value.

When electrons pass a magnetic field, the travelling time is

$$T = \frac{1}{c}\left[L_D + \frac{L_D}{2\gamma^2} + \frac{1}{2}\left(\frac{e}{m\gamma c}\right)^2 \int_0^{L_D} dz \left(\int_0^z B_d(z^{'})dz^{'}\right)^2\right], \tag{60}$$

where L_D is the intersection length and $B_d(z)$ is the transverse magnetic field. Compared

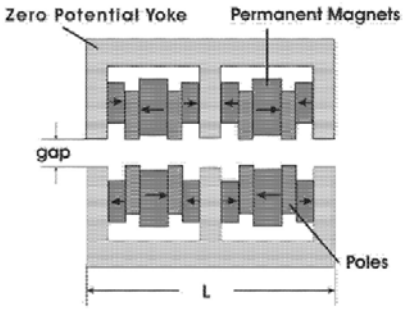

Figure 57: *Illustration of structure of PM phase shifter designed for European XFEL project.*

to the travelling of a photon of L_D/c, the electron will fall behind the optical wave resulting in a phase advance between undulator segments of

$$\phi = -\frac{2\pi\Delta T c}{\lambda_s} = -\frac{\pi}{\lambda_s}\left[\frac{L_D}{\gamma^2} + \left(\frac{e}{m\gamma c}\right)^2 \int_0^{L_D} dz \left(\int_0^z B_d(z^{'})dz^{'}\right)^2\right], \tag{61}$$

where λ_s is the radiation wavelength. Using the vector potential instead $A_x = \int B_d(z^{'})dz^{'}$, Eq. (61) can be expressed as

$$\phi = -\frac{\pi}{\lambda_s}\left[\frac{L_D}{\gamma^2} + \left(\frac{e}{m\gamma c}\right)^2 \int_0^{L_D} A_x^2(z)dz\right]. \tag{62}$$

7.1 Phase shifter error simulation by Genesis 1.3

In order to obtain knowledge of the accuracy with which to set the phase shifter, it is simulated with the FEL simulation code Genesis 1.3. In Genesis, a parameter K_D is used to describe the phase shifter

$$K_D = \frac{e}{mc}\sqrt{< A_x^2 >} = \frac{e}{mc}\sqrt{\frac{1}{L_D}\int_0^{L_D} A_x^2(z)dz}\,. \tag{63}$$

Therefore Eq. (62) becomes:

$$\phi = -2\pi\frac{L_D(1+K_D^2)}{\lambda_s(2\gamma^2)}, \tag{64}$$

where λ_s denotes to the radiation wavelength, which is normally evaluated by the 1D resonance condition $\lambda_{s0} = \lambda_u(1+K_{rms}^2)/2\gamma^2$. Nevertheless the optimized wavelength is always shifted from this 1D resonance value $\lambda_s = \lambda_{s0} + \Delta\lambda_s$, so the phase advance ϕ in Eq. (64) can be expressed:

$$\phi \approx -2\pi\frac{L_D(1+K_D^2)}{\lambda_u(1+K_{rms}^2)} + 2\pi\frac{L_D(1+K_D^2)}{\lambda_u(1+K_{rms}^2)}\frac{\Delta\lambda_s}{\lambda_{s0}}. \tag{65}$$

The first term in the right hand part is always used to represent the phase advance and the second term denotes to the phase advance error because of the wavelength shift. Normally the phase shifter parameter K_D is designed to make the first term equal to

an integer times 2π, which guarantees electrons are synchroneous with the optical field after passing one intersection. But in practise some error is unavoidable that induces phase shifter error $\Delta\phi_0$ to the system. Moreover we use $\delta\phi$ to represent the phase advance shift because of wavelength variation. Therefore after one intersection between two undulators, the phase error $\Delta\phi$ is:

$$\Delta\phi = \Delta\phi_0 - \delta\phi\,. \tag{66}$$

In this equation $\Delta\phi$ is value of ϕ in Eq. (65) after subtracting $2n\pi$, which denotes the phase error. $\Delta\phi_0$ can be directly obtained from the first term of the right hand part in Eq. (65), which is due to the phase shifter error ΔK_D. $\delta\phi$ denotes the phase error because of wavelength shift. However, it should not directly taken from the second term of the right hand part in Eq. (65). The reason is because the wavelength shift induces a slope to the pondermotive phase along the undulator segment. The left part of Fig. 58 shows this.

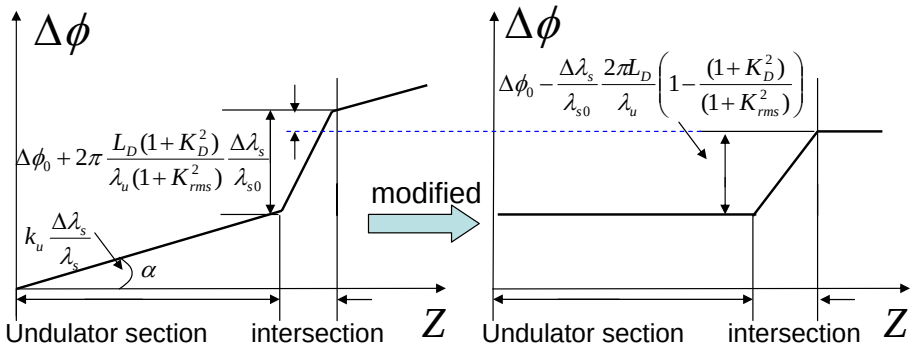

Figure 58: *Illustration of phase shift for the optimized wavelength variation. Left: illustration of phase versus longitudinal position before modification. Right: the phase after modification.*

Normally the slope is straightened when we calculate the pondermotive phase. Due to the angle θ of the slope is:

$$\alpha = \frac{2\pi}{\lambda_u}\frac{\Delta\lambda_s}{\lambda_s}\,, \tag{67}$$

the expression of $\delta\phi$ can be modifed from the second term of right hand part in Eq. (65):

$$\delta\phi = \frac{\Delta\lambda_s}{\lambda_s}\frac{2\pi L_D}{\lambda_u}\left(1 - \frac{1+K_D^2}{1+K_{rms}^2}\right)\,. \tag{68}$$

We use the parameters of SASE1, 0.1 nm to illustrate the value of $\delta\phi$. The wavelength calculated by the 1D resonance condition is 0.0977836 nm and the optimized wavelength is 0.097852 nm, $K_D = 0.383419$ which guanrantees the phase match between two undulator segments. So $\delta\phi = 5.792^o$ So it's difficult to evaluate the suitable value for K_D if the optimized wavelength is not known.

7.2 Two kinds of phase shift error — one direction and alternating error

We investigate the impact of a phase shifter error $\Delta\phi$ by changing the value of K_D. If $\Delta\phi$ has the same sign for each intersection, we call this kind of error one direction error.

If $\Delta\phi$ has the same absolute value for all intersections but the sign is alternating, we call this an alternating phase shift error. Fig. 59 shows these two kinds of errors. In the plot the phase error is chosen $|\Delta\phi| = 10^o$ as an example.

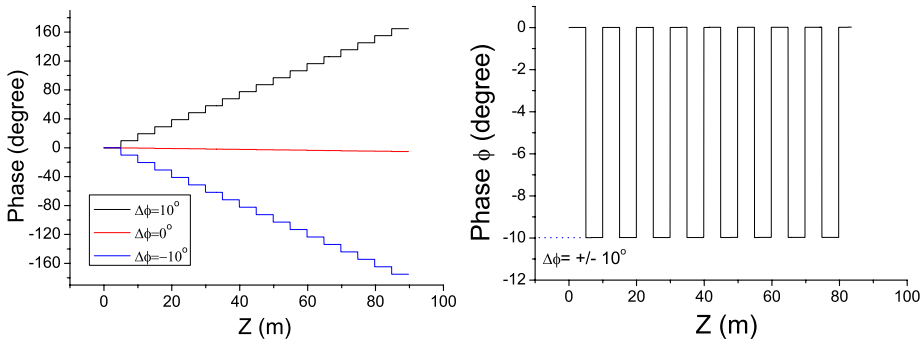

Figure 59: *Illustration of two different kinds of phase shift error. Left: one direction phase shift error. Right: alternating phase shift error.*

7.2.1 One direction phase shifter error

One directional phase shift error continueously changes the phase in one direction. This induces the variation of optimized wavelength. The analytical wavelength change is given in Eq. (68). To show this point, we scan the radiation wavelength in a steady-state simulation and find the optimized value for each $\Delta\phi$, and then compare that value to the number analytically calculated by Eq. (68). Fig. 60 shows the result. One can see that the analytical number matches the the scan number well.

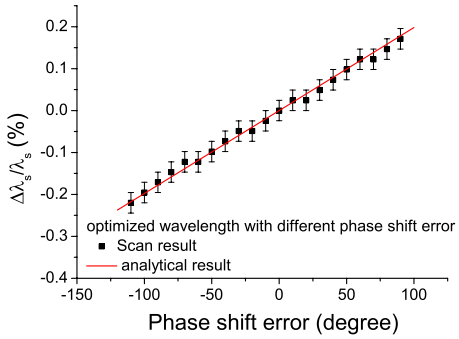

Figure 60: *Comparison of the optimized wavelength by the analytical calculation with a wavelength scan in the simulation.*

As mentioned above, the exact number of $\Delta\phi$ depends on the wavelength shift $\Delta\lambda_s/\lambda_s$ while for the one direction phase shifter error, the optimized wavelength also depends on $\Delta\phi$. We iterate this to first order to evaluate this impact.

The zero order of phase error is $\Delta\phi|_0$, then it induces wavelength shift:

$$\frac{\Delta\lambda_s}{\lambda_s} = \frac{\Delta\phi|_0}{L_u k_u}$$

This wavelength shift contributes to the phase shifter error number is:

$$\delta\phi = \frac{2\pi}{\lambda_u} L_D \left(1 - \frac{1+K_D^2}{1+K_{rms}^2}\right) \frac{\Delta\lambda_s}{\lambda_s}$$

So the ratio of $\delta\phi$ and $\Delta\phi|_0$ is:

$$\frac{\delta\phi}{\Delta\phi|_0} = \frac{L_D}{L_u}\left(1 - \frac{1+K_D^2}{1+K_{rms}^2}\right) \approx \frac{L_D}{L_u}\left(1 - \frac{1}{1+K_{rms}^2}\right), \tag{69}$$

where L_u is the undulator segment length. Normally K_D is small, so the phase shift error change $\delta\phi$ is independent on the zero order phase shifter error $\delta\phi|_0$. For instance for SASE1, $K_{rms} = 2.333$ and $L_D/L_u = 0.2$, the value is $\delta\phi/\Delta\phi|_0 \approx 16.9\%$. To illustrate this, Fig. 61 shows the numerical calculation result. $\Delta\phi|_0$ changes by adjusting the optimized wavelength. The expected phase change is 100^o, but if the wavelength changes, $\Delta\phi = 116^o$, which matches the Eq. (69)

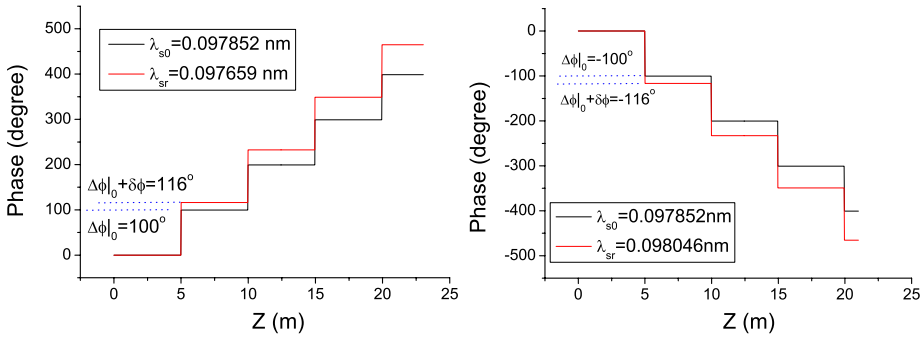

Figure 61: *change of $\Delta\phi$ because of calculation at a wrong wavelength.*

From the discussion above, power degradation relates to the RMS phase shake instead of phase error at each intersection $\Delta\phi$. The RMS phase shake can be calculated from $\Delta\phi$. It is not reasonable to directely set the RMS phase shake as the RMS value of the stepwise shake of phase shown in Fig. 61 but first subtract a straight line. Therefore the RMS phase shake can be calculated by:

$$\sigma_{\Delta\phi} = \sqrt{\frac{\int_0^{L_u}\left(\frac{\Delta\phi}{L_u}x - \frac{\Delta\phi}{2}\right)^2 dx}{L_u}} = \sqrt{1/12}\,|\Delta\phi| \tag{70}$$

Fig. 62 shows the result. As the discussion above, $|\Delta\phi|$ is 16% larger when the wavelenght changes, so the RMS phase shake also increases by 16%.

7.2.2 alternating phase shift error

Because the sign of phase shift error alternates and the absolute value of phase shift error is fixed at each intersection, there is no general change for the alternating phase shift error. So we expect that the optimized wavelength doesn't change. Fig. 63 shows the scan result. One can see that the same wavelengh gives maximum power for all different phase shift errors. This means it is not necessary to scan the wavelength for the alternating phase shift error simulation.

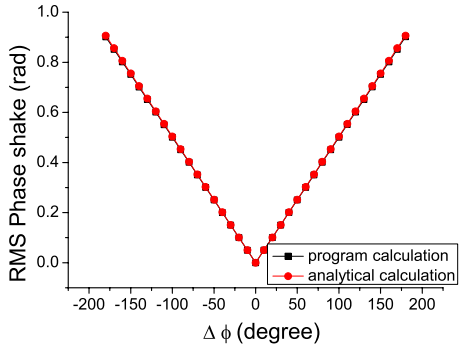

Figure 62: *RMS phase shake for different phase shifter error* $\Delta\phi$.

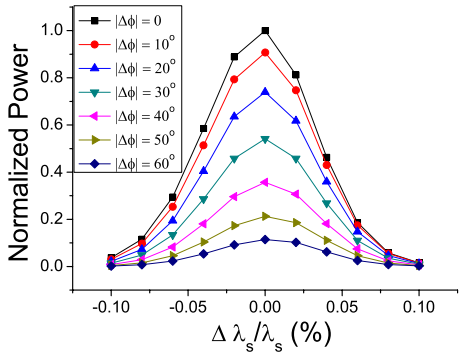

Figure 63: *Normalized power versus wavelength with different alternating phase shift error* ϕ.

From Fig. 59 one can see that the average value of phase error is $<\Delta\phi>=\Delta\phi/2$, so the RMS phase shake for this alternating phase shift error is

$$\sigma_{\Delta\phi} = \left|\frac{\Delta\phi}{2}\right| \tag{71}$$

It is interesting to compare the RMS phase shake between one direction and the alternating phase shift error. According to Eqs. (70) and (71), if the phase shift error ϕ is the same, the RMS phase shake of the alternating error is $\sqrt{3}$ times larger than the one directional error:

$$\frac{\sigma_{\Delta\phi,alternating}}{\sigma_{\Delta\phi,onedirection}} = \sqrt{3} \tag{72}$$

Because the phase shake relates to the power reduction, the one direction error is expected to give a smaller power reduction than alternating error by same phase shift error value ϕ. The simulation result will be shown below.

7.3 Phase shifter tolerance study for SASE1 at 0.1nm

In this section the simulation result of one direction and alternating phase shift error for SASE1 at 0.1nm is illustrated. K_D is varied such that $-\pi < \phi < \pi$.

It has been discussed that the optimized wavelength is different for different ϕ. Fig. 64 compares the simulation results with and without radiation wavelength scan. If the wavelength for an error free phase shifter is selected, the result are totally different.

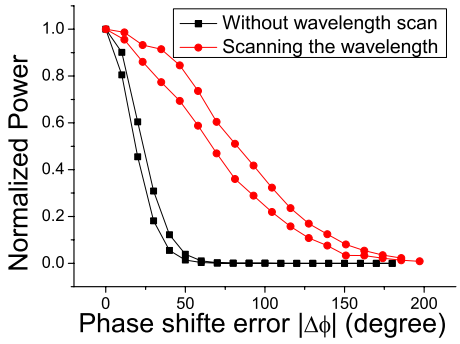

Figure 64: *Illustration of the effect of radiation wavelength scan for the one direction phase error simulation.*

In Fig. 65 the phase shift error calculation result for SASE1 at 0.1 nm is illustrated. For the same phase shift error ϕ, a one directional error reduces the power less (each time adjusting the wavelength) than the alternating power. If the power reduction is shown versus RMS phase shake (on the right), the curves become comparable.

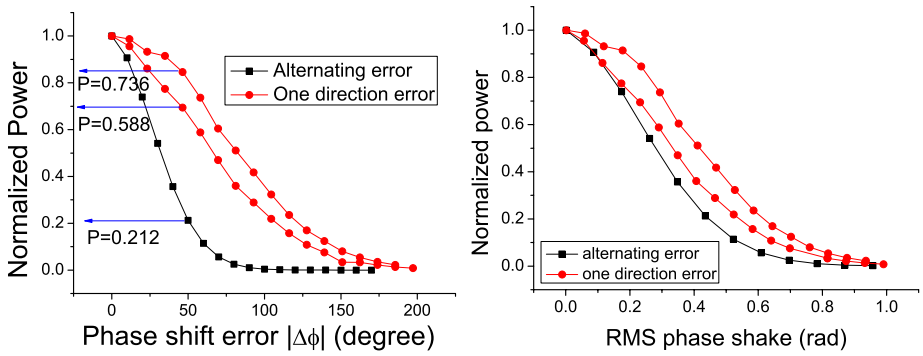

Figure 65: *Comparison of power degradation by one direction and alternating phase shift error. Left: Normalized power against phase error. Right: Normalized power against RMS phase shake.*

Figs. 60 and 63 have shown a wavelength shift for the phase shift in steady state simulations. For time dependent simulations, we choose the phase shift error $\phi = \pm 50^o$ for the one direction and for the alternating error $\phi = 50^o$. Fig. 66 shows the result. Table 2 compares the wavelength shift of time dependent simulation result and the analytical calculation. One can see that the result match.

Then we compare the radiation power by steady-state simulation and time dependent simulation with different phase shift error. From the left plot in Fig. 65 the normalized power of $\phi = 50^o$ or $\phi = -50^o$, one direction error and $\phi = 50^o$, alternating error are respectively 0.736, 0.588 and 0.212. From Fig. 66, the normalized powers are 935, 775 and 316 respectively. Thus, the steady-state and time dependent simulations give similar results.

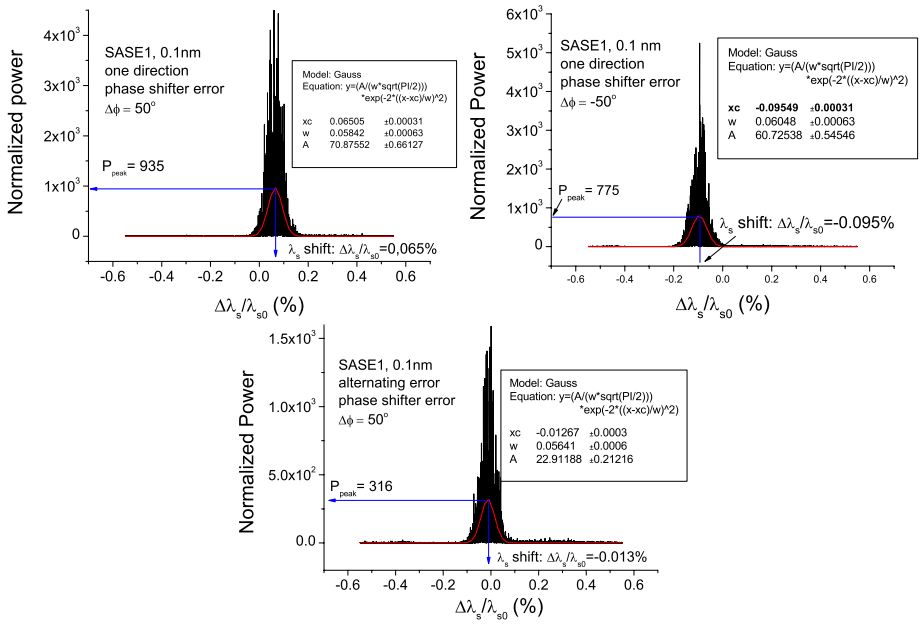

Figure 66: *Time dependent simulation for one direction phase shift error ($\phi = \pm 50^o$) and alternating phase shift error ($\phi = 50^o$)*

Table 2: *Wavelength shift for different phase shift error*

	$\phi = 50^o$ (one direction)	$\phi = -50^o$ (one direction)	$\phi = -50^o$ (alternating)
$\Delta\lambda_s/\lambda_{s0}$ (simulation result)	0.065%	-0.095%	-0.013%
$\Delta\lambda_s/\lambda_{s0}$ (analytical caculation)	0.099%	-0.099%	0

It is also interesting to compare the power degradation by phase shake for the phase shifter error with the periodic errors that have been discussed before. Fig. 67 shows the result. The power degradation by phase shifter error and the other errors is similar.

7.4 Phase shift error simulation result for SASE1 at 0.4 nm and for SASE2.

In this section we list the simulation results for SASE1 at 0.4 nm, SASE2 at 0.1 nm and SASE2 at 0.4 nm by changing electron energy and undulator gap. One can see that the results in this section are similar to the results for SASE1 at 0.1 nm.

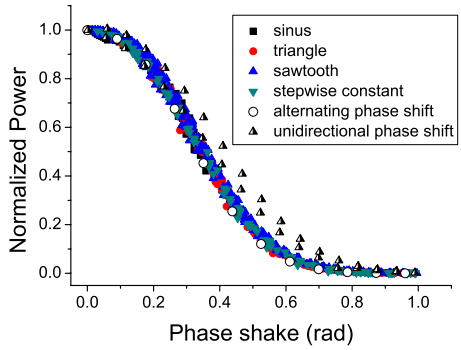

Figure 67: *Comparison of power degradation due to RMS phase shake with different error types.*

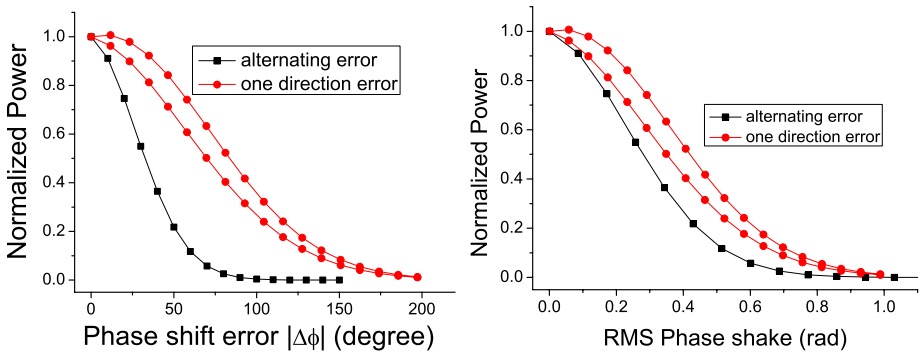

Figure 68: *Comparison of power degradation by one direction and alternating phase shift error for SASE1, 0.4 nm. Left: Normalized power against phase error. Right: Normalized power against RMS phase shake.*

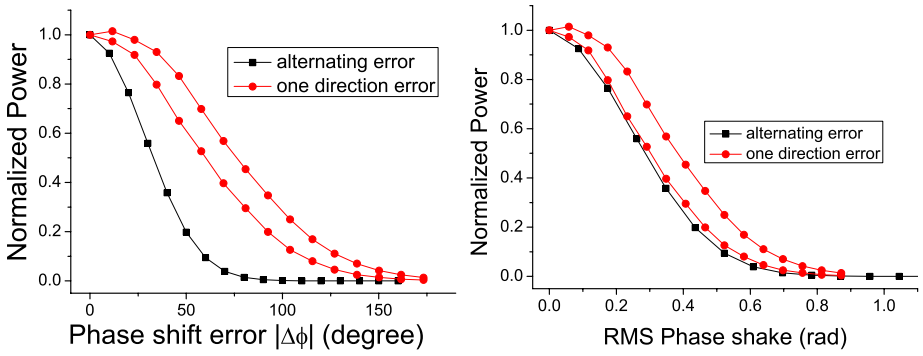

Figure 69: *Comparison of power degradation by one direction and alternating phase shift error for SASE2, 0.1 nm. Left: Normalized power against phase error. Right: Normalized power against RMS phase shake.*

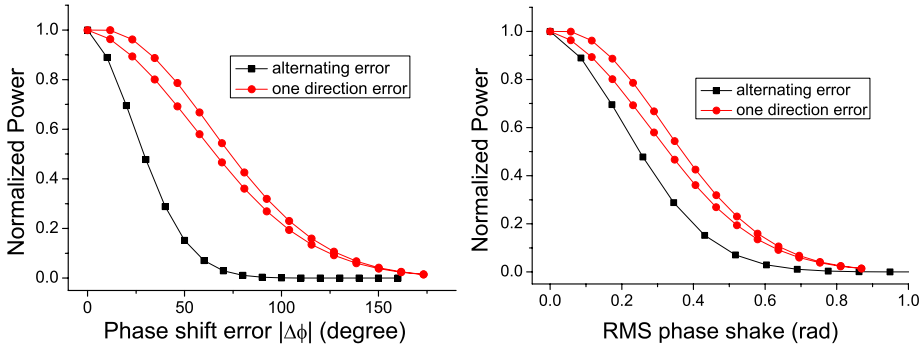

Figure 70: *Comparison of power degradation by one direction and alternating phase shift error for SASE2, 0.4 nm by changing electron energy. Left: Normalized power against phase error. Right: Normalized power against RMS phase shake.*

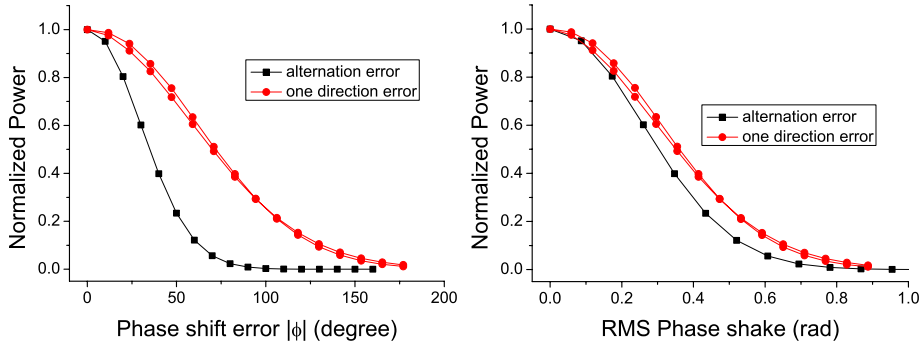

Figure 71: *Comparison of power degradation by one direction and alternating phase shift error for SASE2, 0.4 nm by changing undulator gap. Left: Normalized power against phase error. Right: Normalized power against RMS phase shake.*

8 Error simulation for SASE2

Table 3 lists the parameters for these three operation modes:

Table 3: *SASE2 Parameters*

Wavelength	Electron energy	Energy spread	Undulator period	β-function	K parameter
0.1 nm	17.5 GeV	1.5 MeV	47.9 mm	45 m	2.8
0.4 nm	17.5 GeV	1.5 MeV	47.9 mm	15 m	6.1
0.4 nm	8.75 GeV	1.5 MeV	47.9 mm	15 m	2.8

Because the gap of SASE2 undulator can be adjusted, there are 2 ways to change the wavelength. With 17.5 GeV electron beam, 0.1 nm radiation can be generated for the largest undulator gap and 0.4 nm radiation can be generated by the smallest undulator gap. On the other hand, the longer wavelength 0.4 nm radiation can also be generated

with the largest gap at a lower electron beam energy. Therefore in the simulation for SASE2, three operation modes are: 0.1 nm radiation with largest gap and 17.5 GeV, 0.4 nm radiation with largest gap (smallest K)and change electron energy to 8.75 GeV, 0.4 nm radiation with smallest gap (largest K) and 17.5 GeV electrons. We perform the same simulations as for SASE1. In this section we only list the key plots without the detailed introduction.

8.1 Simulating for SASE2, 0.1 nm mode

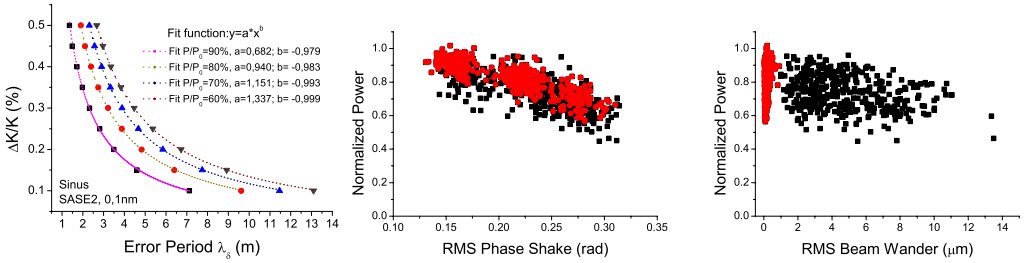

Figure 72: *Results for SASE2 at 0.1 nm. The error distribution is sinus. Left: periodic error distribution showing lines of constant power versus error period and amplitude. Middle: the correlation between the phase shake and the power for random error distributions. The black points show all simulations, the red points the simulations with a beam wander less than 1 μm. Right: the correlation between the beam wander and the power.*

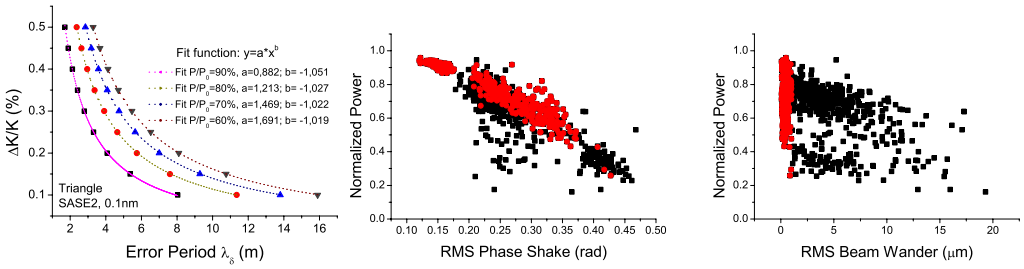

Figure 73: *Results for SASE2 at 0.1 nm. The error distribution is triangle. Left: periodic error distribution showing lines of constant power versus error period and amplitude. Middle: the correlation between the phase shake and the power for random error distributions. The black points show all simulations, the red points the simulations with a beam wander less than 1 μm. Right: the correlation between the beam wander and the power.*

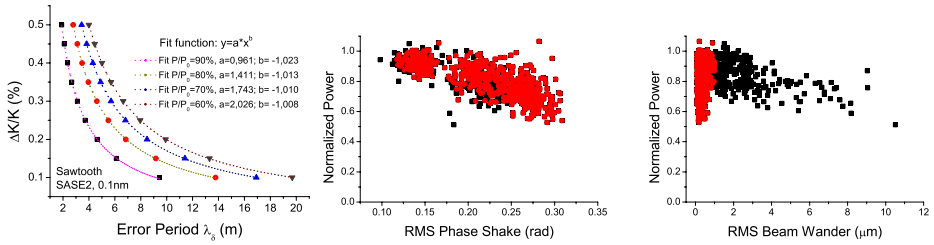

Figure 74: *Results for SASE2 at 0.1 nm. The error distribution is sawtooth. Left: periodic error distribution showing lines of constant power versus error period and amplitude. Middle: the correlation between the phase shake and the power for random error distributions. The black points show all simulations, the red points the simulations with a beam wander less than 1 μm. Right: the correlation between the beam wander and the power.*

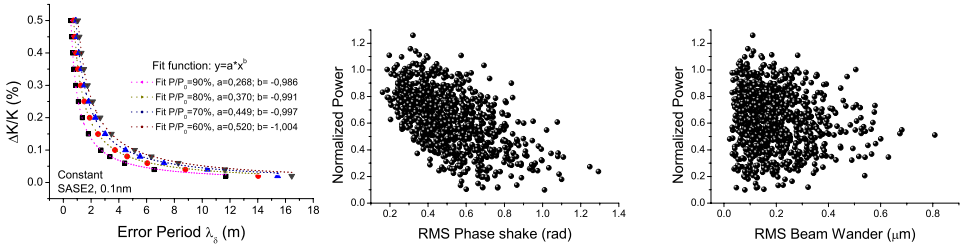

Figure 75: *Results for SASE2 at 0.1 nm. The error distribution is constant. Left: periodic error distribution showing lines of constant power versus error period and amplitude. Middle: the correlation between the phase shake and the power for random error distributions. Right: the correlation between the beam wander and the power.*

8.2 Calculation for 0.4 nm with 17.5 GeV electron beam energy

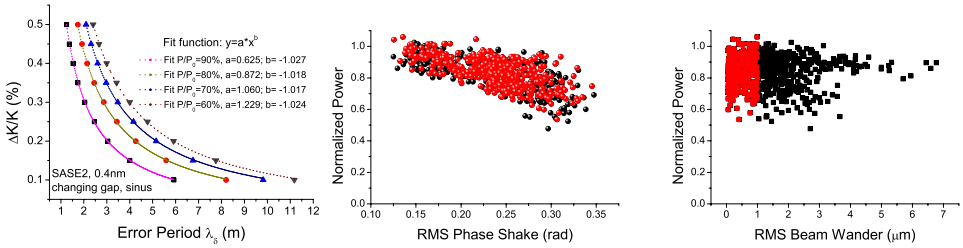

Figure 76: *Results for SASE2 at 0.4 nm. The error distribution is sinus. Left: periodic error distribution showing lines of constant power versus error period and amplitude. Middle: the correlation between the phase shake and the power for random error distributions. The black points show all simulations, the red points the simulations with a beam wander less than 1 μm. Right: the correlation between the beam wander and the power. The wavelength change has been achieved by changing K.*

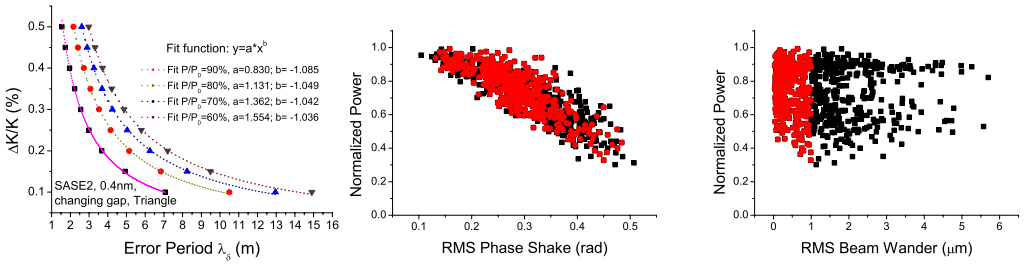

Figure 77: *Results for SASE2 at 0.4 nm. The error distribution is triangle. Left: periodic error distribution showing lines of constant power versus error period and amplitude. Middle: the correlation between the phase shake and the power for random error distributions. The black points show all simulations, the red points the simulations with a beam wander less than 1 μm. Right: the correlation between the beam wander and the power. The wavelength change has been achieved by changing K.*

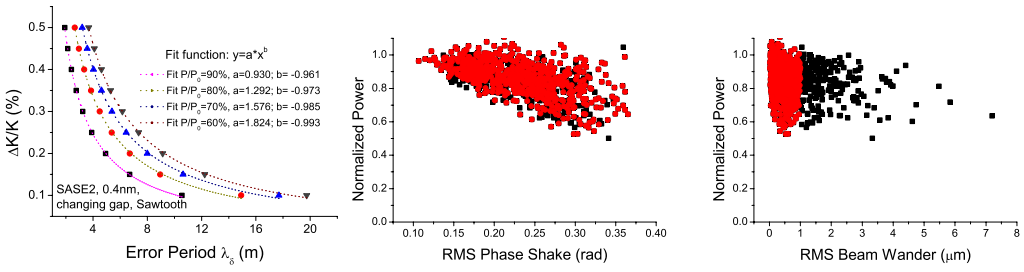

Figure 78: *Results for SASE2 at 0.4 nm. The error distribution is sawtooth. Left: periodic error distribution showing lines of constant power versus error period and amplitude. Middle: the correlation between the phase shake and the power for random error distributions. The black points show all simulations, the red points the simulations with a beam wander less than 1 μm. Right: the correlation between the beam wander and the power. The wavelength change has been achieved by changing K.*

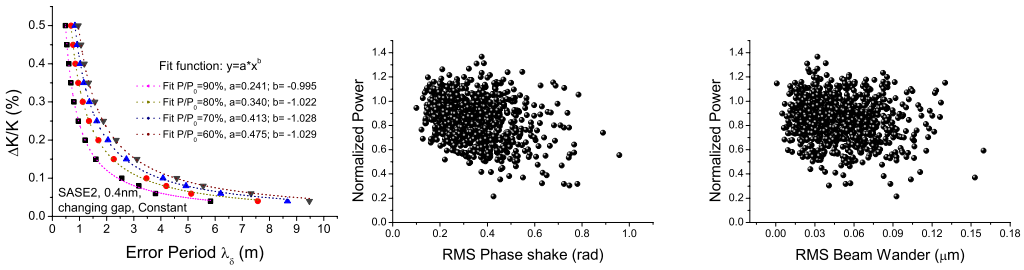

Figure 79: *Results for SASE2 at 0.4 nm. The error distribution is constant. Left: periodic error distribution showing lines of constant power versus error period and amplitude. Middle: the correlation between the phase shake and the power for random error distributions. Right: the correlation between the beam wander and the power. The wavelength change has been achieved by changing K.*

8.3 Calculation for the 0.4 nm for 8.75 GeV electron beam energy

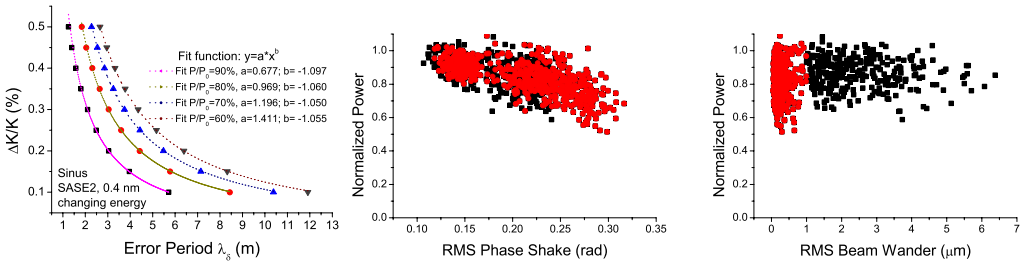

Figure 80: *Results for SASE2 at 0.4 nm. The error distribution is sinus. Left: periodic error distribution showing lines of constant power versus error period and amplitude. Middle: the correlation between the phase shake and the power for random error distributions. The black points show all simulations, the red points the simulations with a beam wander less than 1 μm. Right: the correlation between the beam wander and the power. The wavelength change has been achieved by changing the beam energy.*

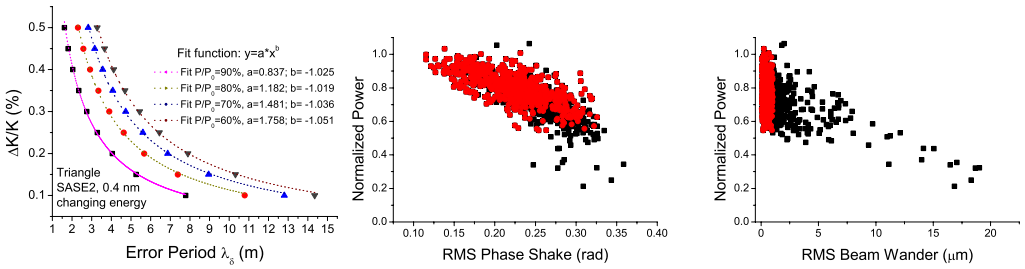

Figure 81: *Results for SASE2 at 0.4 nm. The error distribution is triangle. Left: periodic error distribution showing lines of constant power versus error period and amplitude. Middle: the correlation between the phase shake and the power for random error distributions. The black points show all simulations, the red points the simulations with a beam wander less than 1 μm. Right: the correlation between the beam wander and the power. The wavelength change has been achieved by changing the beam energy.*

8.4 Comparison for 0.1 nm and 0.4 nm of SASE2

In the section for the SASE1 simulation, we compared the error tolerance for 0.1 nm and 0.4 nm. In this section we want to do the same analysis for SASE2. The average beam size of 0.1 nm mode is 42.5 μm, so the Pierce parameter is $\rho = 0.0003857$. The average beam size of 0.4 nm mode by changing gap is 25.5 μm, so $\rho = 0.00091267$, the average beam size of 0.4 nm mode by changing electron energy is 36 μm, so $\rho = 0.0008617$. The 0.1 nm mode has the smallest ρ, its the error tolerance is expected to be the most tight one. Fig. 84 however shows that the error tolerance of 0.1 nm mode is looser than both 0.4 nm results which have larger ρ. By comparing to the corresponding results of SASE1, which matches the evaluation by ρ, the only difference is that in SASE1, both modes

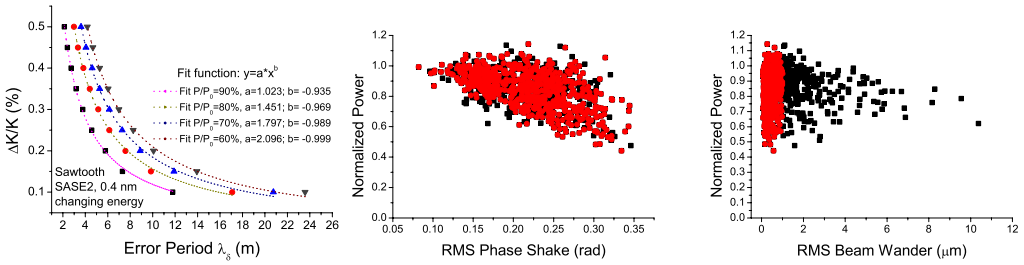

Figure 82: *Results for SASE2 at 0.4 nm. The error distribution is sawtooth. Left: periodic error distribution showing lines of constant power versus error period and amplitude. Middle: the correlation between the phase shake and the power for random error distributions. The black points show all simulations, the red points the simulations with a beam wander less than 1 μm. Right: the correlation between the beam wander and the power. The wavelength change has been achieved by changing the beam energy.*

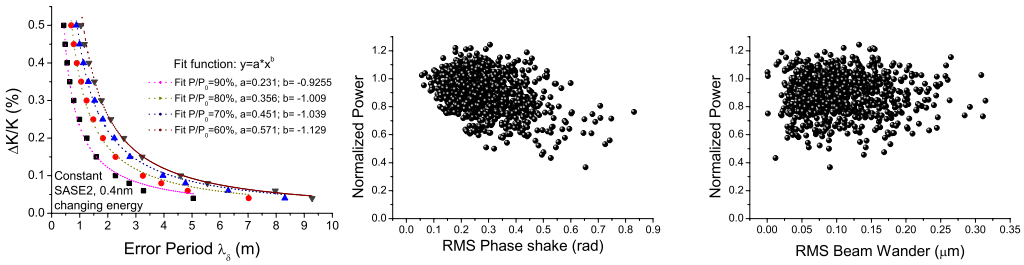

Figure 83: *Results for SASE2 at 0.4 nm. The error distribution is constant. Left: periodic error distribution showing lines of constant power versus error period and amplitude. Middle: the correlation between the phase shake and the power for random error distributions. Right: the correlation between the beam wander and the power. The wavelength change has been achieved by changing the beam energy.*

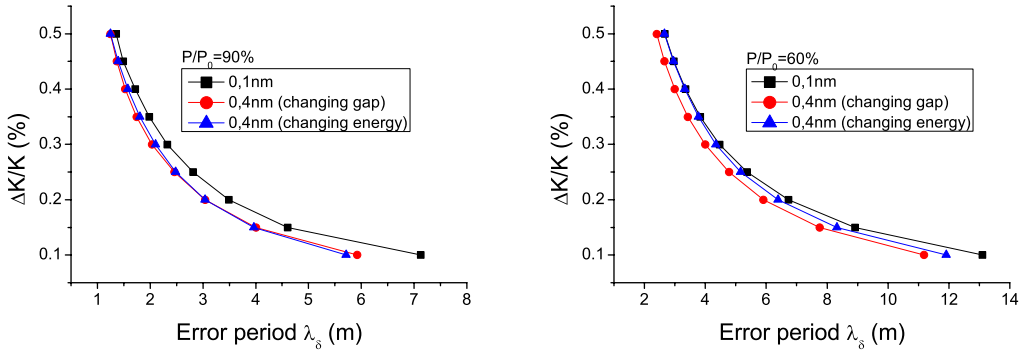

Figure 84: *Comparing the error influence for 0.1 nm and 0.4 nm with sinus error shape. One can see that 0.1 nm has more loose tolerance than 0.4 nm, even though the Pierce parameter of 0.1 nm mode is smaller.*

have the same β function while in SASE2, the β-function is different for 0.1 nm and 0.4 nm: the β-function for 0.1 nm is 45 m while for the 0.4 nm is 15 m.

Therefore in this section, first we change the β-function for 0.1 nm from 45 m to 15 m and compare its error tolerance to the 0.4 nm case and then change the 15 m β-function of 0.4 nm to 45 m to compare the difference in error tolerance.

8.4.1 15 m β-function for 0.1 nm mode

Fig. 85 gives the result without any errors. The saturation length is 161.42 m, the saturation power is 3.5283 GW. The 95% saturation length is 153.35 m, the power at this point is 2.8193 GW. The Pierce parameter is $\rho = 0.00055$.

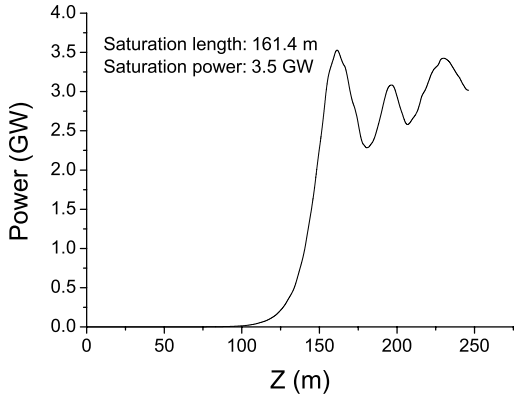

Figure 85: *Power growth for SASE2 0.1 nm mode without error with beta function 15 m.*

Fig. 86 shows the lines of constant power degradation with different error strength and error period. Fig. 87 gives the error tolerance comparing 0.1 nm to 0.4 nm. The tolerance for 0.1 nm is more tough than 0.4 nm and this consistent to the analysis that a larger Pierce parameter brings looser tolerance.

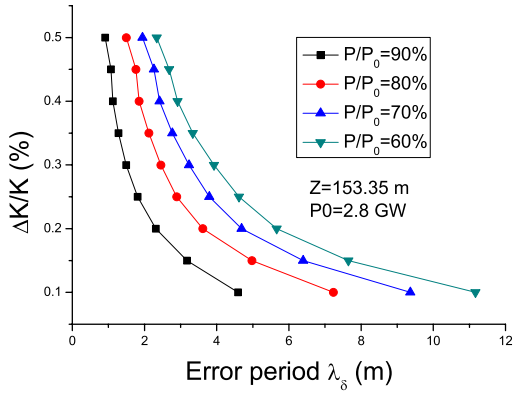

Figure 86: *Impact of error period and strength to the power (SASE2, 0.1 nm with 15 m β-function.*

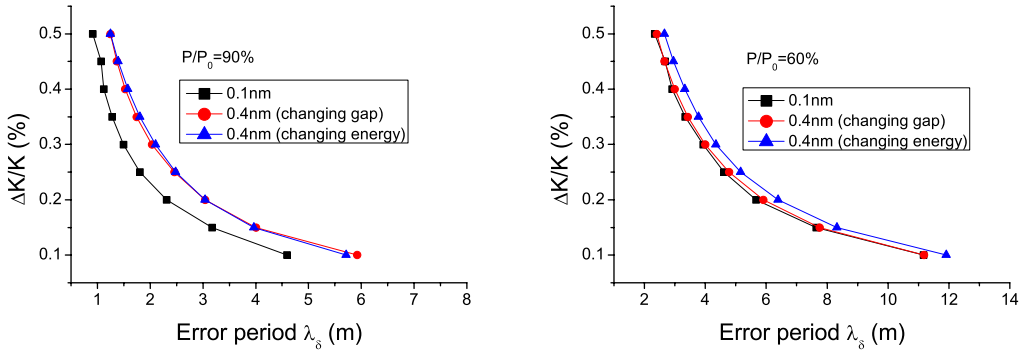

Figure 87: *Comparing the error impact on the power for different wavelengths for SASE2 (The β-function is 15 m for all). One can see the tolerance of 0.1 nm mode is tight which correspond to the analysis that larger Pierce parameter requires looser tolerance.*

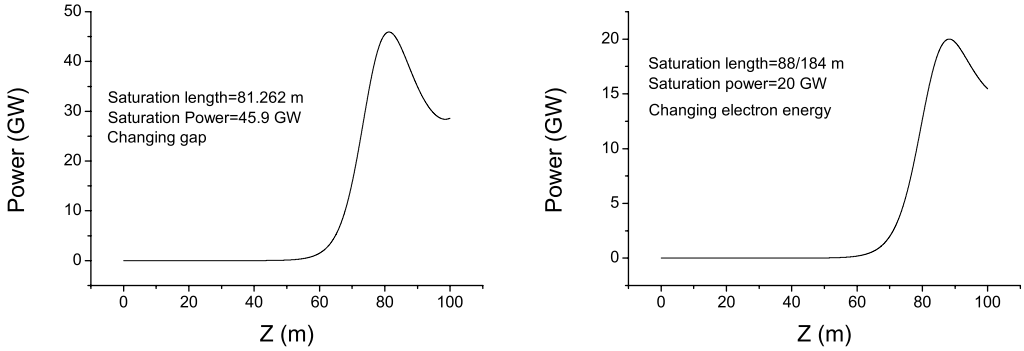

Figure 88: *Power development for 0.4 nm mode without error with β-function 45 m (Left: changing gap, right: changing electron energy).*

8.4.2 45 m β-function for 0.4 nm

In this section we fix the β-function both of 0.1 nm and 0.4 nm to 45 m. The Pierce parameter ρ is 0.0003857, 0.0006676 and 0.0006276 respectively for the modes of 0.1 nm, 0.4 nm by changing gap and 0.4 nm by changing electron energy.

Fig. 88 illustrates the power growth for 0.4 nm for ideal undulator. For the 17.5 GeV electron energy and the smallest undulator gap, the saturation length is 81.26 m and the saturation power is 45.92 GW; for 8.75 GeV electron energy and largest undulator gap, the saturation length is 88.18 m and the saturation power is 20.01 GW. Fig. 89 shows the simulation result for 0.4 nm with 45 m β-function. Fig. 90 shows the error tolerance comparing for 0.1 nm and 0.4 nm. One can see from Fig. 90 that the tolerance is more serious for 0.1 nm, which is consistent to the argument that smaller Pierce parameter brings tougher tolerance. However, for 0.4 nm the tolerance by changing gap is tougher than by changing energy, even though the Pierce parameter by changing gap is larger.

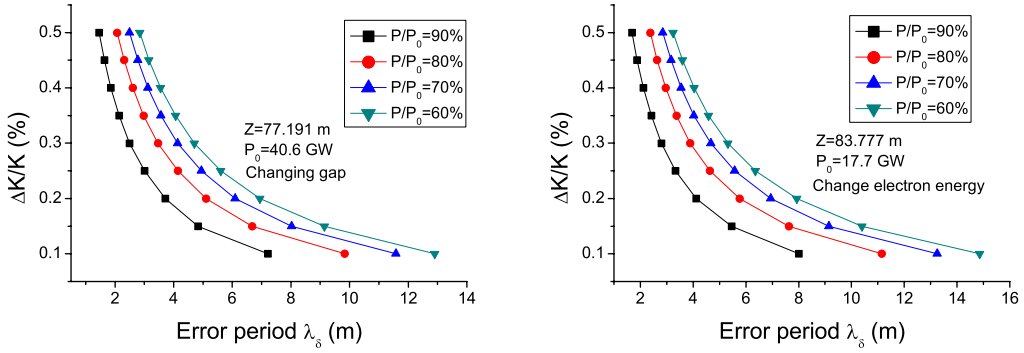

Figure 89: *error impact to the power for 0.4 nm mode with β-function 45 m (Left: changing gap, right: changing electron energy).*

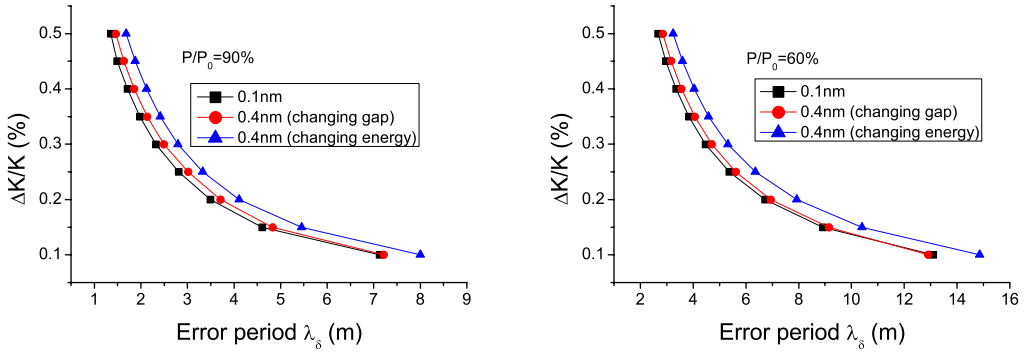

Figure 90: *Comparing the error impact to the power under different wavelength for SASE2 (The β-function is 45 m for all).*

Appendix A: Difference between simulations

By the fitting plots such as Fig. 30, the undulator error tolerance for SASE1 and SASE2 with different operation modes can be evaluated. Table 4 lists the number for the European XFEL undulator structure.

Table 4: *Tolerance levels for SASE 1 and SASE2 at 0.1 and 0.4 nm resulting in a power reduction of 10%. The deformation length in this table are the ones consistent with the present design.*

Type	λ_s	**rms phase shake**	λ_δ	$\Delta K/K$	Δg **(mm)**	ΔT (^oC)
SASE1, sinus	0.1nm	0.146	1.2m	0.366%	0.030	3.66
SASE1, triangle	0.1nm	0.156	10m	0.058%	0.005	0.58
SASE1, saw	0.1nm	0.165	5m	0.148%	0.013	1.48
SASE1, constant	0.1nm	0.183	5m	0.043%	0.004	0.43
SASE1, sinus (energy change)	0.4nm	0.200	1.2m	0.501%	0.042	5.01
SASE1, triangle (energy change)	0.4nm	0.199	10m	0.074%	0.006	0.74
SASE1, sawtooth (energy change)	0.4nm	0.199	5m	0.179%	0.015	1.79
SASE1, constant (energy change)	0.4nm	0.203	5m	0.048%	0.004	0.48
SASE2, sinus	0.1nm	0.160	1.2m	0.571%	0.071	5.71
SASE2, triangle	0.1nm	0.149	10m	0.078%	0.001	0.78
SASE2, saw	0.1nm	0.144	5m	0.185%	0.023	1.85
SASE2, constant	0.1nm	0.167	5m	0.055%	0.007	0.55
SASE2, sinus (gap change)	0.4nm	0.174	1.2m	0.518%	0.056	5.18
SASE2, triangle (gap change)	0.4nm	0.153	10m	0.068%	0.007	0.68
SASE2, saw (gap change)	0.4nm	0.184	5.0m	0.198%	0.021	1.98
SASE2, constant (gap change)	0.4nm	0.174	5.0m	0.049%	0.005	0.49
SASE2, sinus (energy change)	0.4nm	0.156	1.2m	0.554%	0.069	5.54
SASE2, triangle (energy change)	0.4nm	0.151	10m	0.079%	0.010	0.79
SASE2, sawtooth (energy change)	0.4nm	0.177	5.0m	0.227%	0.028	2.27
SASE2, constant (energy change)	0.4nm	0.152	5.0m	0.052%	0.006	0.52

Appendix B: Discussion on the influence of position choice of the point of evaluation

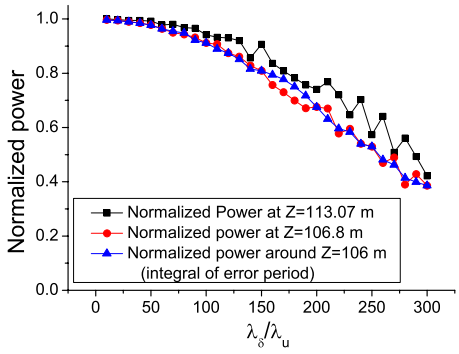

Figure 91: *The normalized power when evaluated for SASE1 at 113.07 m (Black points, corresponding to 95% of the saturation length), at 106.8 m (Red points, corresponding to 90% of the saturation length) and at a position close to 106.8 m which is an exact multiple of the deformation length (Blue points).*

For the evaluation of the error impact on the FEL performance, we have chosen a position along the undulator before saturation is reached, namely 95% of the saturation length. The main reason to choose this method has been explained in Sec. 4.3. Here we address the issue why to take this position along the undulator and not another. For this, one has to consider the following. In order to be able to compare to linear theory, one has to take a value away from saturation (in the exponential gain regime). One can take the points which coincides with 95% of the saturation length, as done in this report, or 90%. The actual choice is to large extent arbitrary. Because the power growth will oscillate along a deformation length, one should in principle always take a point which is a multiple of this deformation length in order to avoid artefacts in the results. Since this would make automation of the procedure difficult, this has not been done. In Fig. 91, these three different options are illustrated. The black squares show the nomalized power at the original 95% of the saturation length, which is $z = 113.07\,\mathrm{m}$ for different error periods. The red point also shows the normalized power but the position is changed to a shorter length which is 90% of the saturation length: $z = 106.8\,\mathrm{m}$. The blue triangle shows the normalized power at the position around $z = 106.8\,\mathrm{m}$ but the length changes to an integer times the error period λ_δ. First it can be seen from Fig. 91 that the normalized power at position of 106.8 m is smaller than the normalized power at 113.07 m. This maybe because at 95% of the saturation length, non-linear effects due to energy loss of the beam already start to play a role. Another interesting thing is that we can see that at the large λ_δ range, the normalized power oscillates as the λ_δ increases, while the oscillation of the red points is much weaker and for the blue curve it is almost gone. Because the curves in the end will be fitted, the oscillations are averaged out of the final results. The remaining deviations are small and do not effect the general results.

Appendix C: Discussion on the relatively large spread in power for random errors

Fig. 32 and similar plots showing the power reduction due to random error distributions have a larger variation in power than those for the periodic error distribution. Even though there is a clear correlation with the same average power reduction for the same RMS phase shake, in this section we try to find some reasons for this.

1. Analysis for the sinus error

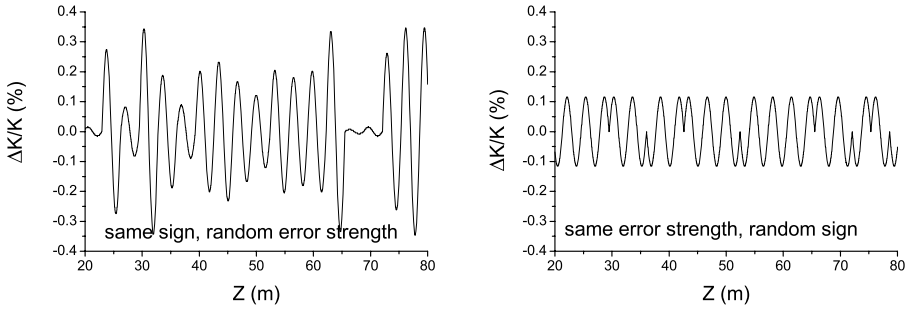

Figure 92: *Two special cases of random sinus errors. Left: random error strength for a constant, positive sign of the sinus. Right: random sign but same error strength for each sinus period.*

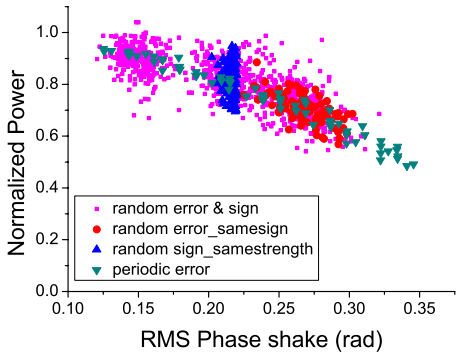

Figure 93: *Four different correlations between phase shake and power for a sinus eror distribution: periodic error (green triangle), random with error strength and sign (pink square), random error strength and same sign (red circle), random sign and same error strength (blue triangle). One can see that the random error simulation has worse correlation than the periodic error. Both the random strength and random coefficient sign can degrade the correlation between phase shake and power, and the random sign has even more influence.*

Fig. 92 shows two kinds of random sinus error. On the left the error strength differs randomly while the sign of the sinus is always the same. On the right the absolute error strength is the same but the sign is random. Both of these random errors generate phase shake. We analyze the two kinds of random sinus error separately.

Fig. 93 compares four different correlations of phase shake and power: periodic simulation, random error both with error strength and sign, random error strength and same sign, random sign and same error strength. Comparing the spread in the case of the same sign, which is shown by red points, to the spread of periodic and totally random simulations, one can see that altough the spread is still larger than the periodic simulation, it is smaller than that of totally random simulation. We are more interested in the result of random sign but same error strength because the rms phase shake value concentrates around a certain value and the spread is large. So we carefully compare these simulation results to the periodic results. Therefore, we choose 61 periodic sinus error points where the phase shake is around 0.22 rad, and calculate the power. The result is showed in Fig. 94. The radiation power spread is still small than the random error result.

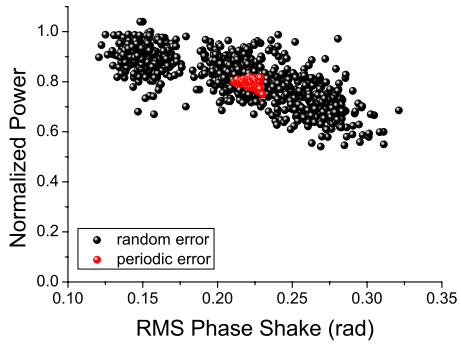

Figure 94: *Comparison of correlation of phase shake and power by periodic error and random error simulation. This time the periodic error phase shake is fixed around 0.22 radians.*

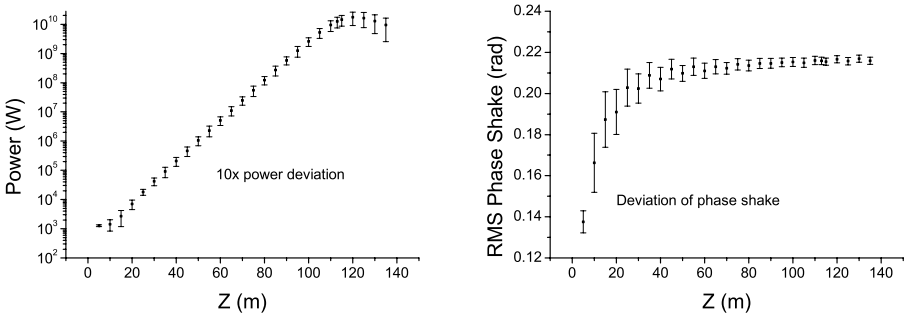

Figure 95: *Mean value and variation range of power and phase shake at different position for 100 random simulations with sign but the same strength.*

Then we compare the simulation the blue points in Fig. 93 and the red point in Fig.94. This time the power and rms phase shake at different position along the undulator are illustrated. The rms phase phase shake at each point is calculated out by the undulator parameter which is from the begining of the undulator to the choosen point. By comparing the results shown in Figs. 95 96 one can see that at each point the spread of random error is larger than that of periodic error. By comparing the rms phase shake distribution, the spread of rms phase shake is homogeneous at each point for the periodic error. For the random error, the spread in rms phase shake is large at the the first several

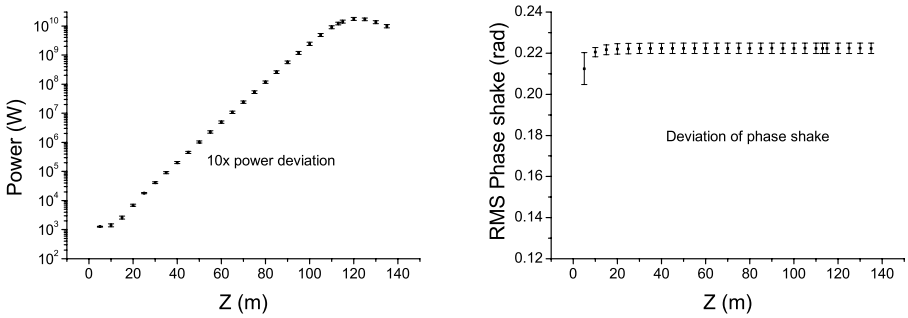

Figure 96: *Mean value and variation range of power and phase shake at different position for 61 periodic sinus error simulation.*

points, at the longer distance along the undulator, the spread is small and close to the spread of periodic error. It seems that at the beginning of the undulator, the spread is large because the phase shake changes significantly for different random simulations. We assume that the local rms phase shake plays an important role for the spread when the deformation length becomes comparable to the 3D gain length of SASE1 (7.96 m). The error period λ_δ utilized in Fig. 95 is 3.2 m. Consequently, there is a large phase shake within a gain length.

To test this assumption, we make the error period λ_δ from 3.2 m to 0.32 m. So in one gain length, enough error periods are included. To guarantee the rms phase shake is the same, we increase the error strength ten times larger. The simulation result is illustrated in Fig. fig:39. One can see that the power spread of this shorter λ_δ is close to the value of periodic error.

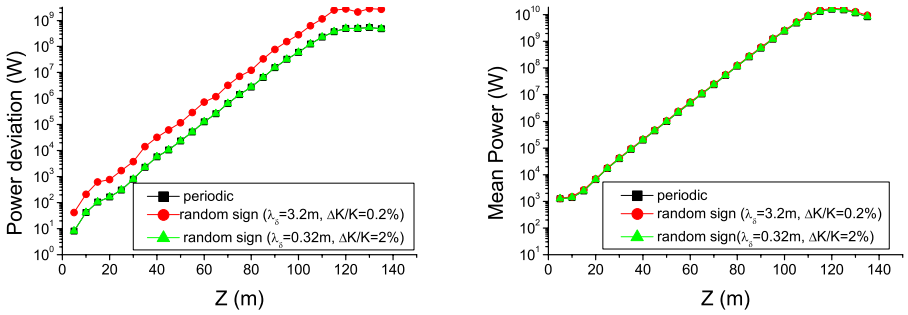

Figure 97: *Comparison of mean power and power deviation for a periodic and random sinus error. Black: periodic error; Red: random sign but same strength* $\lambda_\delta = 3.2\,m, \Delta K/K = 0.2\%$*; Green: random sign but same strength* $\lambda_\delta = 0.32m, \Delta K/K = 2\%$*. One can see that the mean values are close to each other because the phase shake is similar, but the power spreads are different. The random sign error with longer error period has larger values.*

2. Brief analysis of triangle error

Similar to the analysis for sinus error, we also divide the random error into to two random types: constant sign with random error strength and constant error strength with random sign. Fig. 98 shows the different error.

One can see that in Fig. 98, for the same absolute error strength and random error sign, the power spread is very small. We can explain this that if the absolute error strength is same, no matter how the sign is, the rms phase shake is homogenous for each period. Thus in the range of one gain length, the rms phase shake is also homogeneous.

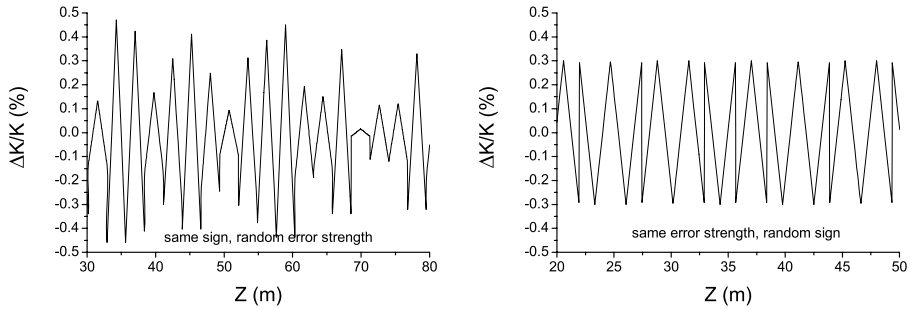

Figure 98: *Two random triangle error types. Left: random error strength for different error period, but he sign is the same. Right: random sign but same error strength for different period.*

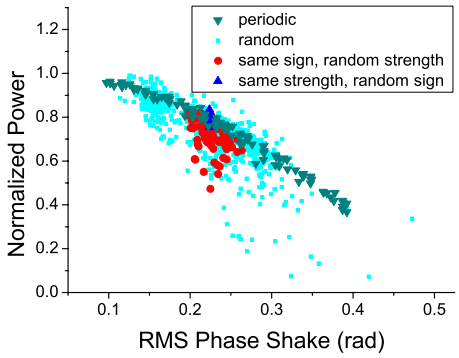

Figure 99: *Four different correlation of phase shake and power for a triangle error: periodic simulation (green triangle), random with error strength and sign (pink square), random error strength and same sign (red circle), random sign and same error strength (blue triangle). One can see that the random error simulation has worse correlation than the periodic error simulation, while random sign doesn't degrade the correlation between phase shake and power, the main reason is random error strength.*

3. Brief analysis of sawtooth error

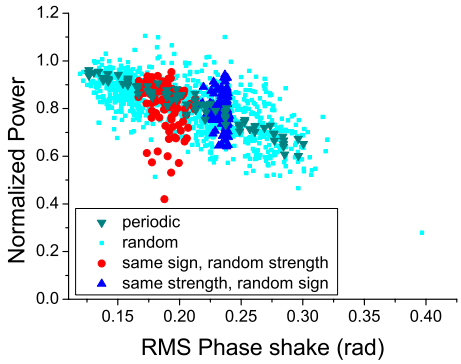

Figure 100: *Four different correlations of phase shake and power for a sawtooth error: periodic simulation (green triangle), random with error strength and sign (pink square), random error strength and same sign (red circle), random sign and same error strength (blue triangle). One can see that the random error simulation has worse correlation than the periodic error simulation, while random sign doesn't degrade the correlation of phase shake and power.*

Appendix D: Details for the random error simulation for different error types

In the sections before for the random error simulation, we only show the plot of correlation of power degradation and rms phase shake. As it has been mentioned, for each kind of error type, we choose 9 combinations of $\Delta K/K$ and λ_δ which contribute three different power degradation: P/P_0=90%, 80%, 70%. Thus for each radiation power degradation, three combinations of $\Delta K/K$ and λ_δ are simulated and for each combination, we calculate the result of 100 random error distributions. The detailed results for each of these simulations are shown in this appendix.

Table 5: *Result presented in this appendix*

Number	Undulator	Wavelength (nm)	Error shape	K or Energy change
1	SASE1	0.1	sinus	
2	SASE1	0.1	triangle	
3	SASE1	0.1	sawtooth	
4	SASE1	0.4	sinus	Energy
5	SASE1	0.4	triangle	Energy
6	SASE1	0.4	sawtooth	Energy
7	SASE2	0.1	sinus	
8	SASE2	0.1	triangle	
9	SASE2	0.1	sawtooth	
10	SASE2	0.4	sinus	K
11	SASE2	0.4	triangle	K
12	SASE2	0.4	sawtooth	K
13	SASE2	0.4	sinus	Energy
14	SASE2	0.4	triangle	Energy
15	SASE2	0.4	sawtooth	Energy

1. SASE1 at 0.1 nm for a sinus error

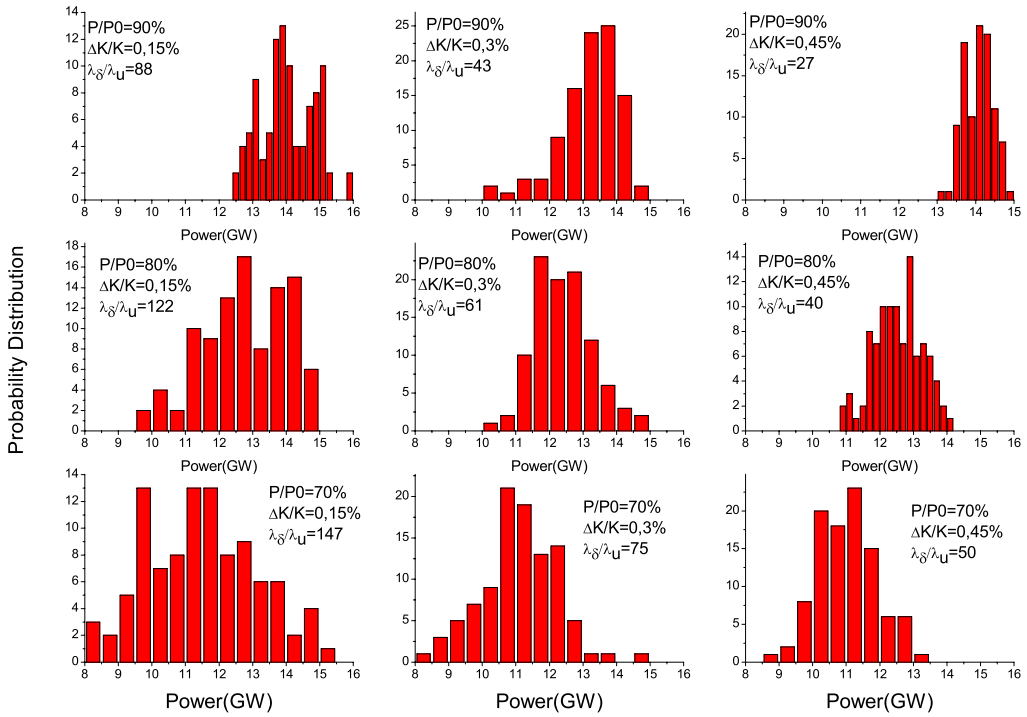

Figure 101: *Results of simulations for SASE1 at 0.1 nm wavelength for a random sinus error distribution. The results from left to right correspond to the same power level of 90% (top), 80% (middle) and 70% (bottom) with increasing error level $\Delta K/K$ or decreasing deformation length λ_δ such that the rms phase shake according to Eq. (17) is constant.*

Table 6: *Summary of the results shown in the Figure above. The rows correspond to the results read from left to right (long to short deformation length, which is equivalent to small to large $\Delta K/K$) and top to bottom (90%, 80% and 70% of the power expected at this position without undulator errors).*

$\Delta K/K$	λ_δ/λ_u	P (GW) Constant	$\overline{P}$ (GW) Mean power	σ_P/P	σ_K	σ_ϕ
0.15%	88	13.763	14.03	5.66%	0.00145	0.156
0.3%	43	13.763	13.191	6.65%	0.00286	0.157
0.45%	27	13.763	14.065	2.69%	0.00429	0.144
0.15%	147	12.234	12.749	9.82%	0.00145	0.216
0.3%	61	12.234	12.406	7.22%	0.00286	0.216
0.45%	40	12.234	12.538	5.74%	0.00428	0.213
0.15%	147	10.704	11.500	14.19%	0.00146	0.260
0.3%	75	10.704	11.110	9.97%	0.00286	0.266
0.45%	50	10.704	11.023	7.96%	0.00429	0.266

2. SASE1 at 0.1 nm for a triangle error

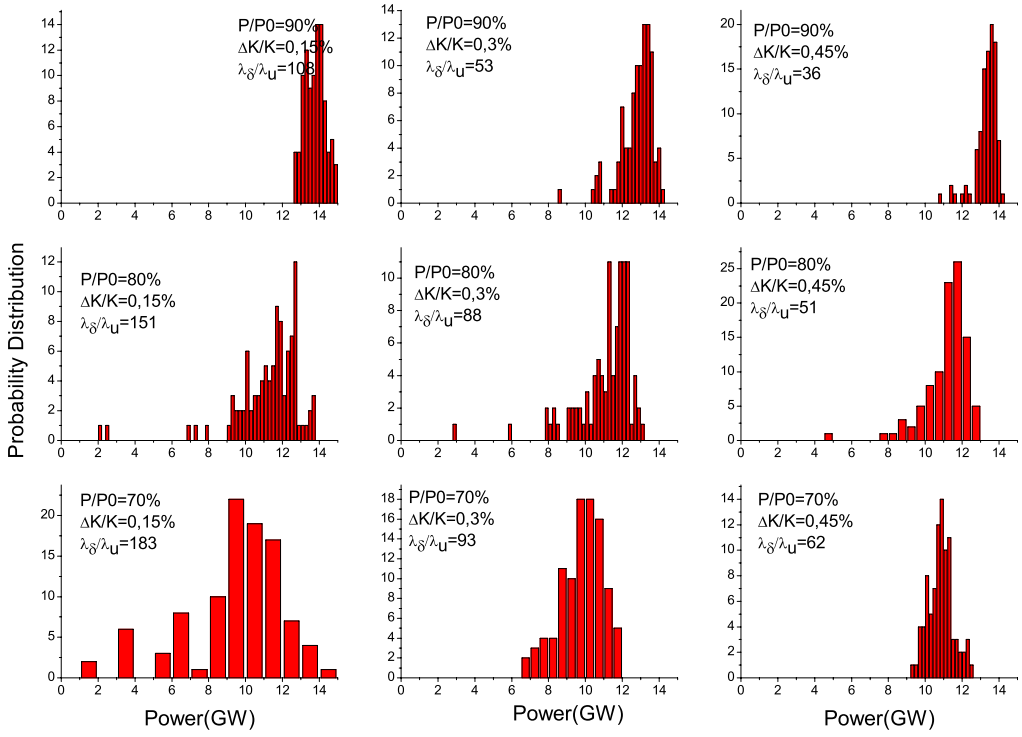

Figure 102: *Results of simulations for SASE1 at 0.1 nm wavelength for a random triangle error distribution. The results from left to right correspond to the same power level of 90% (top), 80% (middle) and 70% (bottom) with increasing error level $\Delta K/K$ or decreasing deformation length λ_δ such that the rms phase shake according to Eq. (17) is constant.*

Table 7: *Summary of the results shown in the Figure above. The rows correspond to the results read from left to right (long to short deformation length, which is equivalent to small to large $\Delta K/K$) and top to bottom (90%, 80% and 70% of the power expected at this position without undulator errors).*

$\Delta K/K$	λ_δ/λ_u	P (GW) Constant	$\overline{P}$ (GW) Mean power	σ_P/P	σ_K	σ_ϕ
0.15%	108	13.763	13.787	4.12%	0.002	0.157
0.3%	53	13.763	12.798	7.18%	0.004	0.164
0.45%	36	13.763	13.333	4.40%	0.006	0.159
0.15%	151	12.234	11.264	16.45%	0.002	0.242
0.3%	88	12.234	11.096	13.94%	0.004	0.232
0.45%	51	12.234	11.154	10.70%	0.006	0.236
0.15%	183	10.704	9.447	28.42%	0.002	0.296
0.3%	93	10.704	9.808	11.91%	0.004	0.269
0.45%	62	10.704	10.837	6.14%	0.006	0.269

3. SASE1 at 0.1 nm for a sawtooth error

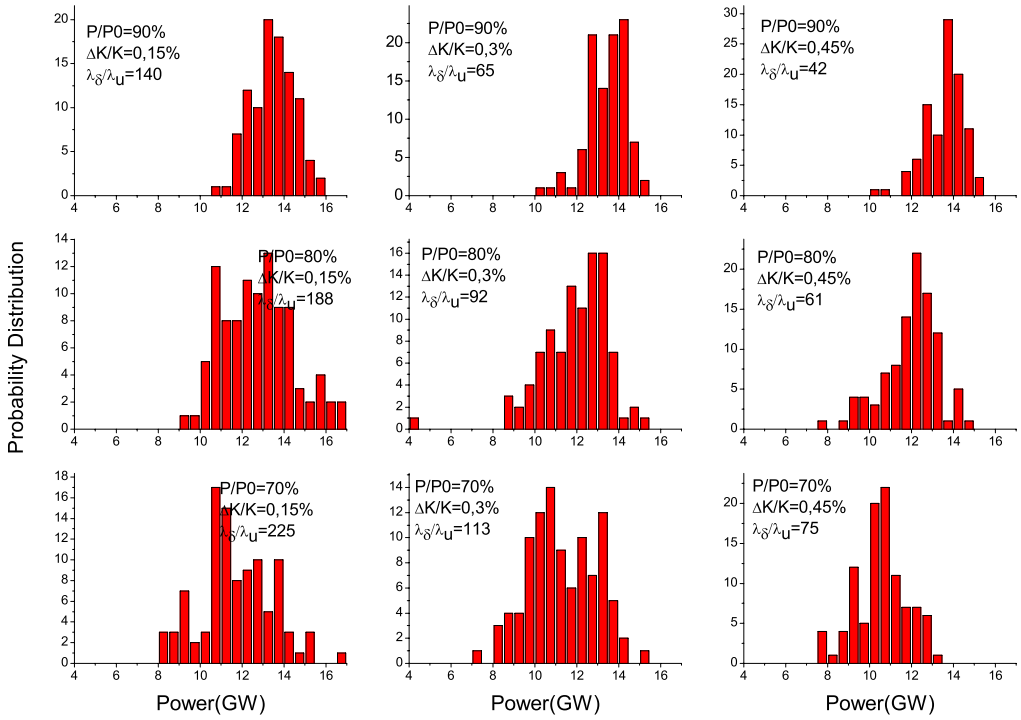

Figure 103: *Results of simulations for SASE1 at 0.1 nm wavelength for a random sawtooth error distribution. The results from left to right correspond to the same power level of 90% (top), 80% (middle) and 70% (bottom) with increasing error level $\Delta K/K$ or decreasing deformation length λ_δ such that the rms phase shake according to Eq. (17) is constant.*

Table 8: *Summary of the results shown in the Figure above. The rows correspond to the results read from left to right (long to short deformation length, which is equivalent to small to large $\Delta K/K$) and top to bottom (90%, 80% and 70% of the power expected at this position without undulator errors).*

$\Delta K/K$	λ_δ/λ_u	P (GW) Constant	$\overline{P}$ (GW) Mean power	σ_P/P	σ_K	σ_ϕ
0.15%	140	13.763	13.440	7.82%	0.00086	0.164
0.3%	65	13.763	13.442	7.16%	0.00165	0.158
0.45%	42	13.763	13.550	6.89%	0.00246	0.155
0.15%	188	12.234	12.728	13.16%	0.00085	0.216
0.3%	92	12.234	11.941	13.20%	0.00166	0.233
0.45%	61	12.234	11.954	10.73%	0.00246	0.218
0.15%	225	10.704	11.748	14.62%	0.00086	0.257
0.3%	113	10.704	11.298	14.25%	0.00166	0.265
0.45%	75	10.704	10.560	11.39%	0.00247	0.266

4. SASE1 at 0.4 nm for a sinus error

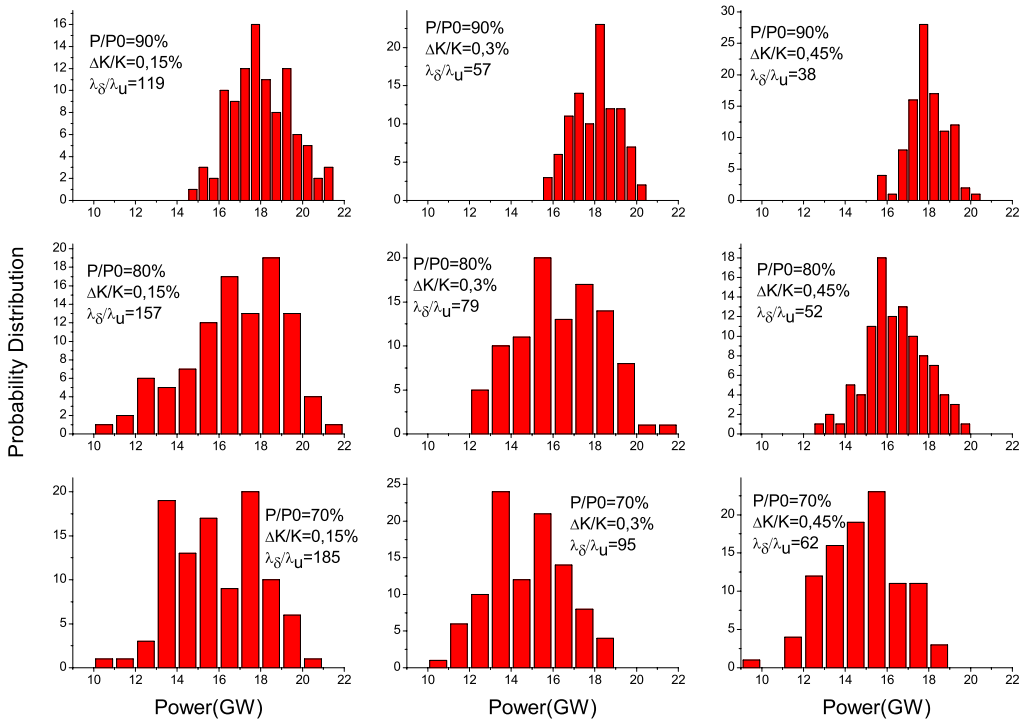

Figure 104: *Results of simulations for SASE1 at 0.4 nm wavelength for a random sinus error distribution. The results from left to right correspond to the same power level of 90% (top), 80% (middle) and 70% (bottom) with increasing error level $\Delta K/K$ or decreasing deformation length λ_δ such that the rms phase shake according to Eq. (17) is constant.*

Table 9: *Summary of the results shown in the Figure above. The rows correspond to the results read from left to right (long to short deformation length, which is equivalent to small to large $\Delta K/K$) and top to bottom (90%, 80% and 70% of the power expected at this position without undulator errors).*

$\Delta K/K$	λ_δ/λ_u	P (GW) Constant	$\overline{P}$ (GW) Mean power	σ_P/P	σ_K	σ_ϕ
0.15%	119	17.843	18.041	7.92%	0.00147	0.209
0.3%	57	17.843	18.039	6.05%	0.00288	0.202
0.45%	38	17.843	17.957	4.89%	0.00428	0.202
0.15%	157	15.860	16.778	14.08%	0.00147	0.273
0.3%	79	15.860	16.387	12.81%	0.00289	0.280
0.45%	52	15.860	16.433	8.85%	0.00429	0.276
0.15%	185	13.878	15.908	13.24%	0.00147	0.324
0.3%	95	13.878	14.730	12.76%	0.00289	0.335
0.45%	62	13.878	14.823	12.35%	0.00430	0.330

5. SASE1 at 0.4 nm for a triangle error

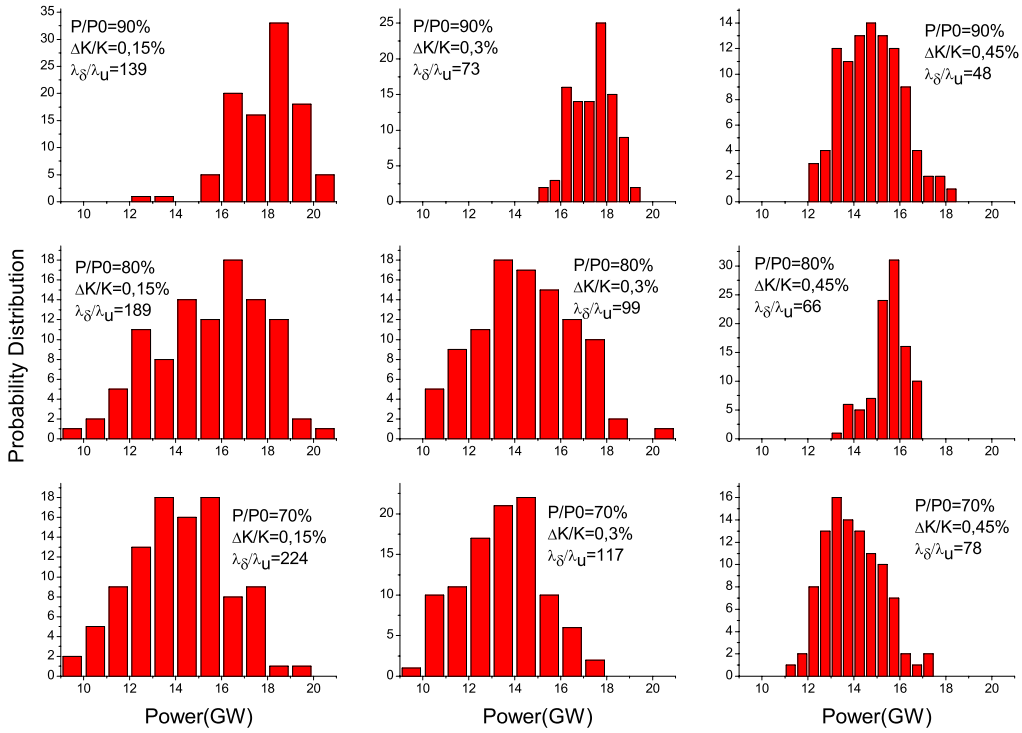

Figure 105: *Results of simulations for SASE1 at 0.4 nm wavelength for a random triangle error distribution. The results from left to right correspond to the same power level of 90% (top), 80% (middle) and 70% (bottom) with increasing error level $\Delta K/K$ or decreasing deformation length λ_δ such that the rms phase shake according to Eq. (17) is constant.*

Table 10: *Summary of the results shown in the Figure above. The rows correspond to the results read from left to right (long to short deformation length, which is equivalent to small to large $\Delta K/K$) and top to bottom (90%, 80% and 70% of the power expected at this position without undulator errors).*

$\Delta K/K$	λ_δ/λ_u	P (GW) Periodic	$\overline{P}$ (GW) Mean power	σ_P/P	σ_K	σ_ϕ
0.15%	139	17.843	17.960	8.18%	0.00205	0.207
0.3%	73	17.843	17.401	5.09%	0.004	0.215
0.45%	48	17.843	14.792	8.83%	0.0061	0.304
0.15%	189	15.860	15.475	14.86%	0.00206	0.288
0.3%	99	15.860	14.513	14.20%	0.00407	0.371
0.45%	66	15.860	15.515	5.16%	0.00604	0.288
0.15%	224	13.878	14.146	14.57%	0.00206	0.328
0.3%	117	13.878	13.446	13.46%	0.00406	0.344
0.45%	78	13.878	13.965	8.94%	0.00603	0.340

6. SASE1 at 0.4 nm for a sawtooth error

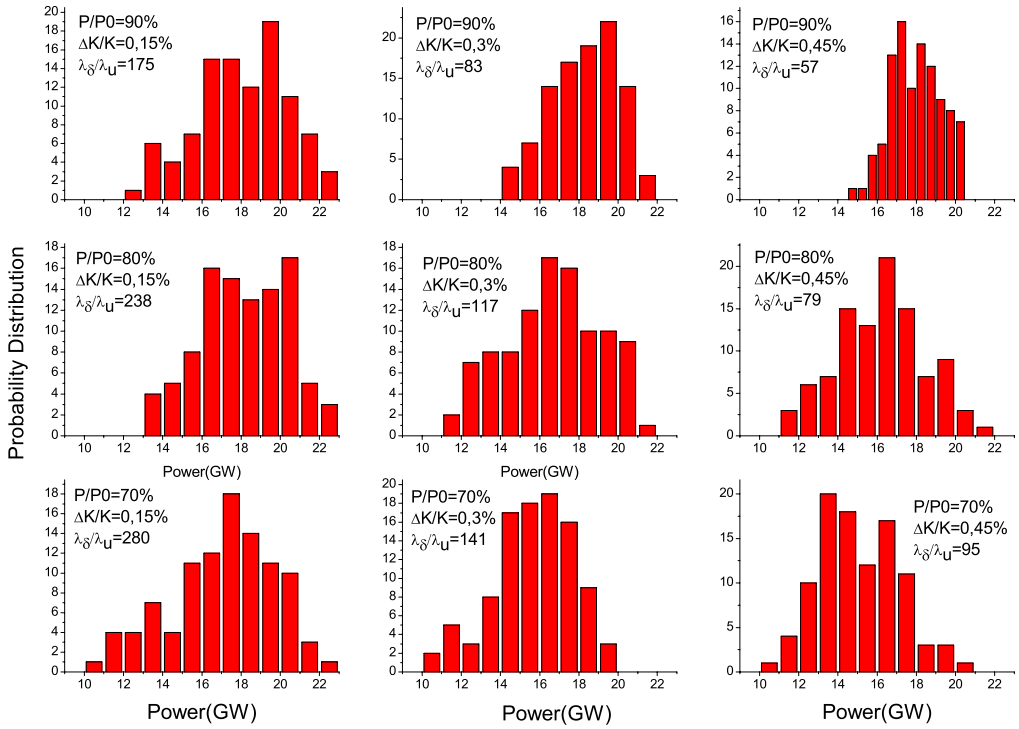

Figure 106: *Results of simulations for SASE1 at 0.4 nm wavelength for a random sawtooth error distribution. The results from left to right correspond to the same power level of 90% (top), 80% (middle) and 70% (bottom) with increasing error level $\Delta K/K$ or decreasing deformation length λ_δ such that the rms phase shake according to Eq. (17) is constant.*

Table 11: *Summary of the results shown in the Figure above. The rows correspond to the results read from left to right (long to short deformation length, which is equivalent to small to large $\Delta K/K$) and top to bottom (90%, 80% and 70% of the power expected at this position without undulator errors).*

$\Delta K/K$	λ_δ/λ_u	P (GW) Periodic	$\overline{P}$ (GW) Mean power	σ_P/P	σ_K	σ_ϕ
0.15%	175	17.843	18.058	13.09%	0.00089	0.200
0.3%	83	17.843	18.287	9.30%	0.00168	0.194
0.45%	57	17.843	17.955	7.08%	0.00249	0.199
0.15%	238	15.860	18.141	11.84%	0.00089	0.265
0.3%	117	15.860	16.732	14.72%	0.00168	0.271
0.45%	79	15.860	16.202	13.64%	0.00249	0.277
0.15%	280	13.878	17.089	15.39%	0.00089	0.304
0.3%	141	13.878	15.691	13.03%	0.00169	0.325
0.45%	95	13.878	15.031	13.57%	0.00249	0.332

7. SASE2 at 0.1 nm for a sinus error

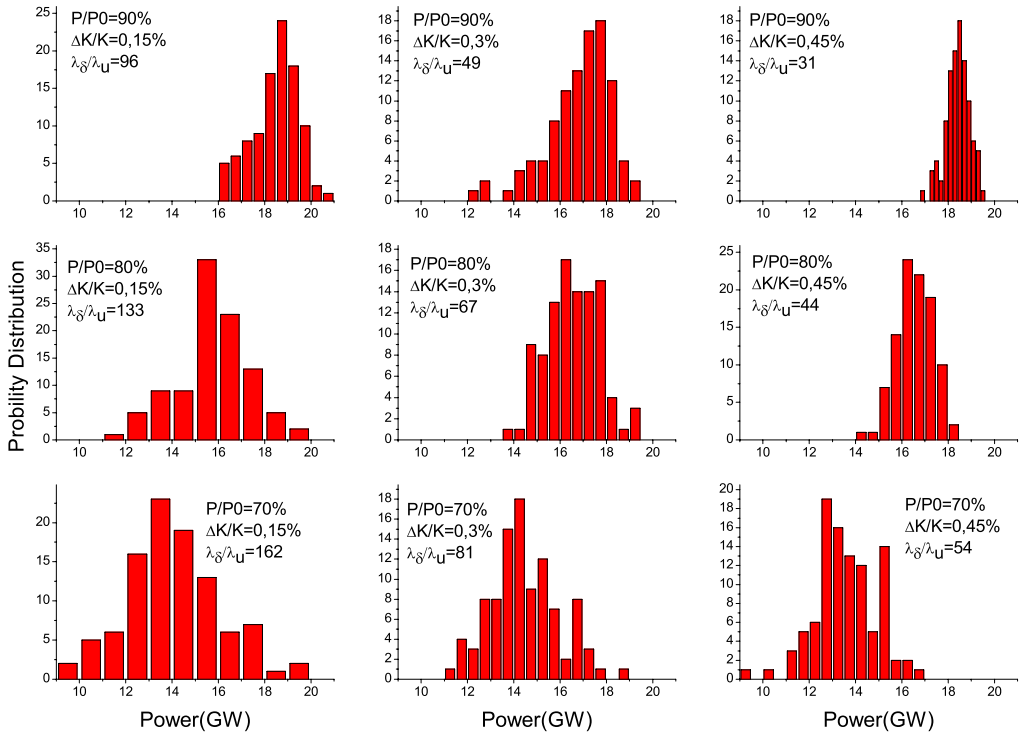

Figure 107: *Results of simulations for SASE2 at 0.1 nm wavelength for a random sinus error distribution. The results from left to right correspond to the same power level of 90% (top), 80% (middle) and 70% (bottom) with increasing error level $\Delta K/K$ or decreasing deformation length λ_δ such that the rms phase shake according to Eq. (17) is constant.*

Table 12: *Summary of the results shown in the Figure above. The rows correspond to the results read from left to right (long to short deformation length, which is equivalent to small to large $\Delta K/K$) and top to bottom (90%, 80% and 70% of the power expected at this position without undulator errors).*

$\Delta K/K$	λ_δ/λ_u	P (GW) Periodic	$\overline{P}$ (GW) Mean power	σ_P/P	σ_K	σ_ϕ
0.15%	96	18.259	18.452	5.38%	0.00123	0.160
0.3%	49	18.259	16.849	8.32%	0.00242	0.168
0.45%	31	18.259	18.415	2.77%	0.00365	0.157
0.15%	133	16.230	15.716	10.21%	0.00123	0.224
0.3%	67	16.230	16.544	6.99%	0.00239	0.220
0.45%	44	16.230	16.544	4.64%	0.00362	0.221
0.15%	162	14.202	14.016	14.77%	0.00123	0.366
0.3%	81	14.202	14.474	10.09%	0.00243	0.270
0.45%	54	14.202	13.582	9.55%	0.00363	0.271

8. SASE2 at 0.1 nm for a triangle error

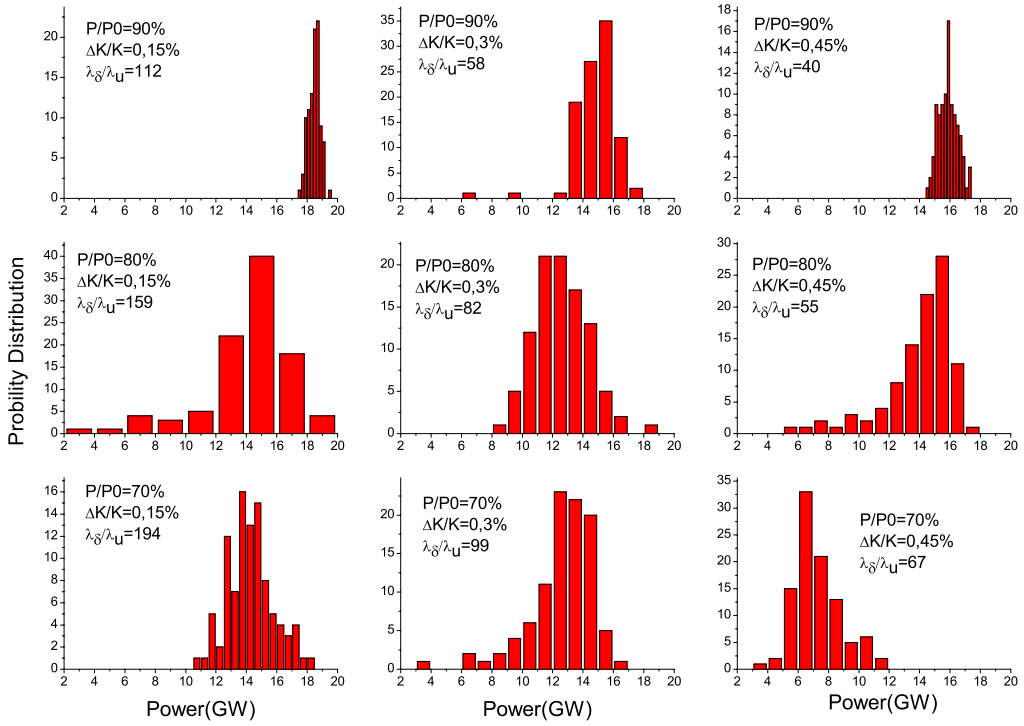

Figure 108: *Results of simulations for SASE2 at 0.1 nm wavelength for a random triangle error distribution. The results from left to right correspond to the same power level of 90% (top), 80% (middle) and 70% (bottom) with increasing error level $\Delta K/K$ or decreasing deformation length λ_δ such that the rms phase shake according to Eq. (17) is constant.*

Table 13: *Summary of the results shown in the Figure above. The rows correspond to the results read from left to right (long to short deformation length, which is equivalent to small to large $\Delta K/K$) and top to bottom (90%, 80% and 70% of the power expected at this position without undulator errors).*

$\Delta K/K$	λ_δ/λ_u	P (GW) Periodic	$\overline{P}$ (GW) Mean power	σ_P/P	σ_K	σ_ϕ
0.15%	112	18.259	18.457	2.09%	0.00172	0.154
0.3%	58	18.259	14.808	9.45%	0.00344	0.226
0.45%	40	18.259	15.869	3.94%	0.00517	0.236
0.15%	159	16.230	14.156	20.38%	0.00174	0.242
0.3%	82	16.230	12.581	14.08%	0.00345	0.325
0.45%	55	16.230	13.975	16.50%	0.00609	0.238
0.15%	194	14.202	14.314	10.44%	0.00173	0.267
0.3%	99	14.202	12.620	16.77%	0.00342	0.279
0.45%	67	14.202	7.305	21.11%	0.00517	0.407

9. SASE2 at 0.1 nm for a sawtooth error

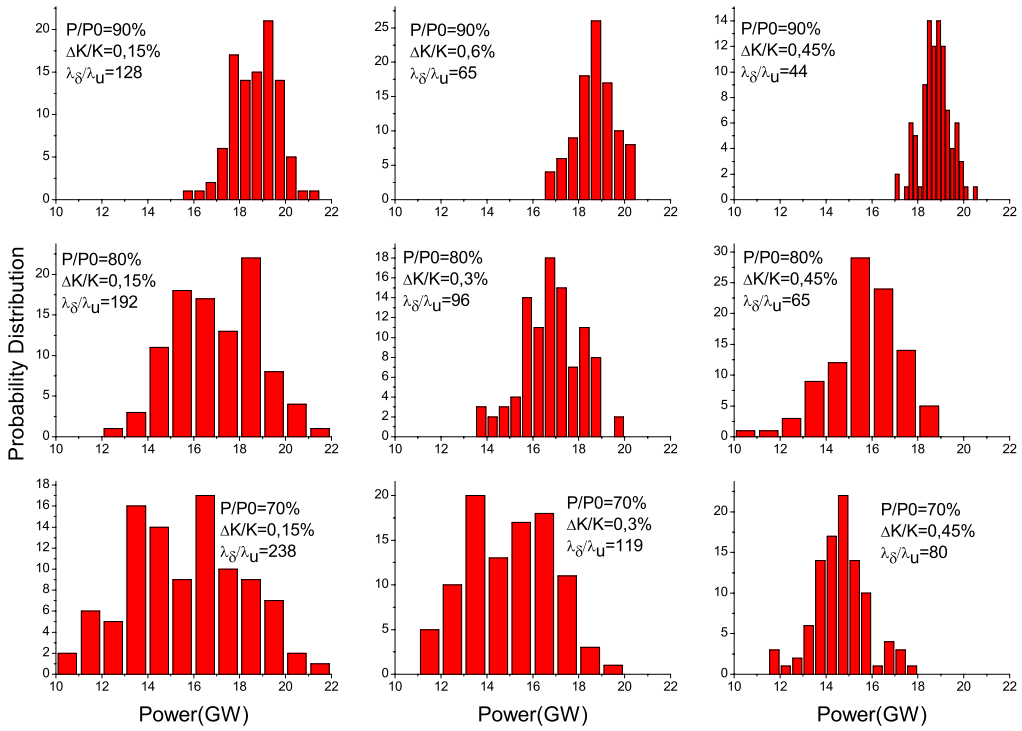

Figure 109: *Results of simulations for SASE2 at 0.1 nm wavelength for a random sawtooth error distribution. The results from left to right correspond to the same power level of 90% (top), 80% (middle) and 70% (bottom) with increasing error level $\Delta K/K$ or decreasing deformation length λ_δ such that the rms phase shake according to Eq. (17) is constant.*

Table 14: *Summary of the results shown in the Figure above. The rows correspond to the results read from left to right (long to short deformation length, which is equivalent to small to large $\Delta K/K$) and top to bottom (90%, 80% and 70% of the power expected at this position without undulator errors).*

$\Delta K/K$	λ_δ/λ_u	P (GW) Periodic	$\overline{P}$ (GW) Mean power	σ_P/P	σ_K	σ_ϕ
0.15%	128	18.259	18.690	5.28%	0.00075	0.138
0.3%	65	18.259	18.698	4.75%	0.00141	0.143
0.45%	44	18.259	18.764	3.42%	0.00209	0.146
0.15%	192	16.230	16.978	10.77%	0.00075	0.205
0.3%	96	16.230	16.824	7.62%	0.00142	0.211
0.45%	65	16.230	15.678	9.61%	0.00210	0.216
0.15%	238	14.202	15.643	15.46%	0.00076	0.255
0.3%	119	14.202	14.975	12.45%	0.00143	0.261
0.45%	80	14.202	14.632	7.91%	0.00210	0.263

10. SASE2 at 0.4 nm with changed gap for a sinus error

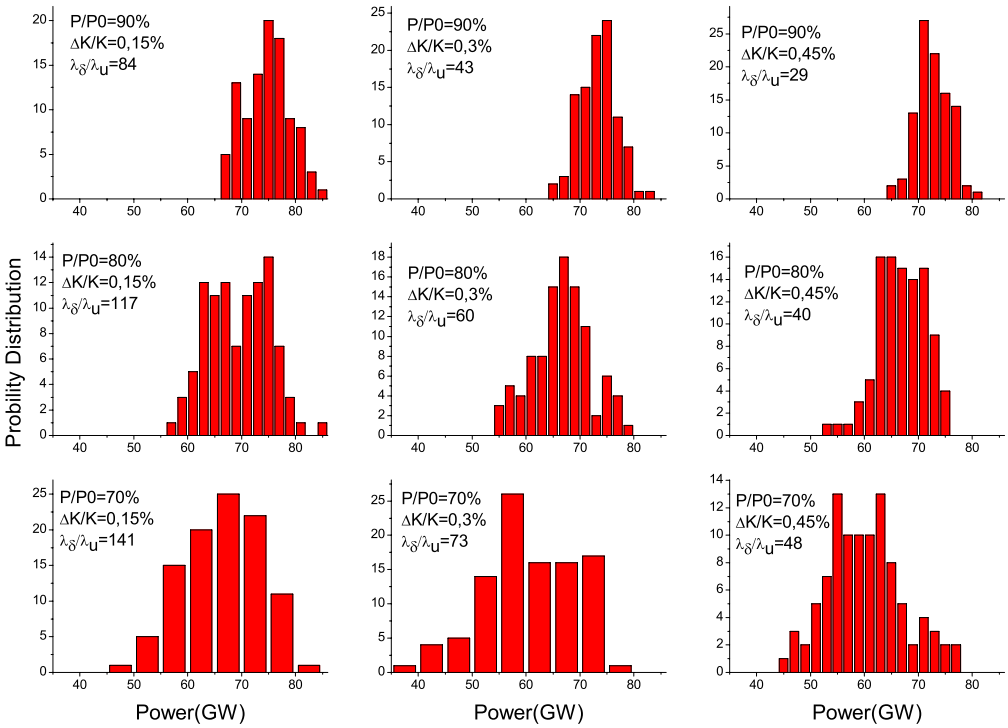

Figure 110: *Results of simulations for SASE2 at 0.4 nm wavelength for a random sinus error distribution. The results from left to right correspond to the same power level of 90% (top), 80% (middle) and 70% (bottom) with increasing error level $\Delta K/K$ or decreasing deformation length λ_δ such that the rms phase shake according to Eq. (17) is constant. The wavelength change has been achieved by changing K.*

Table 15: *Summary of the results shown in the Figure above. The rows correspond to the results read from left to right (long to short deformation length, which is equivalent to small to large $\Delta K/K$) and top to bottom (90%, 80% and 70% of the power expected at this position without undulator errors).*

$\Delta K/K$	λ_δ/λ_u	P (GW) Periodic	$\overline{P}$ (GW) Mean power	σ_P/P	σ_K	σ_ϕ
0.15%	84	72.519	74.713	5.87%	0.00288	0.164
0.3%	43	72.519	73.276	4.86%	0.00540	0.168
0.45%	29	72.519	72.785	4.32%	0.00800	0.171
0.15%	117	64.462	69.412	8.33%	0.00287	0.224
0.3%	69	64.462	66.734	8.12%	0.00543	0.236
0.45%	40	64.462	66.951	6.77%	0.00795	0.237
0.15%	141	56.404	66.248	10.82%	0.00287	0.265
0.3%	73	56.404	60.567	13.67%	0.00544	0.285
0.45%	48	56.404	60.031	11.87%	0.00796	0.287

11. SASE2 at 0.4 nm with changed gap for a triangle error

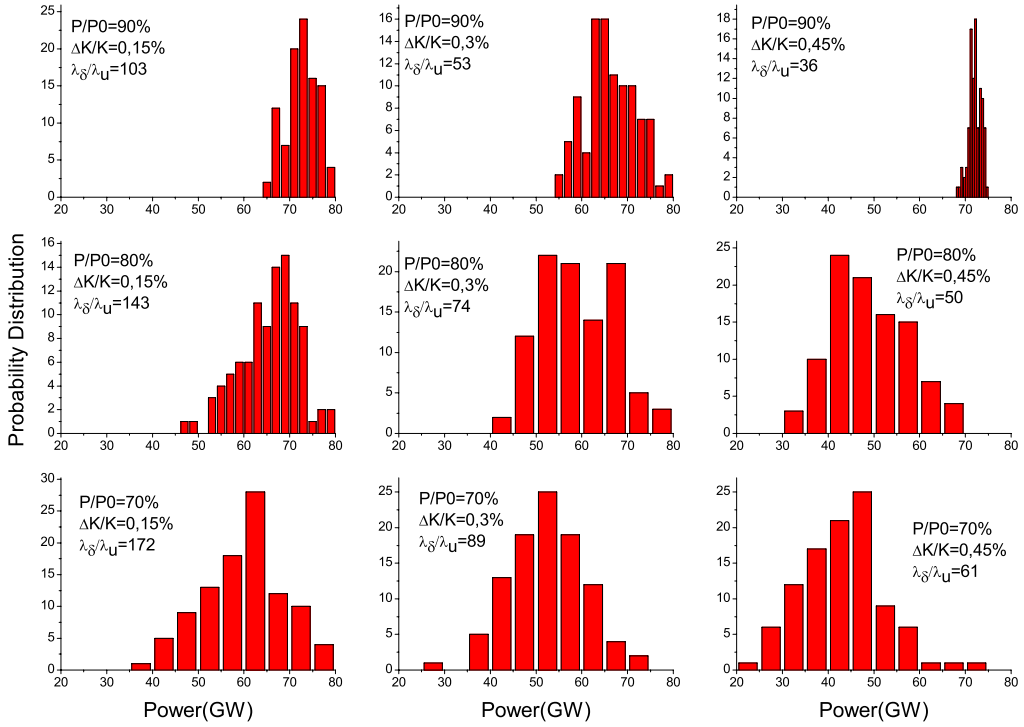

Figure 111: *Results of simulations for SASE2 at 0.4 nm wavelength for a random triangle error distribution. The results from left to right correspond to the same power level of 90% (top), 80% (middle) and 70% (bottom) with increasing error level $\Delta K/K$ or decreasing deformation length λ_δ such that the rms phase shake according to Eq. (17) is constant. The wavelength change has been achieved by changing K.*

Table 16: *Summary of the results shown in the Figure above. The rows correspond to the results read from left to right (long to short deformation length, which is equivalent to small to large $\Delta K/K$) and top to bottom (90%, 80% and 70% of the power expected at this position without undulator errors).*

$\Delta K/K$	λ_δ/λ_u	P (GW) Periodic	$\overline{P}$ (GW) Mean power	σ_P/P	σ_K	σ_ϕ
0.15%	103	72.519	72.628	4.70%	0.00388	0.167
0.3%	53	72.519	66.275	8.30%	0.00754	0.257
0.45%	36	72.519	72.094	1.87%	0.01100	0.177
0.15%	143	64.462	65.473	9.80%	0.00390	0.239
0.3%	74	64.462	58.909	13.91%	0.00759	0.309
0.45%	50	64.462	48.956	17.21%	0.01100	0.360
0.15%	172	56.404	59.568	14.86%	0.00387	0.280
0.3%	89	56.404	52.452	15.56%	0.00769	0.340
0.45%	61	56.404	43.174	20.59%	0.01100	0.417

12. SASE2 at 0.4 nm with changed gap for a sawtooth error

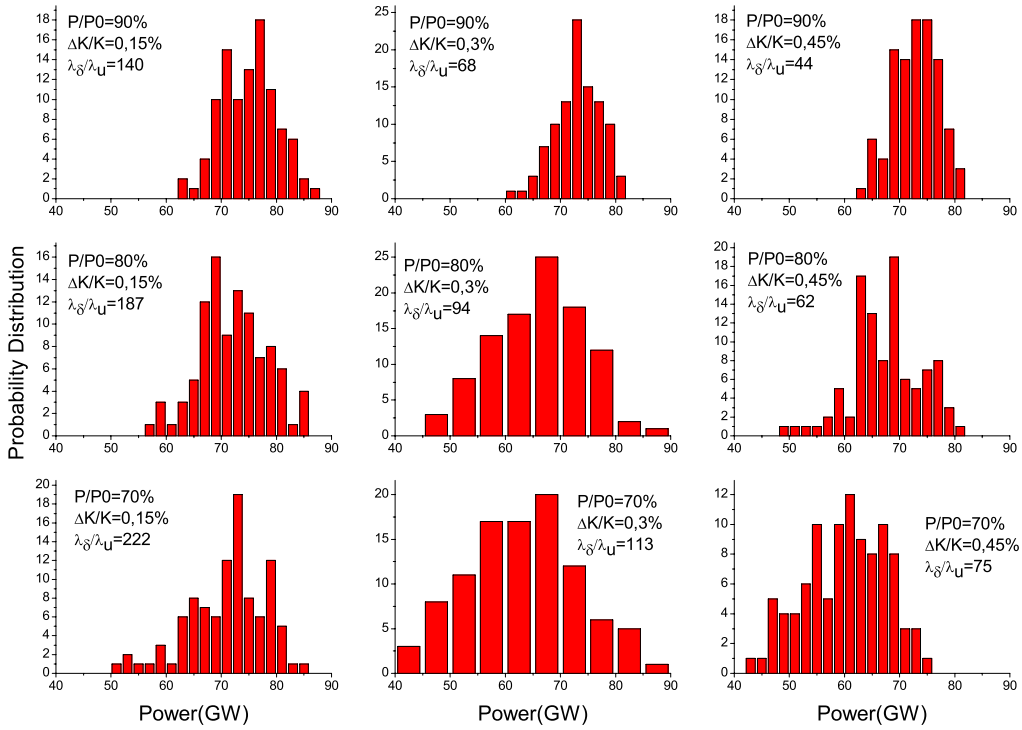

Figure 112: *Results of simulations for SASE2 at 0.4 nm wavelength for a random sawtooth error distribution. The results from left to right correspond to the same power level of 90% (top), 80% (middle) and 70% (bottom) with increasing error level $\Delta K/K$ or decreasing deformation length λ_δ such that the rms phase shake according to Eq. (17) is constant. The wavelength change has been achieved by changing K.*

Table 17: *Summary of the results shown in the Figure above. The rows correspond to the results read from left to right (long to short deformation length, which is equivalent to small to large $\Delta K/K$) and top to bottom (90%, 80% and 70% of the power expected at this position without undulator errors).*

$\Delta K/K$	λ_δ/λ_u	P (GW) Periodic	$\overline{P}$ (GW) Mean power	σ_P/P	σ_K	σ_ϕ
0.15%	140	72.519	74.990	6.76%	0.00190	0.173
0.3%	68	72.519	73.041	5.64%	0.00321	0.173
0.45%	44	72.519	72.845	5.64%	0.00467	0.173
0.15%	187	64.462	72.052	8.59%	0.00193	0.229
0.3%	94	64.462	66.039	12.84%	0.00323	0.236
0.45%	62	64.462	67.514	9.63%	0.00464	0.237
0.15%	222	56.404	71.110	9.98%	0.00192	0.265
0.3%	113	56.404	63.038	16.05%	0.00322	0.285
0.45%	75	56.404	60.124	11.92%	0.00468	0.285

13. SASE2 at 0.4 nm with changed electron energy for a sinus error

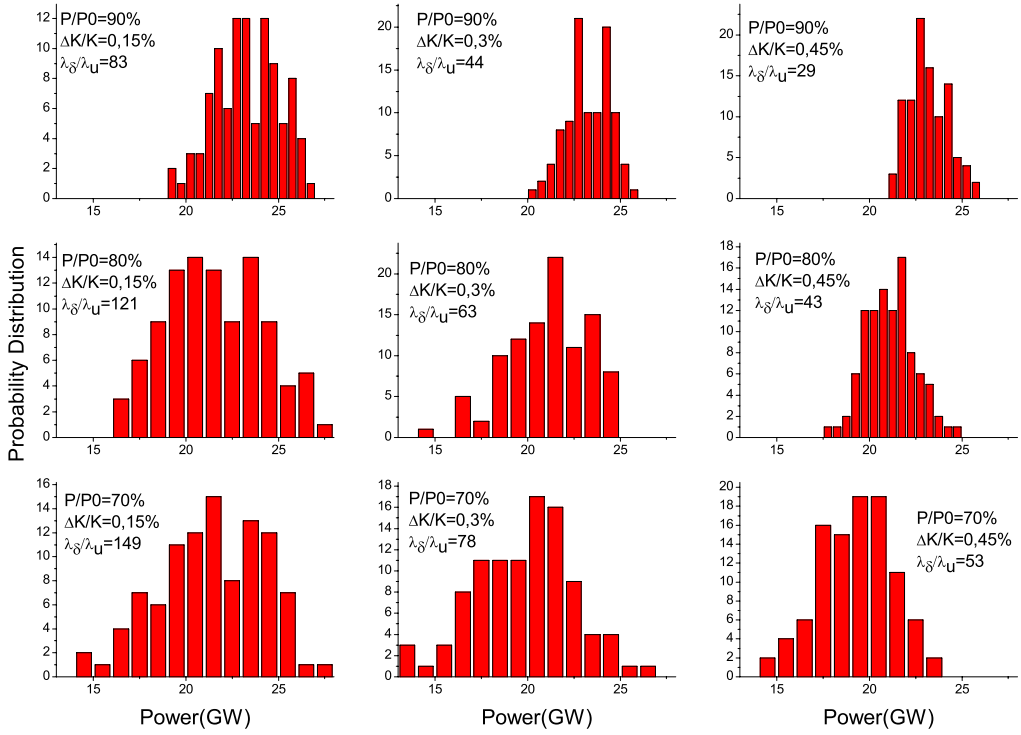

Figure 113: *Results of simulations for SASE2 at 0.4 nm wavelength for a random sinus error distribution. The results from left to right correspond to the same power level of 90% (top), 80% (middle) and 70% (bottom) with increasing error level $\Delta K/K$ or decreasing deformation length λ_δ such that the rms phase shake according to Eq. (17) is constant. The wavelength change has been achieved by changing the beam energy.*

Table 18: *Summary of the results shown in the Figure above. The rows correspond to the results read from left to right (long to short deformation length, which is equivalent to small to large $\Delta K/K$) and top to bottom (90%, 80% and 70% of the power expected at this position without undulator errors).*

$\Delta K/K$	λ_δ/λ_u	P (GW) Periodic	$\overline{P}$ (GW) Mean power	σ_P/P	σ_K	σ_ϕ
0.15%	83	22.831	23.308	7.44%	0.00132	0.136
0.3%	44	22.831	23.260	5.00%	0.00246	0.145
0.45%	29	22.831	23.182	4.51%	0.00367	0.146
0.15%	121	20.294	21.522	12.25%	0.00133	0.197
0.3%	63	20.294	21.100	10.25%	0.00249	0.210
0.45%	43	20.294	21.108	6.34%	0.00366	0.214
0.15%	149	17.758	21.431	13.21%	0.00131	0.235
0.3%	78	17.758	19.807	13.53%	0.00247	0.254
0.45%	53	17.758	19.256	10.40%	0.00364	0.260

14. SASE2 at 0.4 nm with changed electron energy for a triangle error

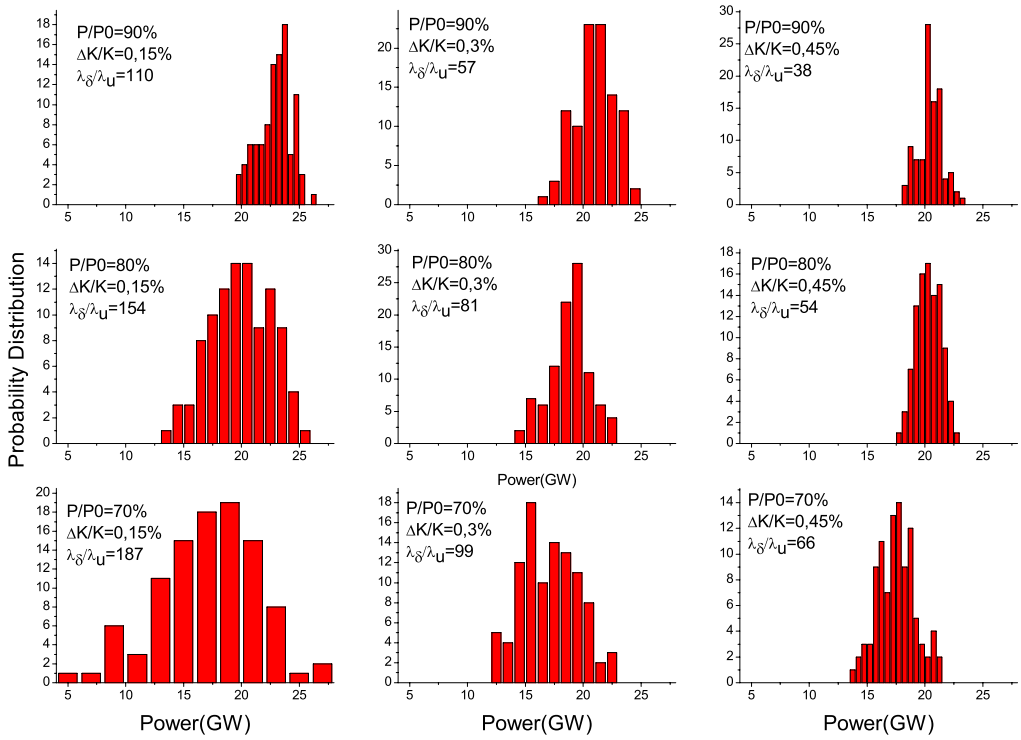

Figure 114: *Results of simulations for SASE2 at 0.4 nm wavelength for a random triangle error distribution. The results from left to right correspond to the same power level of 90% (top), 80% (middle) and 70% (bottom) with increasing error level $\Delta K/K$ or decreasing deformation length λ_δ such that the rms phase shake according to Eq. (17) is constant. The wavelength change has been achieved by changing the beam energy.*

Table 19: *Summary of the results shown in the Figure above. The rows correspond to the results read from left to right (long to short deformation length, which is equivalent to small to large $\Delta K/K$) and top to bottom (90%, 80% and 70% of the power expected at this position without undulator errors).*

$\Delta K/K$	λ_δ/λ_u	P (GW) Periodic	$\overline{P}$ (GW) Mean power	σ_P/P	σ_K	σ_ϕ
0.15%	110	22.831	22.918	6.20%	0.00179	0.162
0.3%	57	22.831	20.977	7.98%	0.00345	0.277
0.45%	38	22.831	20.470	5.04%	0.00516	0.216
0.15%	154	20.294	19.966	13.42%	0.00178	0.208
0.3%	81	20.294	18.830	9.49%	0.00344	0.269
0.45%	54	20.294	20.292	5.04%	0.00510	0.221
0.15%	187	17.758	17.219	24.98%	0.00182	0.261
0.3%	99	17.758	17.077	14.39%	0.00345	0.272
0.45%	66	17.758	17.541	9.22%	0.00518	0.274

15. SASE2 at 0.4 nm with changed electron energy for a sawtooth error

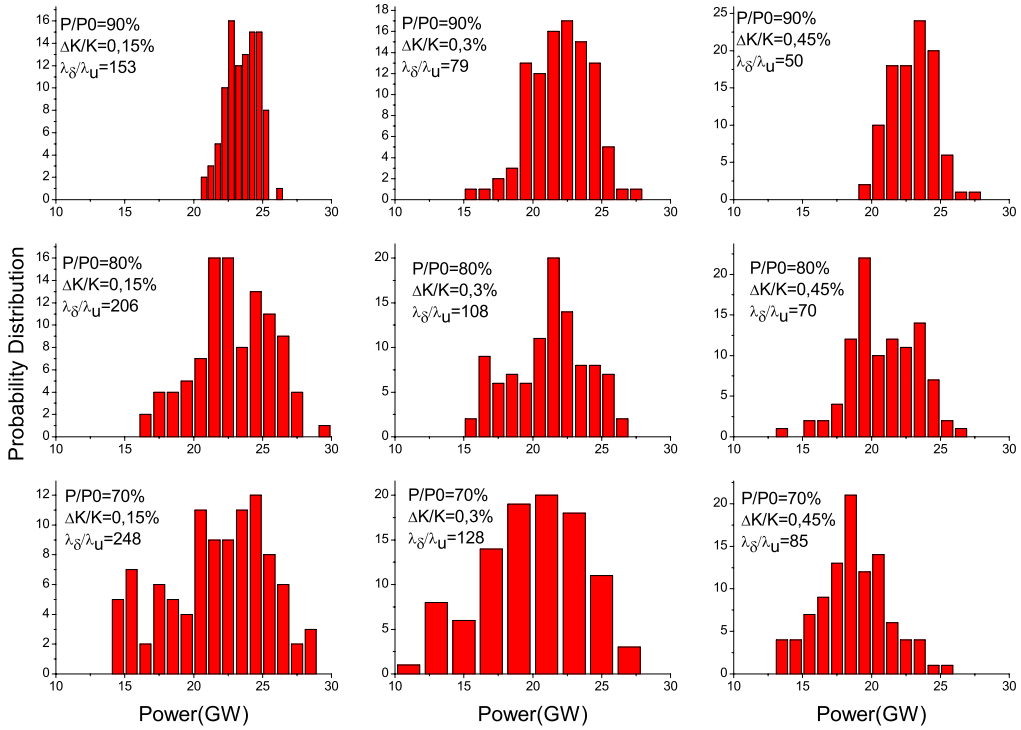

Figure 115: *Results of simulations for SASE2 at 0.4 nm wavelength for a random sawtooth error distribution. The results from left to right correspond to the same power level of 90% (top), 80% (middle) and 70% (bottom) with increasing error level $\Delta K/K$ or decreasing deformation length λ_δ such that the rms phase shake according to Eq. (17) is constant. The wavelength change has been achieved by changing the beam energy.*

Table 20: *Summary of the results shown in the Figure above. The rows correspond to the results read from left to right (long to short deformation length, which is equivalent to small to large $\Delta K/K$) and top to bottom (90%, 80% and 70% of the power expected at this position without undulator errors).*

$\Delta K/K$	λ_δ/λ_u	P (GW) Periodic	$\overline{P}$ (GW) Mean power	σ_P/P	σ_K	σ_ϕ
0.15%	153	22.831	23.501	4.92%	0.00087	0.156
0.3%	79	22.831	21.962	10.01%	0.00148	0.169
0.45%	50	22.831	22.974	6.81%	0.00213	0.163
0.15%	206	20.294	22.868	12.02%	0.00088	0.203
0.3%	108	20.294	21.188	12.87%	0.00148	0.228
0.45%	70	20.294	20.885	11.60%	0.00214	0.227
0.15%	248	17.758	21.709	17.28%	0.00087	0.243
0.3%	128	17.758	19.820	18.77%	0.00147	0.270
0.45%	85	17.758	18.735	13.44%	0.00217	0.274

References

[1] Massimo Altarelli et.al., The European X-Ray Free-Electron Laser Technical Design Report, ISBN 3-935702-17-5

[2] A.M. Kondratenko and E.L. Saldin, Part. Accel. 10, 207 (1980)

[3] R. Bonifacio, C. Pellegrini, and L.M. Narducci, Opt. Commum. 50, 373 (1984)

[4] J. Pflueger, *Undulator Systems and Photon Diagnostics for the European XFEL Project*, Proceedings of the 27th International Free Electron Laser Conference (2005) 378-382

[5] Y. Li, B. Faatz and J. Pflueger, Study of Undulator Tolerances for the European XFEL, TESLA-FEL report 2007-07, DESY, Hamburg.

[6] B.L. Bobbs et.al, Nucl. Instr. and Meth. **A296** (1990) 574-578

[7] B. Faatz, J. Pflueger, Y.M. Nikitina, Nucl. Instr. and Meth. **A393** (1997) 380-384

[8] J. Pflueger, M. Tischer, Nucl. Instr. and Meth. **A483** (1999) 388-393

[9] Y. Li, B. Faatz and J. Pflueger, Magnet Sorting for the XFEL Hybrid Undulator — Comparing Study, TESLA-FEL report 2007-06

[10] S. Reiche, Nucl. Instr. and Meth. **A429** (1999) 243-248

[11] P. Elleaume, J. Chavanne and B. Faatz, Nucl. Instr. Meth. **A455** (2000) 503-523

[12] L.H. Yu, S. Krinsky, R.L. Gluckstern and J.B.J. Zeijts, Phys. Rev. A **45** (1992) 1163-1176

[13] Richard P. Walker, Sincrotrone Trieste ST/M-93/3 (1993)

[14] H.P. Freund and R.H. Jackson, Nucl. Instr. Meth. **A331** (1993) 461-466

[15] A. Friedman, S. Krinski and L.H. Yu, IEEE J. Quant. Electron. **QE 30** (1994) 1295-1302